Aus dem Institut für Chirurgische Forschung
(im Walter-Brendel-Zentrum für Experimentelle Medizin)
der Ludwig-Maximilians-Universität München
Vorstand Prof. Dr. med. Ulrich Pohl

DNA nanotubes - intracellular delivery vehicles *in vivo*

DISSERTATION
zum Erwerb des Doktorgrades der Naturwissenschaften
an der Medizinischen Fakultät der
Ludwig-Maximilians-Universität zu München

Vorgelegt von

Sabine Sellner

aus Freyung

2016

Mit Genehmigung der Medizinischen Fakultät

der Universität München

Berichterstatter:	PD Dr. rer. nat. Markus Rehberg
Mitberichterstatter:	PD Dr. rer. nat. Silke Meiners
	Prof. Dr. rer. nat. Elfriede Nößner
	Prof. Dr. rer. nat. Ludger Klein
Dekan:	Prof. Dr. med. dent. Reinhard Hickel
Tag der mündlichen Prüfung:	15.02.2017

Eidesstattliche Versicherung

Sellner, Sabine

Name, Vorname

Hiermit erkläre ich an Eides statt, dass ich die vorliegende Dissertation mit dem Thema:

DNA nanotubes - intracellular delivery vehicles *in vivo*

selbstständig verfasst, mich außer der angegebenen keiner weiteren Hilfsmittel bedient und alle Erkenntnisse, die aus dem Schrifttum ganz oder annähernd übernommen sind, als solche erkenntlich gemacht und nach ihrer Herkunft unter Bezeichnung der Fundstelle einzeln nachgewiesen habe.

Ich erkläre des Weiteren, dass die hier vorgelegte Dissertation nicht in gleicher oder ähnlicher Form bei einer anderen Stelle zur Erlangung eines akademischen Grades eingereicht wurde.

München, den

Ort, Datum

Unterschrift Doktorandin

„Man sieht oft etwas hundert Mal,

tausend Mal,

ehe es man zum allerersten Mal

wirklich sieht.“

Christian Morgenstern

Contents

1 Abstract

1.1 Abstract

The biomolecule deoxyribonucleic acid (DNA) plays an essential role in the development, function, and reproduction of living organisms. Furthermore, DNA is a natural polymer with unique properties used as raw material for several developments in the physical, medical, and biological sector. The structure of DNA makes it a programmable, functional, and biocompatible basic material for the production of precise structures in the nanometer range. DNA-based nanoconstructs offer great potential to be used as carrier systems for biomedical applications. However, their impact on biological systems and their distribution in cells and tissue is largely unknown.

Therefore, DNA nanotubes with different ligands were produced, using the single-stranded tile method, based on the self-organization of complementary oligonucleotides (ODNs) to tube-like structures in nanometer precision. The functionality and the microdistribution of these DNA structures were investigated under physiological and pathological conditions in the murine muscle tissue and in cultured macrophages.

The use of DNA nanotubes as carrier systems, targeting macrophages in the murine skeletal muscle and their capacity to induce an immune response, was determined in the first part of this thesis. These DNA nanotubes were decorated with immunogenic, unmethylated cytosine-phosphate-guanine (CpG) DNA sequences which are specific for bacterial DNA and are recognized by the innate immune system of vertebrates. The detection of CpG sequences via the endosomal Toll-like receptor 9 (TLR 9) in macrophages after incubation with CpG DNA nanotubes led to the secretion of the proinflammatory cytokine tumor necrosis factor (TNF), while incubation with plain

nanotubes did not induce a significant immune response. To confirm the immunogenic effect of CpG DNA nanotubes *in vivo*, the constructs were microinjected into the murine cremaster muscle. All constructs were taken up by tissue-resident macrophages equally, but only microinjection of CpG DNA nanotubes caused nuclear translocation of the proinflammatory transcription factor NF-κB and the recruitment of leukocytes to the site of injection.

Since DNA nanotubes were selectively ingested by tissue-resident macrophages and because the application of functional CpG motifs specifically affected the immune reaction of macrophages and mast cells, CpG DNA nanotubes were investigated under sterile inflammatory conditions in the next part of the thesis. CpG DNA nanotubes were able to induce phenotypically altered macrophages with high TLR 9 expression in an ischemia-reperfusion (I/R) model. Furthermore, CpG nanoconstructs attenuated leukocyte recruitment. However, plain DNA nanotubes promoted the invasion of leukocytes into the postischemic tissue without causing increased expression of TLR 9 in macrophages.

In the final part of the thesis, the ability of DNA nanotubes to deliver anti-inflammatory drugs was tested. Therefore, the effects and the localization of dexamethasone-conjugated DNA nanotubes (Dex nanotubes) were examined *in vitro* as well as in the I/R model. The anti-inflammatory molecule dexamethasone could be delivered efficiently to target cells using the DNA carrier system *in vitro* and *in vivo*. The pretreatment with Dex nanotubes in a septic *in vitro* model significantly reduced the TNF response by macrophages without affecting the cell viability. Microinjection of Dex nanotubes into postischemic mouse cremaster tissue resulted in a significant reduction of leukocyte recruitment. Immunohistological stainings revealed that the expression of the endothelial adhesion molecules VCAM-1 and ICAM-1 was

diminished after injection of Dex nanotubes, contributing to the attenuated leukocyte transmigration.

Taken together, these results demonstrate that DNA nanotubes can be used as a biocompatible platform for the delivery of bioactive molecules to target macrophages *in vivo*.

1.2 Zusammenfassung

Das Biomolekül Desoxyribonukleinsäure (DNA) ist essentiell für die Entwicklung, Funktion und Reproduktion von lebenden Organismen. Darüber hinaus ist DNA jedoch auch ein natürliches Polymer, das durch seine einzigartigen Eigenschaften zum Ausgangsmaterial für verschiedenste Entwicklungen im physikalischen, medizinischen und biologischen Bereich wurde. DNA ist, durch ihre Struktur, ein programmierbares, funktionalisierbares und biokompatibles Basismaterial für die Herstellung präziser Strukturen im Nanometerbereich. DNA-basierte Nanokonstrukte besitzen großes Potential als Trägersysteme für biomedizinische Anwendungen. Allerdings ist bis jetzt nur wenig über ihren Einfluss auf biologische Systeme und die Verteilung in Zellen und im Gewebe bekannt.

Mittels der *single-stranded tile* Methode, mit der sich komplementäre Oligonukleotide (ODNs) in Nanometergenauigkeit zu Konstrukten selbstorganisieren, wurden DNA-Nanoröhren mit verschiedenen Liganden hergestellt. Diese DNA Strukturen wurden auf ihre Funktionalität und Verteilung unter physiologischen und pathologischen Bedingungen sowohl im murinen Muskelgewebe als auch in kultivierten Makrophagen-Zelllinien untersucht.

Im ersten Teil dieser Arbeit wurden DNA-Nanoröhren als Trägersysteme für die gezielte Anwendung an Makrophagen im murinen Skelettmuskel und auf ihr Vermögen, eine Immunantwort zu induzieren, untersucht. An diese DNA-Nanoröhren waren immunogene, unmethylierte Cytosin-Phosphat-Guanin (CpG) DNA-Sequenzen konjugiert, die spezifisch für bakterielle DNA sind und vom angeborenen Immunsystem der Vertebraten erkannt werden. Die Erkennung der CpG-Sequenzen durch den endosomalen Toll-like Rezeptor 9 (TLR 9) in Makrophagen führte nach

Inkubation mit CpG-DNA-Nanoröhren zur Freisetzung des proinflammatorischen Zytokins Tumornekrosefaktor (TNF), während Inkubation mit unkonjugierten DNA-Nanoröhren keine signifikante Immunantwort induzierte. Um die immunogene Wirkung der CpG-DNA-Nanoröhren auch *in vivo* zu bestätigen, wurden die Konstrukte in den murinen Cremastermuskel mikroinjiziert. Alle Konstrukte wurden gleichmäßig von gewebsständigen Makrophagen aufgenommen, allerdings kam es nur nach Injektion von CpG-Nanoröhren zur nukleären Translokation des proinflammatorischen Transkriptionsfaktors NF-κB und zur Rekrutierung von Leukozyten an die Injektionsstelle.

Da DNA-Nanoröhren spezifisch von Gewebsmakrophagen aufgenommen werden und durch den Einsatz eines funktionellen CpG-Motivs die Immunantwort von Makrophagen und Mastzellen beeinflusst werden konnte, wurden im nächsten Teil dieser Arbeit CpG-DNA-Nanoröhren unter sterilen inflammatorischen Bedingungen untersucht. Nach Ischämie-Reperfusion (I/R) führten CpG-tragende Konstrukte *in vivo* zu phänotypisch veränderten Makrophagen mit hoher Expression von TLR 9. Darüber hinaus konnten inhibierende Effekte von CpG-Nanokonstrukten auf die Leukozytenrekrutierung nachgewiesen werden. Unkonjugierte DNA Nanoröhren förderten hingegen die Einwanderung von Leukozyten ins Gewebe, jedoch ohne eine erhöhte Expression von TLR 9 in Makrophagen hervorzurufen.

Im abschließenden Teil dieser Arbeit wurde die Möglichkeit des Transports von antiinflammatorischen Wirkstoffen durch DNA-Nanoröhren untersucht. Hierfür wurden Dexamethason-konjugierte DNA-Nanoröhren (Dex-Nanoröhren) *in vitro* als auch *in vivo* im I/R-Modell auf ihre Wirkung und Lokalisation untersucht. Durch das DNA-Trägersystem konnte das entzündungshemmende Molekül Dexamethason nicht nur *in vitro*, sondern auch *in vivo*, sehr effizient aufgenommen werden. Im septischen *in vitro* Modell führte die Vorbehandlung mit Dex-Nanoröhren zu einer

reduzierten TNF Antwort durch Makrophagen ohne Einschränkung der Zellvitalität. Die Mikroinjektion von Dex-Nanoröhren in das postischämische, murine Cremaster-Gewebe hatte eine signifikante Reduktion der Leukozytenrekrutierung zur Folge. Immunhistologische Färbungen zeigten, dass die Expression der endothelialen Adhäsionsmoleküle VCAM-1 und ICAM-1 durch Injektion von Dex-Nanoröhren reduziert wird, was zur geringeren Anzahl an transmigrierten Leukozyten beiträgt.

Diese Ergebnisse zeigen, dass sich DNA-Nanoröhren als biokompatible Nanoplattformen für den Transport von bioaktiven Molekülen in Makrophagen *in vivo* eignen und damit ein besonderes therapeutisches Potential besitzen.

2 Introduction

2.1 Nanotechnology

The term nanotechnology is referring to the production, manipulation, and use of materials at dimensions ranging from 1 to 100 nanometers. The prefix “nano-“ derives from the Greek “nanos” (dwarf) and describes the billionth part (=10^{-9}) of something. At this scale, materials gain new physical, chemical, and biological properties that are not shared with non-nanoscale materials with identical chemical composition. The total surface of nanoparticles (NPs) is, compared to the total volume, much larger; therefore, the “reactive” surface is also larger. Furthermore, NPs show a higher conductivity, higher stability, and a lower melting temperature than their larger counterparts. Due to these unique properties, NPs are used in a wide variety of applications such as cosmetics, sunscreen [1], water purification systems [2], and sensors [3]. NPs are entering areas of our daily lives and also the biomedical field. Several classes of engineered NPs are currently applied as nanovaccines [4], nanodrugs [5], or diagnostic imaging tools [6].

2.2 Biological and medical applications of NPs

However, the knowledge about the fate and the biological effects of NPs *in vivo* has not kept up with the pace of these developments. Since NPs have a higher free surface energy than the bulk material, the reactivity of nanomaterials with biomolecules such as proteins or lipids in body fluids is enhanced [7]. As a result, the surface is coated with these molecules. This “biomolecular corona” is in many cases interacting with the NPs´ biological environment and therefore crucially determines the biological features of NPs [8]. For instance, lipoprotein-coated NPs can passively penetrate the cell membrane or attach to it [9], whereas surface ligands such as

proteins are recognized by different cellular receptors that trigger internalization and cellular activation [10].

Also size and solubility affect the interaction of NPs with cells and, particularly, cell-specific parameters such as cell cycle stadium or cell type [11]. The impact of the same NP on different cell populations differs significantly and cannot be assumed for other cell populations. For potential biomedical applications it is therefore important to gain as much knowledge about the impact of certain NP parameters as possible, to draw a general conclusion, and to consider the risks.

The modification of physicochemical properties (such as charge, functional groups, size, and shape) of nanomaterials allows the control of distinct cellular uptake and immunogenicity, factors that influence the distribution and clearance of these particles [12]. To assure the correlation of a particular cellular response to a certain NP or property of a NP, it is of great importance to produce precisely defined structures and to control their properties. A material which allows the determination of many of these properties, because of its high programmability, is DNA.

2.3 DNA nanotechnology

DNA is a central information carrier in biological systems, such as prokaryotic cells, eukaryotic cells, bacteriophages, and viruses. The genetic information is encoded in nucleic acid sequences, which are complementary Watson-Crick base pairings (Fig. 1D). Aside from the biological importance, DNA can be assembled into nanometer-scaled, structurally precise architectures due to its molecular programmability and selective hybridization (Fig. 1F) [13]. In 1982, Nadrian Seeman was the first considering DNA as molecular building material in a non-biological context [14] and he paved the way for structural DNA nanotechnology. From immobile branched

junctions in 1983 [15] to complex three-dimensional structures (Fig. 1G) [16, 17] nowadays, DNA nanotechnology experienced a rapid development.

One of the most important advances made during this development was the use of scaffold DNA strands for creating desired nanoscale shapes [18]. This new technique, called “DNA origami”, was implemented by the group of Paul Rothemund. Analog to the Japanese art of paper folding, Rothemund et al. folded a scaffold DNA strand, consisting of 7249 nucleotides (nt) derived from the bacteriophage M13, into shape with hundreds of shorter oligonucleotides (staple strands) [18]. This method now also allows the formation of larger assemblies by multimerizing single DNA origami constructs as well as building three-dimensional objects by stacking sheets of parallel helices. In this process, staple strands of the inner helix form crossovers with staple strands from three neighboring helices [19]. With a reaction yield of about 90%, DNA origami is a simple and fast method to design and create DNA constructs with about 100 nm in diameter (Fig. 1G). Moreover, it serves as a platform for the arrangement of heteroelements such as proteins [20-22], NPs [23-25], or carbon nanotubes [26] due to the sequence specificity and spatial addressability of DNA nanoconstructs. The pattern of components on top of the nanoconstruct can be quickly and inexpensively reconfigured to perform a different task [27]. Another important feature in the context of biological applications is the stability of DNA origami architectures in cell lysates [28]. Two- and three-dimensional nanoarchitectures assembled by this technique have been deployed in various applications such as single molecule imaging [29], molecular robotics [30], single molecule chemistry [31], or immunostimulation [32]. However, due to the scaffold strand needed, the DNA origami technique is limited in size, complexity, and large scale production.

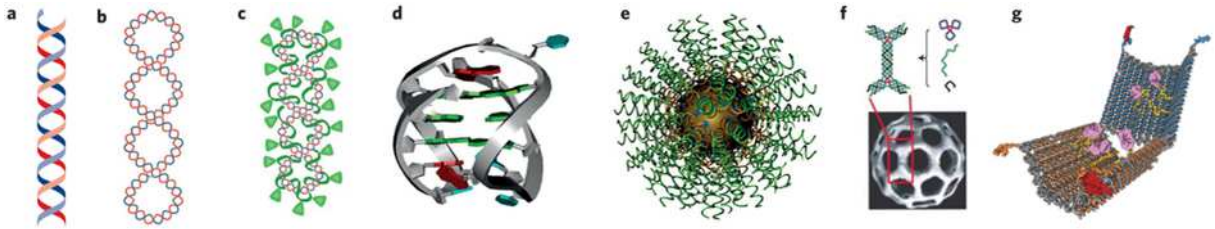

Fig. 1 *Design of DNA nanodevices***.** The double helix structure of DNA is the basis for many DNA nanodevices (**A**). Small circular, double-stranded DNA plasmids are used as vectors for genetic engineering in therapeutic and biomedical applications (**B**). To enhance the efficiency of plasmids they are often complexed with cationic lipids or polyethylenglycol (green) (**C**). Secondary DNA structures, such as G-quadruplexes, are made up of guanine-rich sequences and are used for the molecular recognition of ligands (**D**). Spherical DNA NP conjugates are composed of oriented DNA ODN strands (green) that are packed on an inorganic NP (brown). These constructs have been successfully used for the regulation of genes *in vitro* and *in vivo* (**E**). The sticky-end association of single tiles (top) allows the self-assembly of DNA into polyhedral structures (bottom) (**F**). A three-dimensional DNA origami-based construct with controllable lid for the delivery of molecular payloads (**G**). Reprinted by permission from Macmillan Publishers Ltd: Nature nanotechnology [33] copyright 2015.

A new approach that circumvents these limitations was recently implemented by Wei et al. [34]. The single-stranded tile assembly allows building arbitrary structures with striking speed. In this system, each tile is a single strand with four different binding domains that specify which four other tiles can bind to it. Each tile adopts a specific position and self-assembles to an arbitrary DNA shape, when an appropriate subset of tiles is mixed together (Fig. 6). On the edges of each construct, free binding domains remain which can lead to aggregation. To seal the edges, edge protector strands are added. Wei et al. drastically reduced the manufacturing time with this efficient, modular, and robust method, without producing misfolded by-products. By using a robot to select and mix strands, the authors brought DNA nanotechnology into a rapid prototyping age [27]. It is conceivable that approaches with several thousand strands will generate several kDa huge complex structures, without the use of a scaffold strand in the future.

The spectrum of strategies to create DNA nanoconstructs is broad, but DNA tile assembly and DNA origami are the most popular approaches in DNA nanotechnology.

2.4 DNA nanostructures as drug delivery vehicles

DNA nanoconstructs have caught the interest of the drug delivery community, since the drug cargo can either be attached to the precisely programmed DNA scaffold or enclosed in a three-dimensional structure with targeting ligands attached. Another important benefit for the use of DNA structures as drug delivery tools is: they have been shown to be non-cytotoxic [32, 35]. Furthermore, the stoichiometry can be fully controlled [18, 19] and they survive in cell media, blood serum, and cultured cells for extended periods of time [28, 36, 37]. The stability of DNA constructs towards nucleases can be significantly enhanced by functionalization, e.g., hexanediol [38] or structural compaction.

Douglas et al. created a DNA nanorobot capable of transporting a molecular payload to certain cell subsets under the control of a logic gate [35]. Another powerful implementation is the DNA “nano-claw” which autonomously analyzes multiple molecular cancer cell signatures and, in response, releases target-specific agents [39]. Although there are many sophisticated DNA architectures designed and realized, only a few have been applied to complex biological systems like tissue. Therefore, a rather simple tube design could be more controllable *in vivo* and may allow a general prediction of the bioactivity of DNA structures in contrast to complex multifunctional DNA architectures. To transport drugs efficiently, not only towards the target cells but additionally into target cells, is one of the challenges DNA nanotechnology needs to face. A promising concept is the functionalization of constructs with receptor ligands as guiding or targeting agents. For instance, the conjugation of folate to DNA tubes induced their efficient internalization by folate receptor-bearing cancer cells [40]. But also size is a vital criterion for cellular uptake. Uptake studies with polycation-DNA gene delivery systems (DNA complexed with

polycations) revealed that a size below 100 nm promotes maximal endocytosis by non-specialized cells [41]. Most uptake mechanisms, e.g., clathrin-mediated endocytosis, are receptor-mediated cellular processes. As the size increases, it becomes less likely that receptor binding will occur. However, professional phagocytes such as macrophages, polymorphonuclear granulocytes, or dendritic cells (DCs) are able to internalize objects larger than 500 nm. This requires the recognition of the target by specialized surface receptors (e.g., scavenger receptors) and subsequent actin rearrangement [42, 43]. For the phagocytosis of particles, an actin-dependent extension of the plasma membrane is necessary [44]. The cargo size affects not only uptake pathways but also cytotoxicity and biodistribution.

Negatively charged DNA nanoconstructs are considered to be less toxic than positively charged ones, which have a high affinity to the negatively charged cell membrane and therefore disrupt the membrane integrity [45].

As explained above, successful cellular delivery is substantially driven either by multiple factors regarding the nanoconstruct such as surface charge, size, and shape or by the microenvironment the construct is operating in. The cellular availability of the carrier system is strongly dependent on the biological borders (e.g., blood tissue border, blood brain barrier, or gut mucosa) that need to be crossed. Therefore, critical factors such as construct stability and the delivery across physiologic barriers should be regarded. Acid-catalyzed depurination of DNA at low pH and high concentrations of deoxyribonucleases (DNases) aggravate the crossing of constructs from the blood into the tissue. To mitigate this, direct application into the target tissue is a convenient way to circumvent fast degradation by DNase I, since the concentration of DNase I is in most murine organs significantly lower than in the blood [46]. Microinjection of DNA NPs into the eye [47] and the brain [48] were successful attempts to avoid degradation and to facilitate the transfection of target cells such as neurons and glial

cells. Another interesting target for the administration of functional DNA nanoconstructs are macrophages which are essential components of many types of tissue and contribute to a wide range of pathologies, such as cancer, arthritis, and atherosclerosis [49].

2.5 Monocytes and macrophages

Macrophages have first been described as phagocytic active cells by Ilya Metchnikoff in the 19th century [50]. They are a heterogeneous group of immune cells that are essentially distributed in all tissues and capable of altering their phenotype in order to suit the microenvironment in which they reside. Macrophages are vital participants in the innate and adaptive immune system. Because of multifaceted activities, e.g., the removal of invading pathogens, apoptotic cells, and cellular debris, resolution of inflammation [51], release of cytokines and growth factors, presentation of antigens to T-cells [52], remodeling of matrix components [52, 53], and processing of iron [54], macrophages have been identified as key players in diseases with major influence for the public health. Cancer, autoimmune, chronic inflammatory, degenerative, and metabolic diseases are just a few examples [49].

2.5.1 Monocytes

Blood monocytes are derived from hematopoietic stem cells in the bone marrow and are present in blood and spleen [55]. They consist of two subtypes – inflammatory CCR2^{hi} CX$_3$CR1^{low} Ly6c^{hi} monocytes and resident CCR2^{low} CX$_3$CR1^{hi} Ly6c^{low} monocytes [56]. While Ly6c^{low} monocytes stay in the blood and patrol along vessel walls, Ly6c^{hi} monocytes are not only found in the blood but also in tissues such as skin, lung, lymph nodes, and spleen [57, 58]. There they control the extravascular

environment or transport antigens to lymph nodes and support antigen presentation [57]. Monocytes do not proliferate in a steady state [55, 59], but mature under certain challenges, such as inflammation [60] or atherosclerosis [61] to DCs or macrophages in infiltrated tissues [62, 63]. Since macrophage-colony stimulating factor (M-CSF)-deficient mice show diminished numbers of blood monocytes [64], it has been demonstrated that interleukin-34 (IL-34) and M-CSF strongly push the development of this lineage [60, 65].

2.5.2 Tissue-resident macrophages

Although it has long been the prevailing view that tissue macrophages originate from adult blood monocytes, recent publications revealed that most lineages of tissue macrophages are established during embryonic development from the yolk sac, the fetal liver, or the bone marrow [66-70]. The various sources of development distinguish monocytes from tissue macrophages, which have a limited ability to migrate. Tissue macrophages are extremely heterogeneous in phenotype, homeostatic turnover, and function, thus they are well adapted to the anatomical locations they reside (Fig. 2) [71, 72]. This adaptation also manifests in tissue-specific transcription and epigenetic programs [73, 74]. Bone macrophages, so-called osteoclasts, are specialized in the resorption of bone. This process is associated with a high expression of carbonic anhydrase II [75] in osteoclasts which is known to be important for the acidic degradation of bone material. Another example are microglia, macrophages in the brain. They produce brain-derived neurotrophic factor (BDNF) which is a key modulator of neuronal synaptic plasticity and the formation of memory [76]. Dysfunctions or abnormalities of tissue-resident macrophages in turn lead to a variety of diseases. For instance, osteopetrosis results in insufficient bone resorption due to a defectiv osteoclast development [77].

Furthermore, tissue-resident macrophages are able to dynamically change their activation status and phenotype in response to their environment [78]. The reprogramming of the epigenetic program changes the phenotype of macrophages. Lavin et al. transferred macrophages originating from the peritoneum into the lung and, as a result, the majority of macrophages acquired the gene expression profile of lung macrophages [78]. This study demonstrated that tissue-resident macrophages exhibit a phenotypic plasticity and polarization, occurring during inflammation, which is reversible. These characteristics together with their prominent role in mammalian tissues nominate them as attractive therapeutic targets.

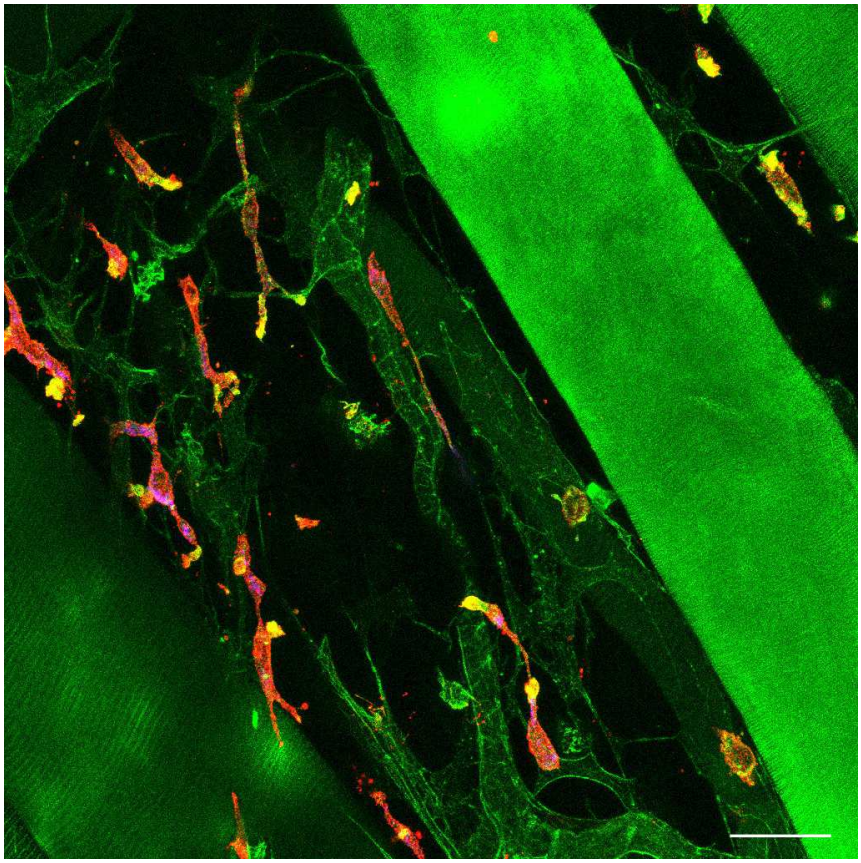

Fig. 2 *Tissue-resident macrophages in the cremaster muscle.* Confocal imaging of tissue-resident macrophages 60 min after intrascrotal injection of carboxyl quantum dot (cQD) NPs. F4/80-positive tissue-resident macrophages (red) phagocytose cQDs (blue) after application into the murine cremaster muscle. These F4/80-positive tissue-resident macrophages line the interstitial tissue between muscle fibers (phalloidin, green). Scale bar: 20 µm.

2.5.3 Activation and polarization of macrophages

Macrophages bridge the two categories of immunity: the innate and the adaptive immune system. The innate immune system detects and responds to various pathogens via a broad range of pattern-recognition receptors, e.g., TLRs and NOD-like receptors (NLRs). These enable them to sense common structural and functional features associated with different classes of microorganisms, foreign substances, or cellular components [79]. Thus, the expression pattern of these receptors is highly dependent on the microenvironment. Subsequent to the encounter of pathogens, receptor activation is translated into different classes of effector responses such as phagocytosis, inflammasome formation [80], and cytokine production.

On the one hand, cytokines can amplify the immune response and on the other hand they directly impact the transmigratory activity of inflammatory leukocytes, largely neutrophils and monocytes, from the blood stream into the affected tissue [81]. Once activated, inflammatory macrophages present the processed antigens via the major histocompatibility complex II (MHC II) to lymphocytes such as T-cells [82]. Subsequently, these T-cells can stimulate B-cells to generate antibodies, specific to the presented antigen, which leads to immediate and long-lasting defense against a specific pathogen.

Monocyte-derived macrophages populate the inflammatory foci, proliferate, and make up the majority of present macrophages. Fundamental for proliferation of all subpopulations, under physiologic and pathologic conditions, is the growth factor M-CSF [72, 83]. In contrast to monocyte-derived macrophages, resident macrophages though having the ability to proliferate, the proliferation is tightly regulated and dampened once normal tissue numbers are obtained [83, 84]. However their importance is stated by the observation that the depletion of resident macrophages

with chlodronate liposomes leads to an altered immune response due to the absence of inflammatory mediators, such as chemokines, cytokines, lipid mediators, and a disrupted host defense [85-87].

In general, macrophages actively scan their microenvironment and certain stimuli polarize the cells into another phenotypic and functional subpopulation. The “M1-M2 paradigm” describes two well-studied macrophage subsets established according to their gene expression profiles and their functional activities [88]. M1 macrophages promote host defense and antitumor immunity via the production of reactive oxygen and nitrogen species and pro-inflammatory cytokines (TNF, IL-12, and IL-1β) [89]. Alternatively activated macrophages (M2 macrophages) facilitate wound repair, regulate glucose metabolism, suppress inflammation and antitumor immunity [90]. “Regulatory macrophages” are a third population, which are generated in the presence of TLR agonists and Immunoglobulin G (IgG) complexes [91]. Other factors turning the macrophage development into a regulatory direction are IL-10 [92], apoptotic cells [93], or prostaglandins [94]. Due to the production of the immunosuppressive cytokines IL-10 and TGF-β, these cells have the propensity to induce an anti-inflammatory T_H2 and regulatory T-cell response to dampen chronic inflammatory and antitumor responses.

2.6 Leukocyte recruitment from the microcirculation

Leukocytes, also called white blood cells, are a group of immune cells that fulfill specific effector functions within the immune defense in lymphoid and peripheral tissue. Leukocytes can be classified in two major lineages: the myeloid lineage including neutrophils, eosinophils, basophils, and monocytes, and the lymphoid

lineage including B-cells, T-cells, and natural killer cells [95]. They are generated from hematopoietic stem cells in the bone marrow and circulate through the blood and the lymphatic system. In order to eliminate invading microorganisms or in the incidence of a sterile tissue injury, leukocytes extravasate the bloodstream from postcapillary venules into the interstitial space. The recruitment of leukocytes into inflamed tissue is considered to be a fundamental part of inflammatory processes, however leukocytes are also required to support repair mechanisms of the tissue.

The current model of leukocyte recruitment is described by a well-defined series of steps termed the leukocyte-adhesion cascade. The interactions, occurring between blood-borne leukocytes and endothelial cells (ECs), are characterized by capture and rolling of leukocytes at the endothelium and firm adhesion to ECs. Next, leukocytes start to crawl on the luminal site and transmigrate through the vessel wall. Upon their arrival at the abluminal site of the vessel, leukocytes exhibit movements along pericyte processes, then breach the pericyte layer, and finally detach from the vessel wall to migrate towards an inflammatory focus [96].

These serial steps are initiated by the release of pathogen-associated molecular patterns (PAMPs) from invading microorganisms or damage-associated molecular patterns (DAMPs) released from damaged or dead cells. The perception of PAMPs or DAMPs is mediated by a heterogeneous group of pattern recognition receptors, such as TLRs, NLRs, or C-type lectin receptors (CLRs). These receptors can be expressed intracellularly or on the surface of tissue-resident sentinel cells, such as macrophages, mast cells, or DCs. These cells respond to the danger signals by releasing chemokines (e.g., CXCL-1, CXCL-8), cytokines (e.g., IL-1, IL-6, TNF), or chemoattractants (e.g., $LTB_{4,}$ PAF). Proinflammatory mediators, such as IL-1 and TNF, activate ECs to express adhesion molecules (selectins, integrins, VCAM-1, and ICAM-1) which facilitate the different steps of leukocyte transmigration. Subsequently,

the gradients of soluble or surface-bound chemotactic factors (e.g., CXCL-1) guide leukocytes to the injury, where they remove dead cells and promote tissue repair (Fig. 3). Hence, leukocytes strongly contribute to tissue homeostasis. Since leukocyte migration is fundamental for adequate immune response, deficiencies in this process can have drastic consequences. An insufficient leukocyte response leads to recurrent bacterial and fungal infections, whereas exaggerated numbers of leukocytes contribute to a multitude of prominent diseases such as rheumatoid arthritis, Crohn`s disease, multiple sclerosis, or cancer [97]. Gaining control of leukocyte migration is the challenge that novel therapeutic approaches for inflammatory diseases need to face.

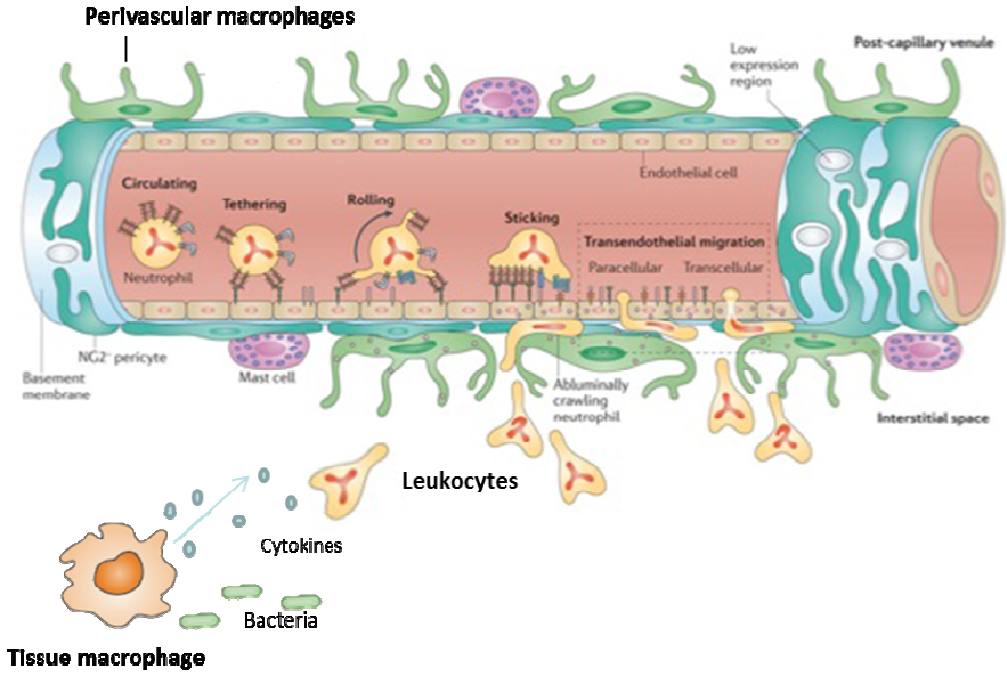

Fig. 3 *Leukocyte recruitment into inflamed tissue***.** Invading pathogens induce an inflammatory response in tissue-resident immune cells. The activation of these immune cells leads to the generation and release of chemoattractants that attract leukocytes from the blood stream. Leukocytes follow a multistep adhesion cascade, starting with rolling on the endothelium, adherence, and finally transmigration into the interstitial space. During this series of steps they follow the chemotactic gradient to the site of infection, where they phagocytose pathogens and cellular debris. Figure adapted and modified from Weninger et al. 2014. Reprinted by permission from Macmillan Publishers Ltd: Nature Reviews Immunology [81] copyright 2014.

2.7 Ischemia-reperfusion injury

Ischemic heart disease is the leading cause of death in developed countries [98]. After an initial restriction of blood supply, classically induced by an embolus, the imbalanced metabolic tissue supply causes tissue hypoxia. The subsequent restoration of reperfusion and reoxygenation is responsible for exacerbated tissue injury and inflammation [99]. The mortality of ischemic heart diseases is often related to microvascular dysfunction, enhanced vascular permeability, and the recruitment of leukocytes from postcapillary venules [100]. The detrimental effects of I/R injury result from the induction of cell death programs such as apoptosis and necrosis. Although I/R injury induces a sterile environment, innate immunological mechanisms, such as complement activation and adaptive mechanisms, are contributing to severe tissue damage [101].

Leukocytes are key modulators of I/R injury since they are the source of proinflammatory cytokines, reactive oxygen species, and proteases, which are able to enhance the postischemic tissue damage [102]. On the other hand, leukocytes support the regeneration and the healing of postischemic tissue, e.g., by maintaining tissue homeostasis by phagocytosis of apoptotic cells [103, 104]. Tissue macrophages are contributing to a proinflammatory milieu through the release of soluble proinflammatory mediators, e.g., TNF. These mediators stimulate ECs to upregulate adhesion molecules that facilitate rolling, capture, and transmigration of leukocytes. Leukocyte-endothelial cell adhesion and platelet-leukocyte aggregation aggravate microvascular dysfunction [105].

The activation of macrophages and other immune cells in an inflamed environment is partly mediated through pattern-recognition receptors such as TLRs. Although the I/R injury occurs in a sterile environment, the consequence of I/R is phenotypically

similar to the immune response towards invading pathogens. Recent studies have implicated TLR signaling in various ischemic diseases, e.g., inhibition of TLR 4 signaling protected the myocardium from I/R injury [106] and preconditioning with TLR 2, TLR 3, TLR 4, TLR 7 and TLR 9 ligands induced ischemic tolerance and reduced cerebral ischemic damage [107-111].

2.8 Toll-like receptor 9

So far, 10 functional TLRs have been identified in the mouse and are largely divided into two subgroups depending on their cellular localization and respective PAMP ligands. One group is expressed on the cell surface and the other group, composed of TLR 3, TLR 7, TLR 8, and TLR 9, are expressed in intracellular vesicles such as the endoplasmic reticulum (ER), endosomes, lysosomes, and endolysosomes, where they recognize microbial nucleic acids [112].

The ligands of the endosomal TLR 9, unmethylated CpG-DNA from bacteria and DNA-containing immune complexes from necrotic cells [113, 114], activate the myeloid differentiation primary response gene 88 (MyD88)-dependent NF-κB signaling (Fig. 4) as well as PI3K/Akt signaling which improves cell survival [115]. Unmethylated CpG ODNs have immunogenic properties and therefore hold great promise for therapeutic applications in a wide range of TLR 9-dependent pathologies, such as tumor-mediated immunosuppression, allergies, or asthma [111, 112].

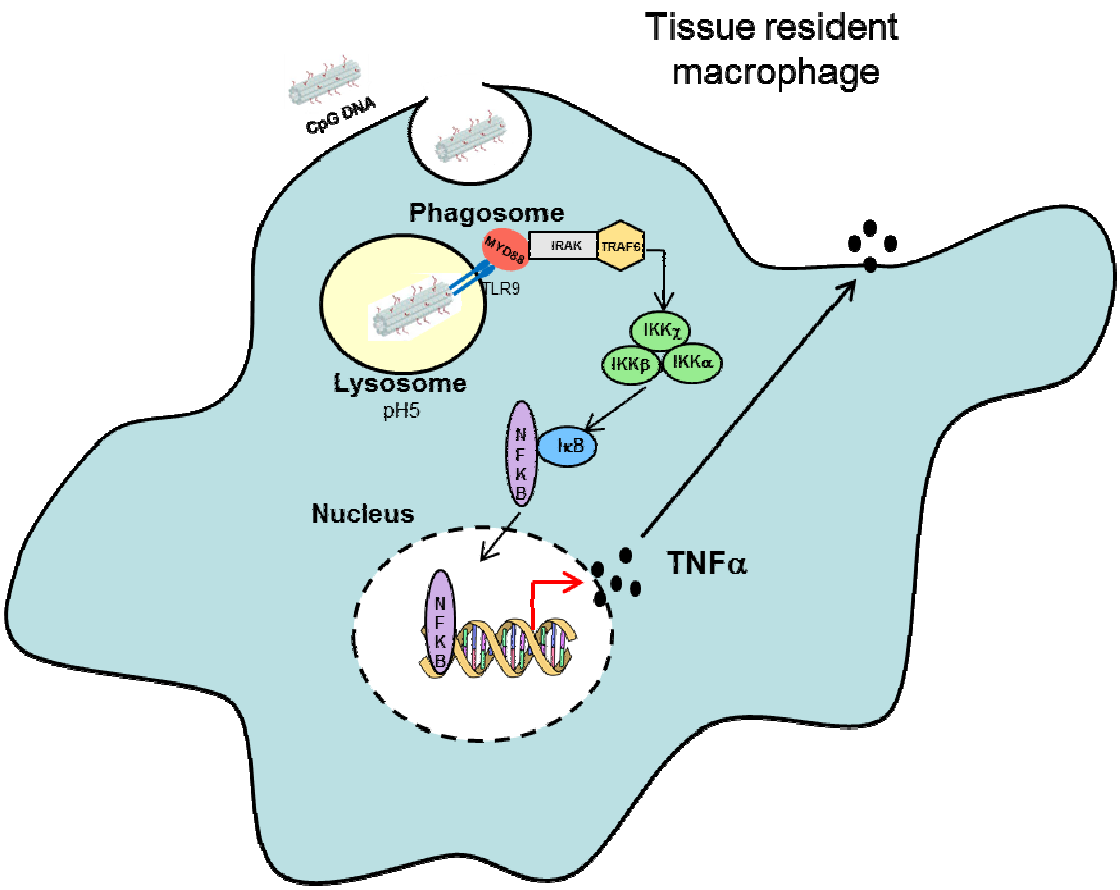

Fig. 4 *TLR 9 signaling in tissue-resident macrophages after CpG DNA internalization***.** Tissue-resident macrophages phagocytose CpG DNA from the extracellular space and transfer it in acidic endolysosomal compartments. The lysosome contains TLR 9, which recognizes CpG DNA and as a result, induces an intracytoplasmatic signaling cascade. The TLR 9 signal activates MYD88 followed by the activation of the IRAK-TRAF6 complex. The IKK complex, made of IKKα, IKKβ, and IKKχ, is a central regulator of NF-κB. Phosphorylation of the IKK complex by TRAF6 results in the degradation of IκB and the translocation of NF-κB from the cytoplasm into the nucleus, where it facilitates the expression of inflammatory cytokines such as TNF.

Asthma or allergic reactions are dominated by a T_H2-weighted imbalance, which promotes IgE production and eosinophilic response. The redirection of this T_H2 response in favor of a T_H1 response is achieved by the application of CpG DNA. Otherwise, CpG DNA can even act beneficial in a sterile inflammation, for example during cerebral ischemia [116]. It has been shown, that preconditioning with CpG DNA increased TNF levels in the serum, which reduced the ischemic damage after stroke [110].

2.9 Aim of the study

As explained above, DNA-based nanostructures are gaining importance in biological and biomedical research since they can be modified with a plethora of (bio)chemical moieties with nanoscale precision and full control over stoichiometry. Particularly, the nanoscale programmability and ease of fabrication of DNA-based nanostructures have sparked interest. However, the *in vivo* behavior of such constructs at the microscopic tissue/cell level as well as their inflammatory potential are largely unknown.

The aim of this work was to investigate the potential of DNA nanoconstructs as innovative platform for the efficient and biocompatible delivery of drugs *in vivo* to macrophages, which are key players in homeostasis, immune defense, and disease.

For this purpose, immunostimulatory CpG ODNs or immunosuppressive dexamethasone were conjugated to DNA nanotubes. In *in vitro* experiments, the uptake efficiency and the impact on cellular cytokine production in macrophage cell lines were studied. In further *in vivo* experiments, the local distribution, the bioactivity, and the effects of these DNA constructs on leukocyte recruitment were investigated under physiological and pathological conditions (I/R) in the murine cremaster muscle.

3 Material and Methods

3.1 Material

All used consumables are listed in the Appendix.

3.2 Methods

3.2.1 Design and assembly of DNA nanotubes

DNA nanotube design, assembly, and characterization were mainly done by Samet Kocabey and Tim Liedl (Department of Physics, LMU) in close cooperation and with conceptual input from the author of this thesis. For the sake of completeness and to deepen the understanding of DNA nanotubes the design, assembly and characterization of DNA nanotubes are included in this thesis.

3.2.1.1 Design of 8-helix DNA nanotubes

DNA nanotubes were designed using the single-stranded tile (SST) method, where each tile oligonucleotide is 42 bases long and consists of four domains with 10 or 11 bases. Each domain is complementary to one domain on the neighboring tile [34, 117]. We designed 8-helix tubes consisting of 48 individual tile ODNs folding into 8 parallel double helices. Tile strands located at the ends of the tube contain non-pairing poly-A sequences in order to prevent sticky end formation and polymerization. For CpG labeling, the 3´ ends of 24 tiles (every second tile in each helix) were extended by 20 bases containing the immune stimulatory CpG motif, GACGTT, twice (CpG 1826: TCCATGACGTTCCTGACGTT). For control tubes, that do not carry the CpG motif, tiles without CpG extension were used. All ODNs were purchased from Eurofins Operon MWG (Ebersberg, Germany) with HPSF purification.

3.2.1.2 Design of 6-helix DNA nanotubes

DNA nanotubes were designed using SST, where each SST ODN has 21 base long domains complementary to the adjacent domains on the neighboring tiles. 15 individual SST were used to fold 6-helix nanotubes. The domains at the end of the nanotube contain non-pairing poly-A sequences to prevent polymerization. To generate a pH-responsive DNA nanoconstruct, 3 of the tiles were extended with an i-motif sequence (CCCTAACCCTAACCCTAACCC) facilitating the release of dexamethasone handles at acidic pH. For dexamethasone conjugation, 3 of the tile ODNs extended with the i-motif sequence or a random sequence were hybridized with dexamethasone-conjugated single-stranded ODNs. All unmodified ODNs (HPSF purified) and amine-modified ODNs (HPLC purified) were purchased from Eurofins Operon MWG (Ebersberg, Germany) (see the Supporting Information, Table S1 for the sequences).

3.2.1.3 Dexamethasone conjugation

Amine-modified single-stranded ODNs were conjugated with dexamethasone using the method developed by Acedo et al. [118]. In brief, dexamethasone (0.4 g, 1 mmol, Sigma) was reacted with succinic anhydride (0.15 g, 1.5 mmol) and DMAP (0.13 g, 1 mmol) in pyridine at room temperature for 20 h. The reaction mixture was concentrated by drying in vacuum evaporator, then re-dissolved in 150 ml of DCM/MeOH (4:1), and washed twice with 75 ml of 1 M sulfuric acid and water. The organic white solid formed after the reaction, dexamethasone succinic acid (0.25 g, 0.5 mmol), was reacted with N-hydroxysuccinimide (70 mg, 0.6 mmol) and DCC (125 mg, 0.6 mmol) in 5 ml of THF at room temperature for 20 h. After several filtration

and washing steps, the final residue was dissolved in 5 ml DMF (10 mM) and stored at 4 °C for months. For DNA coupling, 10 µl of 5´amine-labeled ODN (100 µM) and 10 µl of dexamethasone-NHS (10 mM) were mixed in Tris buffer (50 mM, pH 7.4) and incubated at room temperature overnight. On the next day, the solution was centrifuged at 13000 g for 5 min and supernatant was collected. The solution was evaporated to remove DMF in a vacuum centrifuge and redissolved in water. The centrifugation and evaporation steps were repeated several times. Finally, dexamethasone-conjugated ODNs (Dex ODNs) were purified using 3 K Amicon Ultra 0.5 ml centrifuge filters for further use in dye labeling and assembly.

3.2.1.4 Enzymatic dye labeling of tiles

To visualize the DNA nanotubes *in vivo*, the 3´ ends of some of the tile strands were enzymatically labeled with Atto488-dUTP or Atto546-dUTP [119]. For Dex nanotubes 6 of the tiles at the middle part of the structure and Dex ODNs were enzymatically labeled with Atto488-dUTP and Atto647N-dUTP respectively. Further, Atto-dUTPs (80 µM, purchased from Jena Bioscience, Jena, Germany), $CoCl_2$ (5 mM), terminal transferase enzyme (16 U/µl, Roche, Penzberg, Germany), and all DNA tiles (400 pmol) were mixed in 20 µl 1x TdT reaction buffer. The solution was incubated at 37 °C for 60 min. Then, 2.5 µl of NaOAc (3 M) was added and the solution was filled up to 80 µl with ice-cooled ethanol (99 %). After 1 h of incubation at -20 °C, samples were centrifuged at 13000 g for 30 min. Then, samples were washed with 70 % ethanol for 10 min again and the supernatant was discarded. The remaining pellet was re-dissolved in distilled water. For CpG-labeled tubes, 24 of the unmodified tiles and for the control tubes, 40 of the core tiles were used for dye labeling. For CpG ODNs, 24 of the tiles with CpG sequence were labeled with dye.

3.2.1.5 DNA nanotube assembly and purification

For the annealing of DNA nanotubes, 800 nM (8-helix tubes) or 1µM (6-helix tubes) of each tile (dye-modified and unmodified) were mixed with folding buffer (10 mM Tris-HCl, 1 mM EDTA, pH 8.0, 20 mM $MgCl_2$). The DNA nanotubes were folded over the course of 16 h (5 min at 80 °C, cooling down to 65 °C at 1 °C/min, cooling down to 25 °C at 2.5 °C/h). The assembled 8-helix nanotubes (CpG nanoconstructs) were then purified using 30 K Amicon Ultra 0.5 ml centrifuge filters (30000 MWCO, Millipore, Schwalbach, Germany) in order to remove excess strands that were not folded into the structures. For 8-helix nanotube (Dex nanotubes) purification, 100 K Amicon Ultra 0.5 ml centrifuge filters (100000 MWCO, Millipore, Schwalbach, Germany) were used. 100 µl of assembled DNA tube solution was completed up to 500 µl with folding buffer, filled into the centrifuge filter, and centrifuged 3 times at 13000 g for 6 min. After every centrifugation step, the flow-through was removed and the filter was refilled up to 500 µl with buffer. After final centrifugation, the remaining solution at the bottom of the filter (~ 50 µl) was pipetted out and the concentration of tubes was determined by measuring the optical density at 260 nm. Overall, 50 – 60 % of the initial amount of DNA nanotubes was obtained after purification.

3.2.1.6 Gel electrophoresis and transmission electron microscopy

To analyze DNA nanotubes, the samples were run in an agarose gel. 2 % agarose was dissolved in 0.5 x TBE buffer by heating to boiling. After cooling, $MgCl_2$ was added to 11 mM final concentration and the solution was poured into a gel cask for solidification. 10 µl of each filter-purified DNA tube sample were mixed with 2 µl of 6x loading dye before loading into the gel pockets. 6 µl of 1 kb ladder was also loaded

adjacent to the samples. The gel was run for 2 h at 70 V in an ice-cooled water bath to prevent heat-induced denaturation of DNA nanotubes. After running, the gel was stained with ethidium bromide (0.5 µg/ml) for 30 min.

DNA nanotubes were visualized by electron microscopy using a JEM-1011 (JEOL, Freising, Germany) transmission electron microscope (TEM). The DNA nanotubes were incubated on plasma-exposed (240 kV for 1 min) carbon-coated grids and then negatively stained with 1 % uranyl acetate for 15s.

3.2.1.7 Stability of DNA nanotubes

Stability of DNA nanotubes and pUC 18 double stranded-plasmid were tested in DNAse I-containing buffer, mice serum and fetal calf serum (FCS) separately. For DNAse I experiments 50 ng/µl of each sample was incubated in buffer at 37 °C for different time periods. To emulate *in vivo* conditions, the DNAse I concentration was adjusted to 1.97 U x 10^{-4} U/g wet weight [46]. For further experiments, mice serum was diluted 37 times to mimic conditions prevalent in the skeletal muscle [46]. The DNA nanotubes were also incubated in pure FCS (not heat-inactivated) for up to 2 h. Zeta potential and size measurements were performed with a Zetasizer Nano (Malvern Instruments, Malvern, UK) at 100 nM nanotube concentration.

3.2.1.8 Gel electrophoresis to test the functionality of pH-responsive Dex tubes

To test the i-motif-dependent release of single-stranded Dex ODNs, 100 µl of DNA nanotubes were filled up with 50 mM MES buffer (pH 5.5) to 500 µl and incubated at 37 °C for 30 min. Then, the samples were centrifuged 3 times at 13000 g for 6 min

using 100 K Amicon filters. The samples were analyzed by running a 2 % agarose gel (0.5 x TBE, 11 mM $MgCl_2$) as described in 3.2.1.6.

3.2.2 Cell culture

3.2.2.1 RAW 264.7 cells

Murine RAW 264.7 macrophage-like cells were purchased from American Type Culture Collection (Rockville, USA) and grown in Dulbecco´s modified eagle medium (DMEM) supplemented with 10 % FCS, 4 mM L-Glutamin and 1 g/L D-Glucose at 37 °C and 5 % CO_2. For passaging, medium was removed, cells were washed twice with phosphate-buffered saline (PBS) and 3 mL of pre-warmed Trypsin-EDTA (0.5 %) was added and incubated for 15 min at 37 °C. Digestion was stopped by adding 7 mL pre-warmed DMEM. After resuspension in culture medium, RAW 264.7 cells were collected in falcon tubes and centrifuged (1100 rpm, 5 min, room temperature). Cells were resuspended and transferred to a new flask or seeded for experiments. RAW 264.7 cells were split every 2 to 3 days.

3.2.2.2 Stimulation of RAW 264.7 cells

Cells were seeded on 24-well culture plates at a density of 4 x 10^5 cells and cultivated for 24 h. For stimulation, RAW 264.7 cells were incubated with DNA nanotube constructs or CpG ODNs for up to 12 h. Culture supernatants were collected and stored at -80 °C for further analysis. Cells were washed and resuspended in DMEM, and uptake of DNA constructs and ODNs was visualized using a confocal laser-scanning microscope (Leica SP5, Leica Microsystems, Wetzlar, Germany) equipped with a GaAsP hybrid detection system (Leica HyD).

3.2.2.3 MH-S cells

MH-S, a murine alveolar macrophage cell line was purchased from American Type Culture Collection (Rockville, USA). Cells were grown in complete RPMI-1640 medium supplemented with 10 % FCS and 0.05 mM 2-mercaptoethanol at 37 °C and 5 % CO_2. For passaging, medium was removed, cells were washed twice with PBS, and 3 mL of pre-warmed Trypsin-EDTA (0.5 %) was added and incubated for 5 min at 37 °C. Digestion was stopped by adding 7 mL pre-warmed RPMI-1640. After resuspension in culture medium, MH-S cells were collected in falcon tubes and centrifuged (1100 rpm, 5 min, room temperature). Cells were resuspended and transferred to a new flask or seeded for experiments. MH-S cells were split every 3 to 4 days.

3.2.2.4 Flow cytometry

Upon incubation with DNA nanoconstructs, cells were washed with culture medium and transferred with 250 µl PBS into BD Falcon round bottom tubes. The fluorescence intensity of incorporated Cy3-coupled DNA constructs was determined by a Gallios flow cytometer (Beckman Coulter Inc, Brea, USA) in order to quantify the uptake of DNA nanoconstructs. Post-acquisition analysis was performed using FlowJo software (Tree Star, Ashland, US).

3.2.2.5 Enzyme-linked immunosorbent assay (ELISA)

Cell culture supernatants were collected after treatment with different DNA nanoconstructs and stored at -80 °C until analysis. The concentration of TNF in

culture supernatants was determined by enzyme-linked immunosorbent assay (ELISA) according to the manufacturer´s instructions (R&D Systems, Wiesbaden, Germany). Concentrations were calculated with a standard curve.

3.2.2.6 Water-soluble tetrazolium salt (WST) cell viability assay

MH-S cells were seeded into 96-well plates at a density of 1 x 10^5 cells per well. After adding 50 nM of Dex DNA constructs, LPS (10 ng/ml), Ethanol (70 % for 2 min) and dexamethasone (40 ng/ml and 1µg/ml) the supernatant was discarded at different timepoints (1 h, 3 h, 6 h, and 12 h) and 10 % Roche WST reagent was added to the plate. After 15 min of incubation at 37 °C and 5 % CO_2 the absorbance at 490 nm was determined using an InfiniteF200 microplate reader (Tecan, Männedorf, Switzerland).

3.2.3 *In vivo* imaging

3.2.3.1 Animals

Male C57BL/6 mice at the age of 10-12 weeks were purchased from Charles River (Sulzfeld, Germany) and MacGreen mice (JAX, Stock Number: 018549) were obtained from The Jackson Laboratory (Bar Harbor, USA). Male, heterozygous CX_3CR1-EGFP mice were generated as previously described and backcrossed to the C57BL/6 background for six to ten generations [120]. All experiments were performed using mice at the age of 10-12 weeks. Animals were housed under conventional conditions with free access to food and water. All experiments were performed

according to German legislation for the protection of animals and approved by the Regierung von Oberbayern, München, Germany.

3.2.3.2 Surgical procedure

The surgical preparation was performed as described by Baez with minor modifications [121]. Briefly, mice were anesthetized by i.p. injection of a ketamine/xylazine mixture (100 mg/kg ketamine and 10 mg/kg xylazine). The left femoral artery was cannulated in a retrograde manner for administration of 2 µm FluoSpheres (Invitrogen, Carlsbad, CA, USA) for measurement of blood flow velocities. The right cremaster muscle was exposed through a ventral incision of the scrotum. The muscle was opened ventrally in a relatively avascular zone, using careful electrocautery to stop any bleeding, and spread over the pedestal of a custom-made microscopy stage. Epididymis and testicle were detached from the cremaster muscle and placed into the abdominal cavity. Throughout the procedure, as well as after surgical preparation during *in vivo* microscopy, the muscle was superfused with warm buffered saline. The body temperature was maintained at 37 °C using a heating pad placed under the mouse. After *in vivo* microscopy, tissue samples of the cremaster muscle were prepared for immunohistochemistry. Blood samples were collected by cardiac puncture for the determination of systemic leukocyte counts using a Coulter ACT Counter (Coulter Corp., Miami, USA). Anaesthetized animals were then euthanized by an intra-arterial pentobarbital overdose (Narcoren, Merial, Hallbergmoos, Germany).

3.2.3.3 Mouse model of I/R

For the analysis of postischemic cellular responses to DNA constructs, a postcapillary venule segment of the cremaster muscle was randomly chosen. After having obtained baseline recordings of leukocyte firm adhesion and transmigration in the segment, ischemia was induced by clamping all supplying vessels at the base of the cremaster muscle using a vascular clamp (Martin, Tuttlingen, Germany). After 30 min of ischemia, the vascular clamp was removed, reperfusion was restored, and firm adhesion and transmigration of leukocytes were recorded again. Immediately after removing the vascular clamp, DNA nanoconstructs were microinjected next to the vessel and measurements were repeated at 30 min, 60 min, and 90 min after injection. Blood flow velocity was determined as described above previously [122]. After *in vivo* microscopy, tissue samples of the cremaster muscle were prepared for immunohistochemistry.

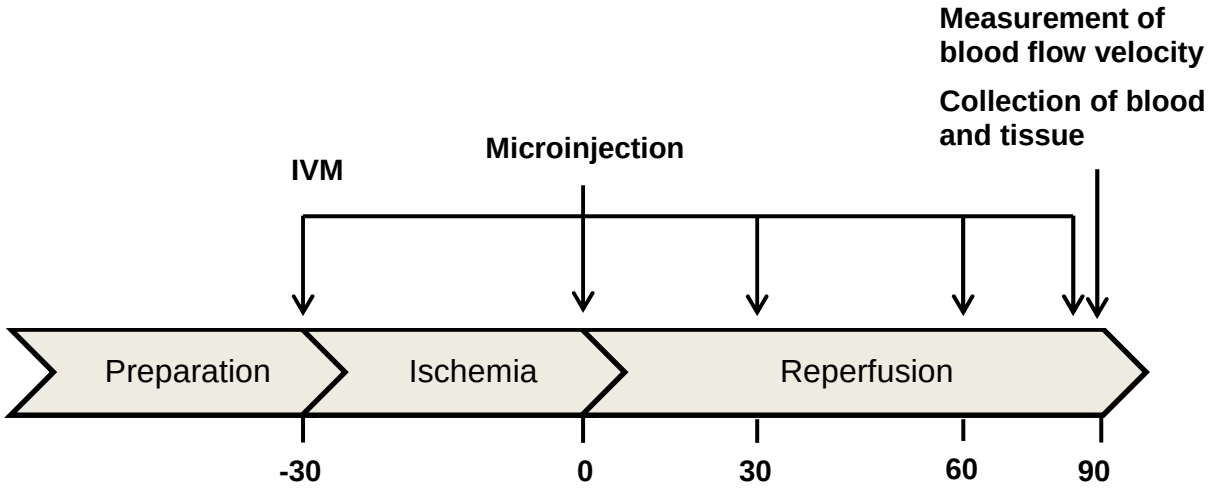

Fig. 5 *Experimental protocol for the analysis of leukocyte recruitment after ischemia and reperfusion*

3.2.3.4 *In vivo* microscopy

The setup for *in vivo* microscopy was centered around a VisiScope.A1 imaging system, equipped with an LED light source for fluorescence epi-illumination. For DNA nanotubes or ODN excitation the 470 nm or 550 nm LED modules (exposure time 700 ms), and for transillumination the 655 nm LED module (exposure time 10 ms) were used in a fast simultaneous mode. Light was directed onto the specimen via a triple dichroic filter NC316973 (z 405/488/561 rpc; Chroma Technology Corp., Bellows Falls, USA). Microscopic images were obtained with a water dipping objective (20 x, NA 1.0). Light from the specimen was separated with a beam splitter (T 580 lpxxr Chroma Technology Corp., Bellows Falls, USA) and acquired with two Rolera EM^2 cameras and VisiView Imaging software (Visitron Systems GmbH, Puchheim, Germany). Oblique transillumination was obtained by positioning a mirroring surface (reflector) directly below the specimen and tilting its angle relative to the horizontal plane as described previously [123].

3.2.3.5 Microinjection of DNA nanotubes and LysoTracker dye

Local administration of 250 +/- 100 pl of fluorescently labeled DNA nanotubes (500 nM), CpG DNA nanotubes (500 nM), CpG ODNs (12 µM), or saline into the cremaster muscle was performed via perivenular microinjection in regions at a distance of 25 to 75 µm from a postcapillary venule. Dex nanotubes (1.5 µM), Dex nanotubes w/o imotif (1.5 µM), DNA tubes (1.5 µM), and Dex ODNs (4.5 µM) were immediately microinjected after removing the vascular clamp during I/R as previously described. Venules with diameters ranging between 25 and 35 µm were selected for the experiments. Microinjection was performed under visual control of the intravital

microscope, with a long distance air objective (20 x, NA 0.4 Olympus), using borosilicate glass micropipettes - pulled with a micropipette puller - which were connected to the injection system consisting of a micromanipulator and a microinjector. The tip pressure during injection was 3000 hPa and the tip diameter < 1 µm. The vessel and the surrounding tissue were visualized during a time period of 1 min at baseline conditions before injection and up to 90 min after injection. For LysoTracker Red DND-99 co-microinjection, the stock solution was diluted to a concentration of 750 nM in saline and further diluted to an end concentration of 75 nM in the respective CpG DNA nanotube sample. For LysoTracker Red DND-99 and LysoTracker Green DND 26 co-microinjection, the stock solution was diluted to a concentration of 750 nM in saline and further diluted to an end concentration of 75 nM in the respective Dex nanotubes sample. Different fluorescent labels (as described above) did not affect the distribution and localization of DNA nanoconstructs.

3.2.3.6 Quantification of leukocyte kinetics and microhemodynamic parameters

To quantify the sequential steps of leukocyte extravasation, *in vivo* microscopy records were analyzed offline using ImageJ software (National Institutes of Health, Bethesda, USA). Firmly adherent cells were determined as those resting in the associated blood flow for more than 30 sec and related to the luminal surface per 100 µm vessel length. Transmigrated cells were counted in regions of interest, covering 75 µm on both sides of a vessel over 100 µm vessel length, and are presented per 10^4 μm^2. Green fluorescent beads (FluoSpheres 2 µm, Invitrogen, Carlsbad, USA) were injected via the femoral artery catheter and their passage through the vessels of

interest was recorded (filter T580lpxxr, LED 470 nm, exposure 50 ms, cycle time 1 min). Centerline blood flow velocity was determined by measuring the progression of free flowing fluorescent beads in subsequent images in the blood stream.

3.2.3.7 Immunostaining

After dissection of the cremaster muscle, the tissue was fixed with 2 % paraformaldehyde for 15 min at room temperature, then blocked and permeabilized in PBS, supplemented with 2 % bovine serum albumin (BSA) and 0.5 % Triton X-100 for 1 h at room temperature. This blocking solution was used to dilute primary antibodies at 1:100 and the tissue was incubated at 4°C over night with the antibody solution. Before incubation with secondary antibodies (1:400 in blocking solution) and TO-PRO3®-Iodide (1:1000 in blocking solution) for 2 h at room temperature, the tissue was washed twice with PBS for 5 min. After washing, immunostained cremaster muscles were mounted in PermaFlour™ Aqueous Mounting Medium on glass slides. For localization of microinjected DNA constructs in Csfr1-EGFP mice as well as colocalization with LysoTracker dye, the dissected cremaster muscle was mounted in a custom-made imaging chamber and was immediately viewed. Images were obtained using a Leica SP5 confocal laser-scanning microscope - equipped with a Leica HyD GaAsP hybrid detection system - with an oil-immersion lens, as previously described [124]. Images were processed with ImageJ software and figures were assembled in Photoshop 9 (Adobe Systems, Mountain View, USA).

3.2.3.8 CpG DNA nanotubes *in vivo*

Experimental groups

In a first set of experiments, mice (n=6 each group) received saline, DNA nanotubes, CpG DNA nanotubes, or CpG ODNs 20 min after the preparation of the cremaster muscle via microinjection. Additional experiments were performed in mice (n=6) receiving cromolyn (0.2 mg/kg), an inhibitor of mast cell degranulation, as a bolus via intra-arterial injection 30 minutes before cremaster preparation and subsequent application of CpG DNA nanotubes. The animals were randomly assigned to the experimental groups.

3.2.3.9 CpG DNA nanotubes *in vivo* during I/R injury

Experimental groups

Mice (n=6 each group) received saline, DNA nanotubes, CpG DNA nanotubes, or CpG ODNs via microinjection into the postischemic cremaster muscle tissue. The animals were randomly assigned to the experimental groups.

3.2.3.10 Dex nanotubes *in vivo* during I/R injury

Experimental groups

Mice (n=6 each group) received saline, DNA nanotubes, Dex nanotubes, Dex nanotubes w/o i-motif, Dex ODNs, or dexamethasone (1 µg/ml) via microinjection into the postischemic cremaster muscle tissue. The animals were randomly assigned to the experimental groups.

3.2.4 Statistical analysis

GraphPad Prism 6 (GraphPad Software Inc., La Jolla, USA) was used for statistical analysis. Groups were compared with one-way ANOVA followed by a multiple comparison test (Tukey´s test). In all cases, p values of $p<0.05$ were considered to be significant.

4 Results

4.1 DNA nanotubes as intracellular delivery vehicles *in vivo*

4.1.1 Design, assembly, and characterization of DNA nanotubes

DNA nanotube design, assembly, and characterization were mainly done by Samet Kocabey and Tim Liedl (Department of Physics, LMU Munich) in close cooperation and with considerable conceptual input from the author of this thesis. The fundamental structure of DNA nanotubes consists of 48 different ODNs, each of which is 42 base pairs long. These ODNs self-assemble into a tube-like architecture comprised of eight parallel double helices and a designed length of ~40 nm and a diameter of ~8 nm (Fig. 6) [34, 117]. The assembly takes place during a temperature-controlled annealing process. For assembly of CpG nanotubes, 20-nt long CpG sequences (CpG 1826) with two highly immunostimulative GACGTT motifs were conjugated to DNA nanotubes.

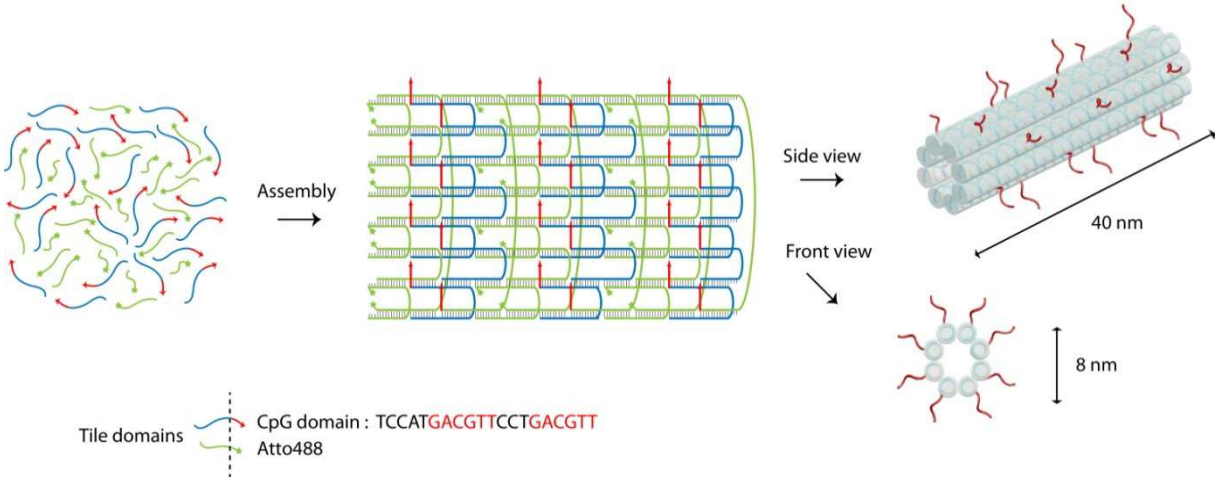

Fig. 6 *Schematic illustration of CpG-decorated DNA nanotubes.* Left: Mixture of 48 different DNA tiles, containing CpG domains (red arrows) or Atto488 dye (green star). Middle: Tiles assembled to a secondary tube structure. Blue and green tile domains contain random sequences and vertical lines indicate the base pairing. Right: 3D side and front views of 8-helix DNA nanotubes. Red extensions on the tube surface represent CpG domains and transparent cylinders indicate double helices. Taken from Sellner et al. [125].

For the presentation of the CpG 1826 sequences on the surface of the DNA nanotubes, 24 of the 48 tile strands were extended on their 3' ends with the CpG 1826 sequence (Fig. 6). CpG 1826 belong to B-type CpG sequences and induce an immune response via the recognition of the murine TLR 9 located in endosomal cellular compartments [32, 126].

Unfolded CpG 1826 (CpG ODNs) and DNA nanotubes without CpG motifs (plain tubes) served as control samples in all performed experiments. The correct assembly of CpG tubes and plain tubes was analyzed by gel electrophoresis and TEM. The prominent bands for CpG tubes and plain tubes (Lane 2+3 in Fig. 7A) and the decreased mobility of CpG DNA tubes (Lane 2) compared to plain tubes (Lane 3) indicate the correct assembly of the structures. TEM micrographs revealed the monodisperse composition of the DNA tube architectures, which are with the measured length of 41 +/- 1 nm and the measured diameter of 8 +/- 1 nm in agreement with the designed dimensions (Fig. 2B and 2C).

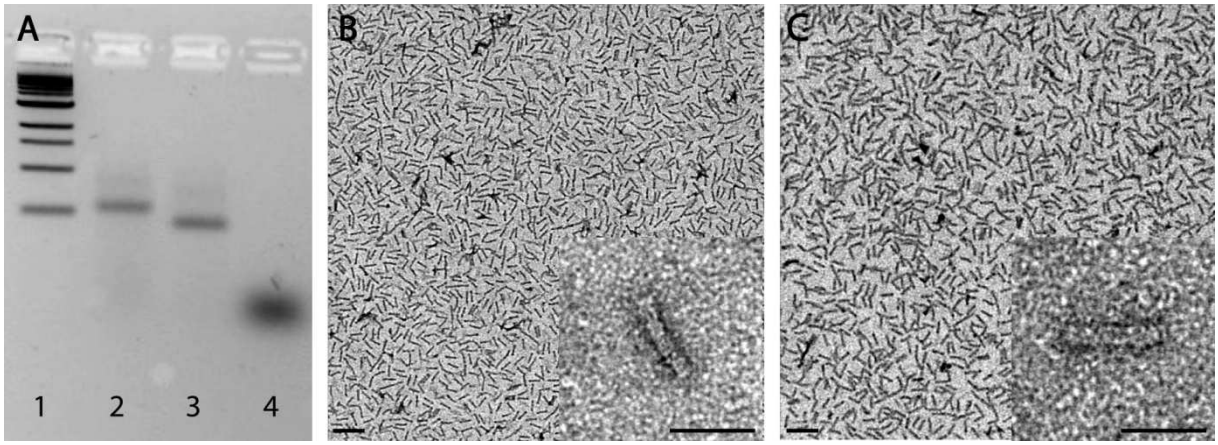

Fig. 7 *Structural characterization of DNA nanotubes.* (**A**) Structural analysis of assembled nanotubes by gel electrophoresis after purification. 1) 1 kb ladder, 2) CpG tube 3) plain tube and 4) CpG ODNs. Transmission electron micrographs of (**B**) CpG tubes and (**C**) plain tubes. Scale bars: 100 nm (left) and 40 nm (inset). Taken from Sellner et al. [125].

A prerequisite for the application *in vivo* is the stability of DNA nanoconstructs in a biological environment. Therefore, DNA tubes were treated with different concentrations of DNAse I and in different serum conditions for various incubation times to analyze the structure stability. Next to CpG ODNs and plain tubes, a double-stranded plasmid (pUC 18) was used as a control sample.

For 2 h DNA tubes withstand the degradation caused by DNAse I at a concentration which is equivalent to concentrations in murine organs such as pancreas, liver, or testis (0.5 U/ml) and is about 40 times higher than the one in skeletal muscle [46]. At the same concentration of DNAse I (0.5 U/ml) plasmid pUC18 degraded completely within 30 min (Fig. 8A). DNA tubes resisted the treatment with a high dose of DNAse I (10 U/ml) up to 15 min whereas plasmid pUC18 was cleaved by DNAse I instantaneously (Fig. 8B). Furthermore, DNA nanotubes revealed stable over an incubation period of 24 h in serum at a concentration prevalent in the muscle tissue (Fig. 8C). CpG DNA nanotubes showed only little degradation under the same conditions and time periods (Fig. 8C). However, treatment with pure serum leads to a complete degradation of all samples over the course of 2 h (Fig. 8D).

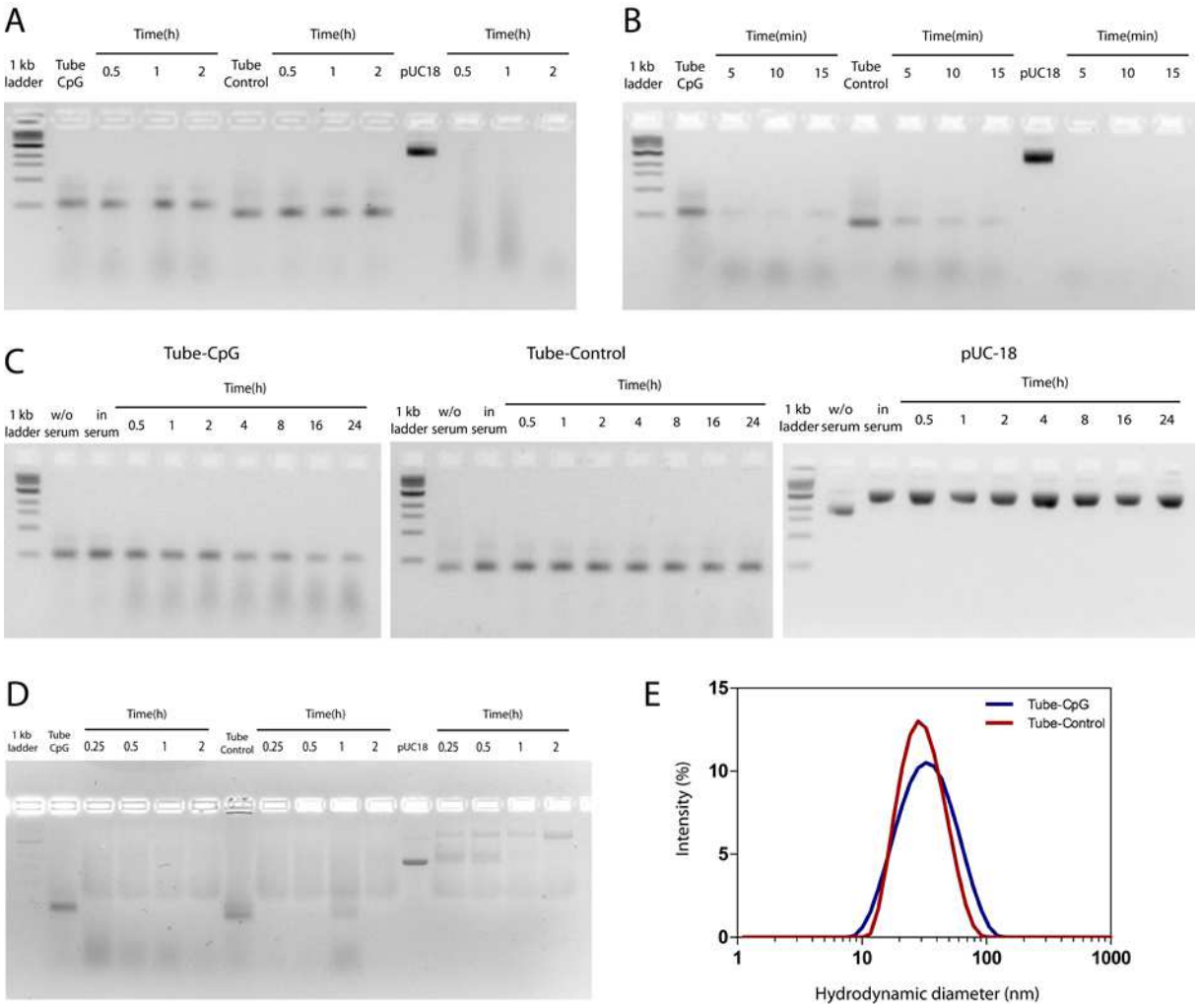

Fig. 8 *Stability of DNA nanotubes.* (A) Gel analysis of CpG tube, plain tube, and pUC 18 (left to right) incubated in the reaction buffer containing 5 x 10^{-1} U/ml DNAse I at 37 °C for 2 h. (B) Gel analysis of CpG tube, plain tube, and pUC 18 (left to right) incubated in reaction buffer containing high concentration of DNAse I (10 U/ml) at 37 °C for 15 min. (C) Gel analysis of CpG tube, plain tube and pUC 18 (left to right) incubated in 37x diluted mice serum. (D) Gel analysis of CpG tube, plain tube and pUC 18 (left to right) incubated in pure FCS (not heat-inactivated) for 2 h. E) DLS analysis of CpG tubes and plain tubes. Taken from Sellner et al. [125].

4.1.2 Release of inflammatory cytokines after stimulation with DNA nanotubes and ODNs *in vitro*

The purpose of designing CpG DNA tubes was to create efficient immunostimulatory constructs. A simple approach to test the response of immune cells to DNA nanoconstructs is to measure the cytokine release. Therefore, macrophage-like RAW 264.7 cells were incubated either with CpG DNA nanotubes (5 nM), plain DNA nanotubes (5 nM), CpG ODNs (120 nM), CpG ODNs (120 nM) mixed with plain tubes (5 nM) or LPS (10 ng/ml), which served as positive control. Subsequently, the release of TNF into culture supernatants was measured by ELISA. Within 1 h of incubation, all constructs could be observed in intracellular vesicles of RAW 264.7 cells (Fig. 9).

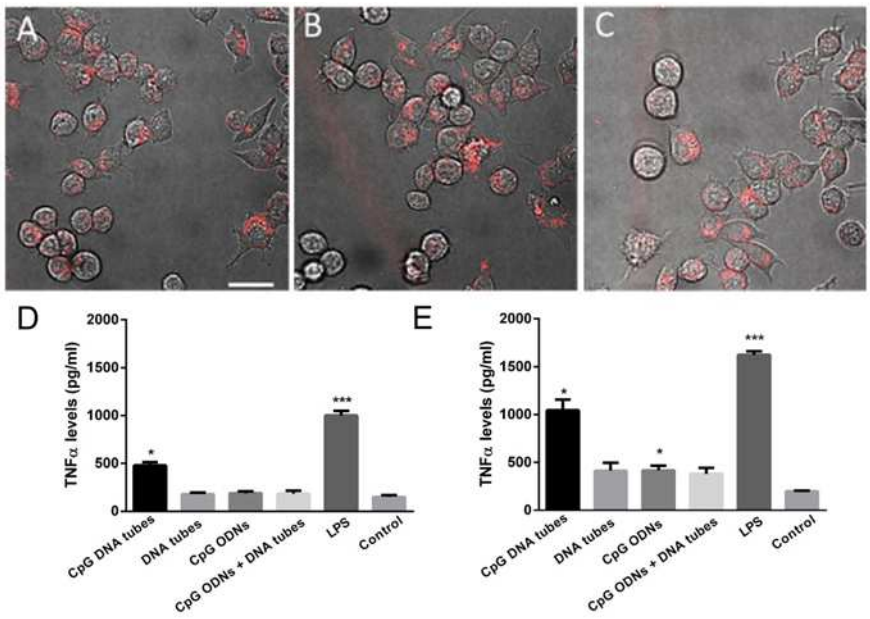

Fig. 9. *Uptake of DNA nanoconstructs and TNF response by RAW 264.7 cells.* RAW 264.7 cells were incubated with 5 nM of (**A**) plain tubes, (**B**) CpG tubes, and 120 nM of (**C**) CpG ODNs for 3 h at 37 °C. The different DNA nanotubes (red) were internalized by RAW 264.7 cells. (**D, E**) ELISA analysis of TNF levels in supernatants of $4x10^5$ RAW 264.7 cells incubated for (**D**) 1 h and (**E**) 3 h with 5 nM of CpG tubes, 5 nM of plain tubes, 120 nM of CpG ODNs, 120 nM of CpG ODNs + 5 nM of DNA tubes, and LPS (10 ng/ml), which served as positive control or without additive (control) (n=3, mean+/-SEM; *p<0.05, ***p<0.001 vs. control). Scale bar: 20 µm. Taken from Sellner et al. [125].

Flow cytometric measurements confirmed the uniform cellular uptake of fluorescently labeled CpG tubes, plain tubes, plain tubes + CpG ODNs, and CpG ODNs by RAW 264.7 cells (Fig. 10). Furthermore, the viability of RAW 264.7 cells, up to 18 hours of incubation with DNA nanoconstructs, was not affected (Fig. 11). Although there are no differences in cellular uptake and viability, the cellular production of TNF varied between the different groups. Incubation with CpG DNA tubes led within 1 h to a 3-fold and within 3 h to a 5-fold higher induction of TNF release compared to untreated cells (Fig. 9D, E). Treatment with plain tubes, CpG ODNs, and CpG ODNs + plain tubes induced only a slight increase of TNF after 3 h (Fig. 9E).

These results allow the conclusion that CpG DNA nanotube structures are immunogenic within 3 h of treatment. The complexation of CpG ODNs on the DNA tubes seems to be essential for the recognition of CpG sequences and the subsequent cellular TNF production.

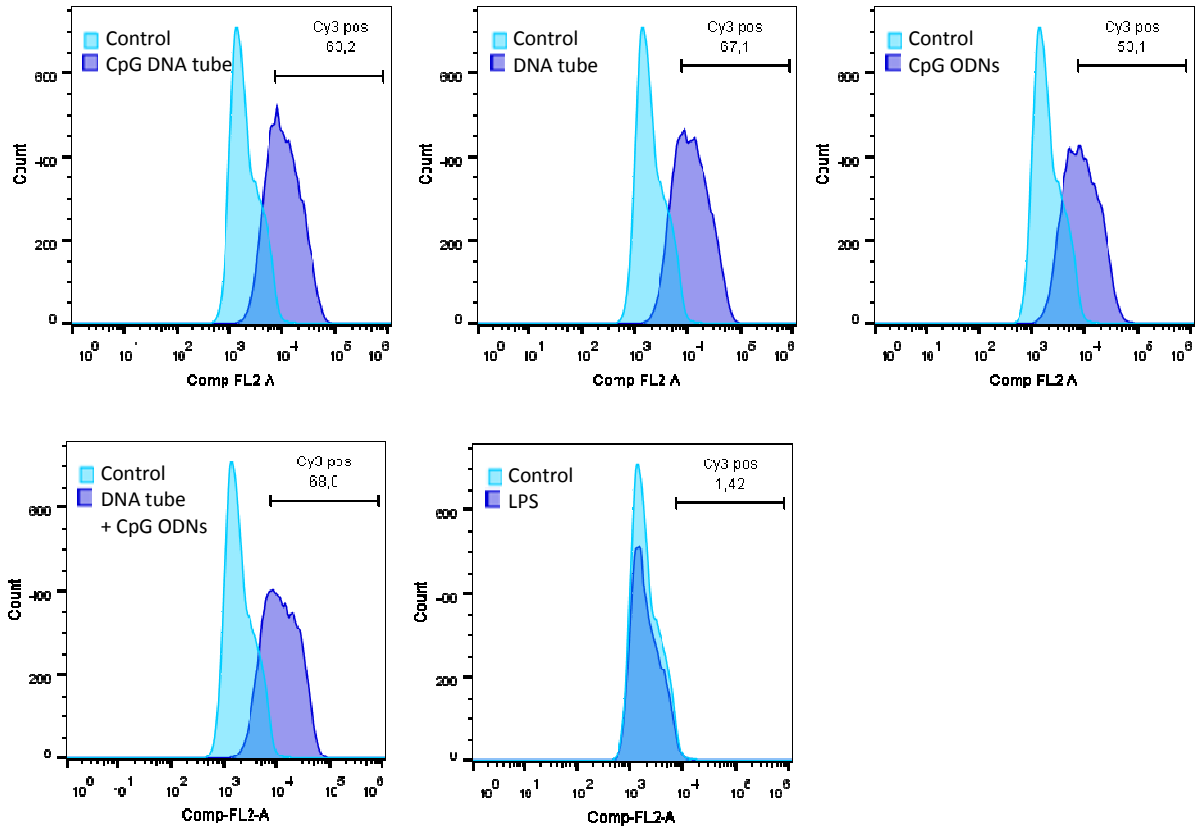

Fig. 10 *Uptake of DNA nanoconstructs by RAW 264.7 macrophages after 1 h of incubation.* Representative histograms show a fluorescence shift indicating the uptake of Cy3-coupled DNA nanoconstructs by RAW 264.7 macrophages. Cells were incubated with different DNA nanoconstructs (5 nM CpG DNA tubes, 5 nM DNA tubes, 120 nM CpG ODNs, 120 nM CpG ODNs + 5 nM DNA tubes), LPS (10 ng/ml) or without additive (control) for 1 h at 37°C. Taken from Sellner et al. [125].

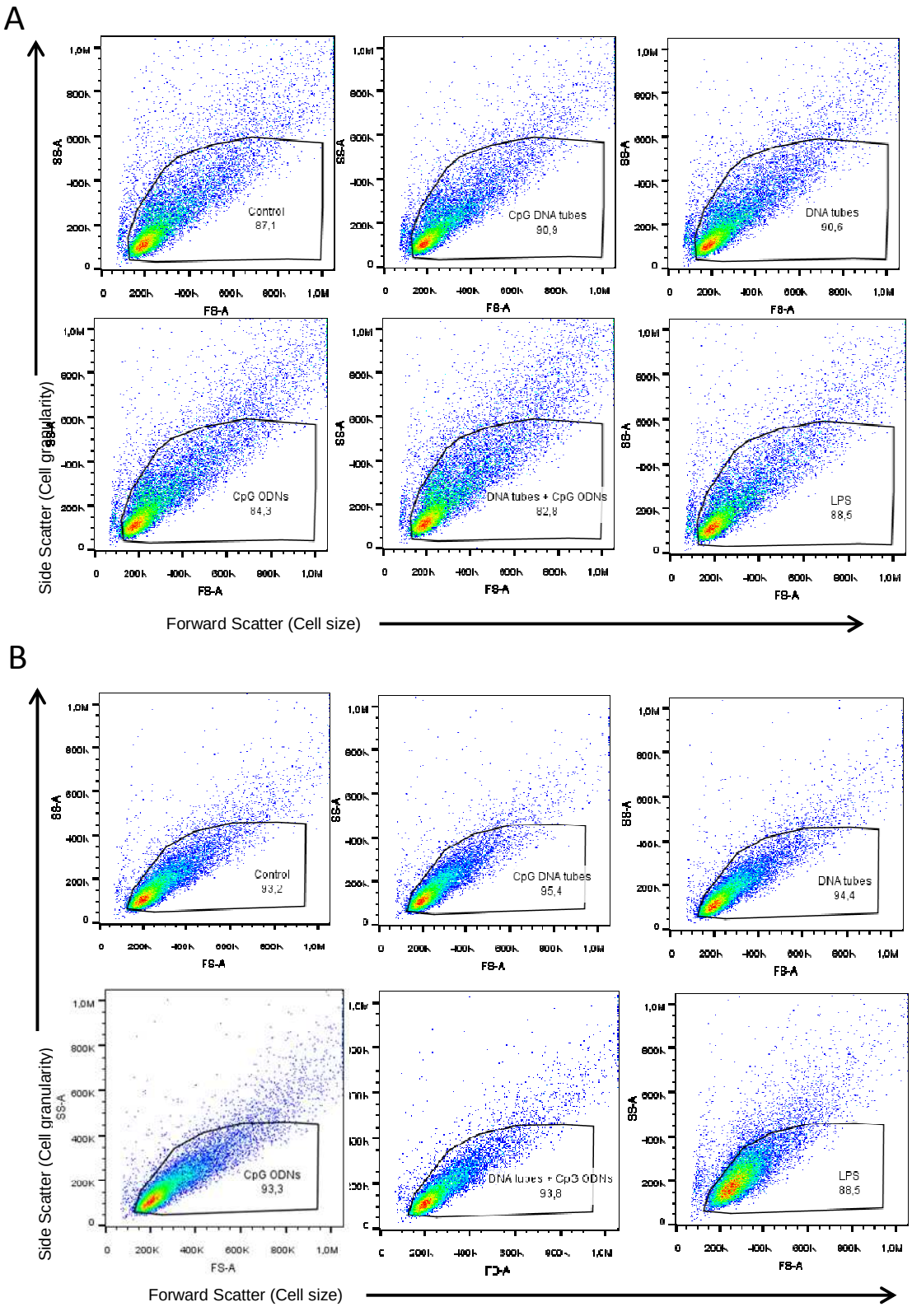

Fig.11 *Cell viability after incubation with DNA nanoconstructs.* FACS analysis of RAW 264.7 macrophage viability after incubation with different DNA nanoconstructs (5 nM CpG DNA tubes, 5 nM DNA tubes, 120 nM CpG ODNs, 120 nM CpG ODNs + 5 nM DNA tubes), LPS (10 ng/ml) or without additive for 1 h (**A**) and 18 h (**B**) at 37 °C. The numbers indicate the percentage of viable cells within the sample. Taken from Sellner et al. [125].

4.1.3 Localization of DNA nanotubes in skeletal muscle tissue after microinjection

Next, the behavior of DNA nanotubes in the skeletal muscle tissue was investigated. For this purpose, fluorescently labeled DNA nanoconstructs were microinjected into the murine cremaster muscle in 25 µm to 50 µm distance to a venule. *In vivo* fluorescence microscopy was performed to visualize the DNA constructs for 60 min.

Perivascular and tissue-resident cells in the vicinity of the injection site, internalized CpG DNA nanotubes within 5 min after microinjection (Fig. 12A and B). This uptake pattern was the same for all DNA nanoconstructs (Data not shown).

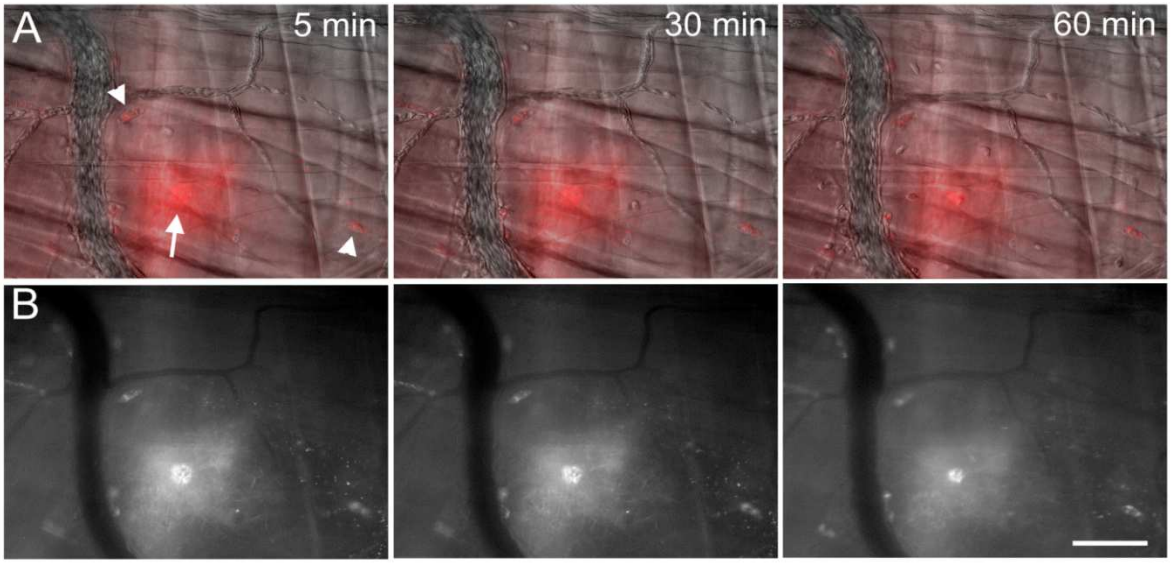

Fig. 12 *Distribution of CpG DNA nanotubes in the cremaster tissue. In vivo* fluorescence microscopy images of CpG tube (red) distribution after microinjection into the cremaster muscle revealed a rapid uptake of CpG tubes by tissue-resident cells (arrowheads) in the vicinity of the application site (arrow). At 30 min and 60 min, transmigrated leukocytes are visible in the tissue adjacent to the postcapillary venule (**A, B**) to the injection site. The fluorescence channel images (**B**) are merged with the corresponding transmitted light images from the cremaster tissue (**A**). Images were taken at the indicated time points after microinjection of 250 nl of CpG tubes and selected from a movie. Scale bar: 50 µm. Taken from Sellner et al. [125].

The identification of these perivascular and tissue-resident cells was achieved by repeated microinjection of DNA nanoconstructs into the cremaster muscle of Csf1r-EGFP transgenic (MacGreen) mice [127]. In these mice, macrophages and to some extend polymorphonuclear leukocytes express green fluorescent protein under the control of the CSF-1R (c-fms) promoter.

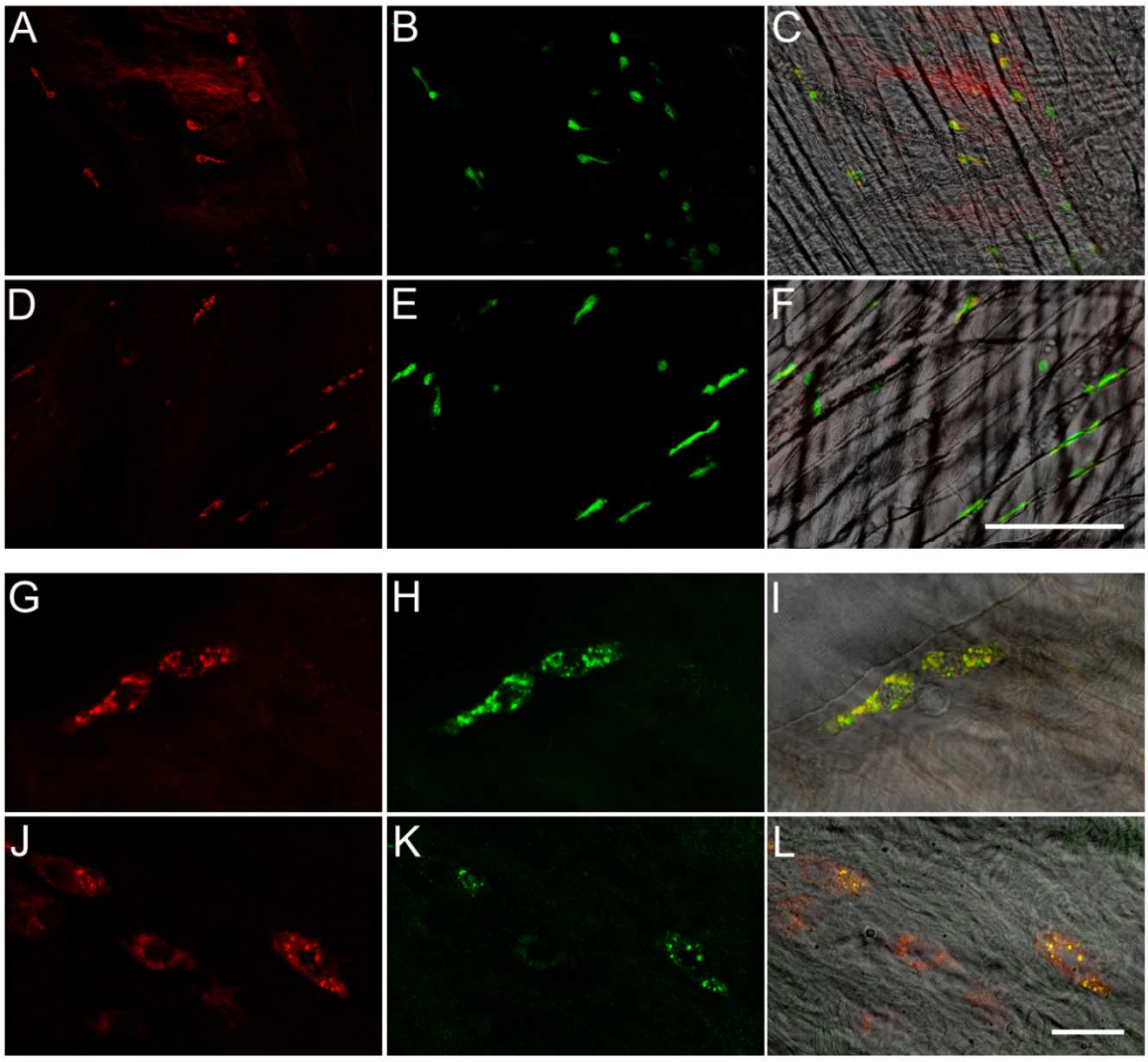

Fig. 13 *DNA nanotubes are localized in the endolysosomes of tissue macrophages.* Confocal imaging of CpG tubes (**A-C**) and plain tubes (**D-F**) microinjected in the cremaster muscle of MacGreen mice. Images show that DNA nanotubes (**A**, **D**, red) were internalized by EGFP-positive macrophages (**B**, **E**, green). The fluorescence channel images (**A**, **B**, **D**, **E**) are merged with the corresponding transmitted light images depicting the muscle tissue (**C**, **F**). Scale bar: 30 µm. Confocal imaging of co-microinjected DNA nanotubes (red) and LysoTracker (green) showing the presence of CpG tubes (**J**) as well as plain tubes (**G**) in the late endolysosomes (**H**, **K**). Merged image (**I**, **L**). Scale bar: 15 µm. Taken from Sellner et al. [125].

After microinjection of CpG tubes, plain tubes, and CpG ODNs, the constructs could be localized in vesicular structures of $EGFP^+$ tissue-resident macrophages (Fig. 13A-F). Simultaneous microinjection of DNA nanostructures and LysoTracker dye demonstrated that DNA nanostructures are localized in the endolysosomes of tissue-resident macrophages (Fig. 13G-L).

Consistent with the *in vitro* results, the cellular uptake pattern of CpG tubes, plain tubes, and CpG ODNs *in vivo* are identical. However, plain tubes and CpG tubes accumulate along muscle fibers, which have been pierced by glass capillaries during microinjection (Fig. not shown). Furthermore, CpG as well as DNA tubes were attached to extracellular matrix components, presumably collagen fibers (Fig 12 and Fig. 13).

4.1.4 Microinjection of CpG tubes induces leukocyte adhesion and transmigration

In additional experiments, the impact of DNA nanotubes on leukocyte recruitment was investigated. Using near-infrared transillumination *in vivo* microscopy, firm adherence and transmigration of leukocytes were analyzed in the mouse cremaster muscle up to 90 min after microinjection of DNA nanoconstructs.

30 min after application of CpG tubes the numbers of firmly adherent leukocytes (3.5 +/- $0.31/10^4$ μm^2) at the vessel walls of postcapillary venules were significantly increased compared to the injection of plain tubes (0.75 +/- $0.35/10^4$ μm^2) or CpG ODNs (0.64 +/- $0.48/10^4$ μm^2)(Fig. 14A). As shown in Figure 14B, these significant higher numbers of adherent leukocytes after CpG nanotube administration maintained over 60 min of observation since the numbers of adherent leukocytes

after CpG nanotube microinjection (2.89 +/- 0.23/10^4 μm^2) was five times higher than in the control group receiving saline (0.67 +/- 0.31/10^4 μm^2). The numbers of adherent leukocytes after CpG ODN microinjection remained low (0.87 +/- 0.26/10^4 μm^2), whereas administration of plain tubes elevated the numbers of adherent cells after 60 min (2.31 +/- 0.56/10^4 μm^2) 4-fold compared to the saline group. In accordance with the typical length of time for the different steps of leukocyte recruitment upon administration of inflammatory mediators [128] the number of adherent leukocytes declined 90 min after injection of CpG DNA nanotubes (Data not shown).

After adhesion, leukocytes subsequently transmigrate from the vessel lumen into the inflamed tissue. To test whether local microinjection of the different constructs resulted in a directed transmigration of leukocytes into the adjacent tissue, a comparison of the numbers of transmigrated cells on the vessel side ipsilateral to the application site with those on the contralateral side was conducted. In line with the leukocyte adherence data, the numbers of transmigrated leukocytes were significantly increased within the ipsilateral vessel side after CpG DNA microinjection (Fig. 14D, 60 min: 7.3 +/- 0.32/10^4 μm^2) as compared to saline (Fig. 14D, 60 min: 1.3 +/- 0.51/10^4 μm^2) at all investigated time points (Fig. 14C and D). However, microinjection of CpG ODNs or plain DNA tubes had no effect on leukocyte transmigration.

Taken together, these data demonstrate the immunogenic properties of CpG-decorated DNA tubes. CpG DNA nanotubes recruit leukocytes to the site of injection, whereas plain DNA tubes and CpG ODNs lack this capacity.

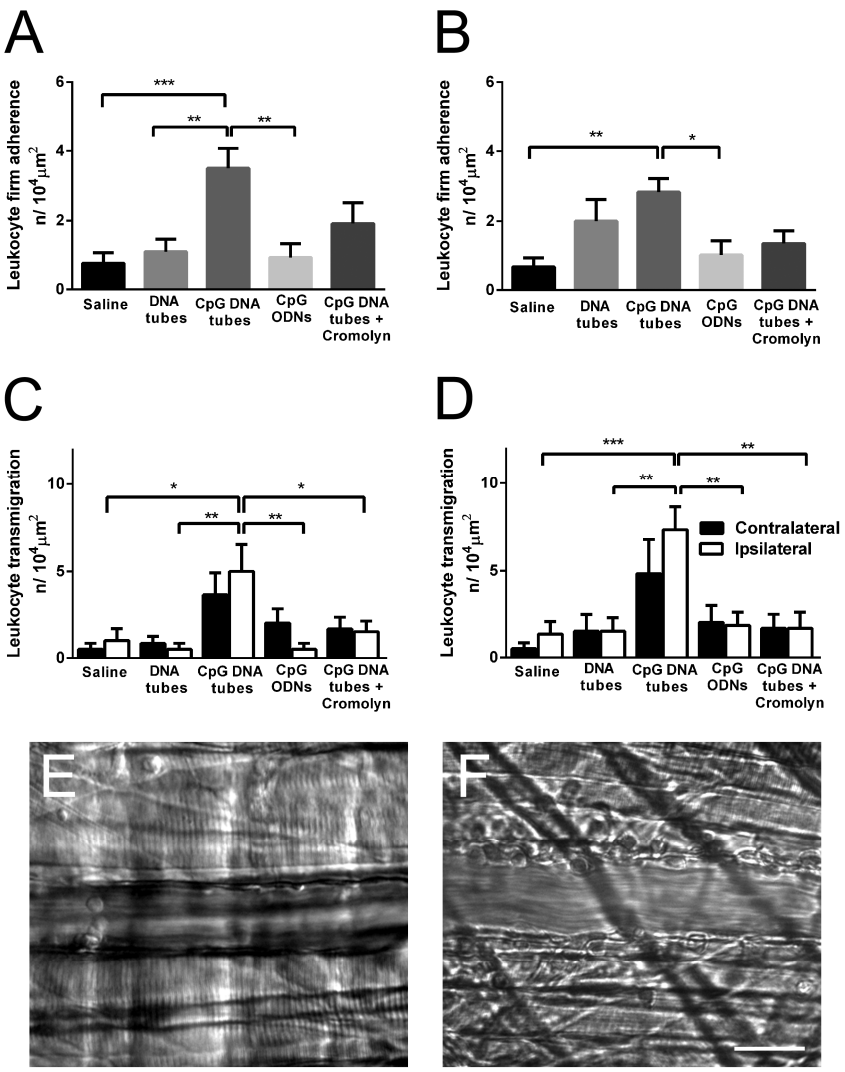

Fig. 14 *Quantitative analysis of intravascular adherence and transmigration of leukocytes after microinjection of DNA nanoconstructs.* Leukocyte adherence was quantified in postcapillary venules in the cremaster muscle using *in vivo* transillumination microscopy at 30 min (**A**) and 60 min (**B**) upon microinjection of CpG tubes, DNA tubes, CpG ODNs, or saline. The numbers of adherent leukocytes were significantly increased at 30 min and 60 min after CpG tube injection. Pretreatment with cromolyn prior to CpG tube injection diminished leukocyte adherence. Leukocyte transmigration was quantified on the vessel side ipsilateral to the microinjection site (white bars) and on the contralateral side (black bars) at 30 min (**C**) and 60 min (**D**) after microinjection. CpG tube injection elicited leukocyte transmigration into the tissue. Cromolyn pretreatment attenuated the leukocyte transmigration induced by microinjection of CpG tubes (n=6, mean+/-SEM; *p<0.05, **p<0.01, ***p<0.001 vs. all groups). (**E**, **F**) depicts representative *in vivo* microscopy images of postcapillary venules in the cremaster muscle 30 min after microinjection of either saline (**E**) or CpG tubes (**F**) with adherent as well as transmigrated leukocytes. Scale bar, 25 µm. Taken from Sellner et al. [125].

4.1.5 Mast cell inhibition abolishes CpG tube-evoked leukocyte adhesion and transmigration

Mast cells are well known for their role in allergy, since they are important immune cells involved in the recognition of pathogens and the initiation of immune responses [129]. After activation, mast cells are able to release proinflammatory mediators from their characteristic granules, which subsequently facilitate the exit of leukocytes from postcapillary venules [130]. As previously reported, surgical preparation of the cremaster muscle does not activate mast cells and does not contribute to the low baseline levels of preparation-induced leukocyte recruitment [124, 131]. To determine whether mast cells are involved in leukocyte recruitment elicited by microinjection of CpG DNA nanotubes, mice received the mast cell degranulation inhibitor cromolyn prior to microinjection.

Cromolyn pretreatment diminished the numbers of adherent (Fig. 14B, 60 min, 1.3 +/- 0.33/10^4 µm^2) and the numbers of transmigrated leukocytes (Fig. 14D, 60 min, 1.7 +/- 0.71/10^4 µm^2) after microinjection of CpG tubes compared to non-treated mice (Fig. 14B, adherence 60 min, 2.8 +/- 0.24/10^4 µm^2, Fig. 14D, transmigration 60 min, 7.3 +/- 0.48/10^4 µm^2). These values were in the range of the control group (Fig. 14B, adherence 60 min, 0.7 +/- 0.32/10^4 µm^2, Fig. 14D, transmigration 60 min, 1.3 +/- 0.62/10^4 µm^2).

4.1.6 Systemic leukocyte counts and microhemodynamic parameters

To guarantee the comparability of all experimental groups, inner vessel diameter, blood flow, and wall shear stress of all examined vessels were determined. To exclude anomalies, systemic leukocyte counts in the peripheral blood of animals were measured at the end of the experiment. There were no significant differences in inner vessel diameter, blood flow, wall shear stress, or systemic leukocyte counts between all groups (Table 1).

Experimental group	Inner vessel diameter [µm]	Blood flow velocity [mm/s]	Wall shear rate [1/s]	Systemic leukocyte counts [$*10^6$ /ml]
Sham	29.2 ± 2.0	3.1 ± 1.2	4157.6 ± 1650.2	3.6 ± 1.4
Saline	27.8 ± 1.2	2.8 ± 0.7	3978.1 ± 1075.8	2.4 ± 0.7
CpG nanotubes	31.8 ± 3.1	3.1 ± 1.1	3800.0 ± 1175.2	2.7 ± 1.5
DNA nanotubes	25.8 ± 0.8	3.5 ± 0.3	5312.6 ± 291.2	1.8 ± 0.1
CpG ODNs	27.3 ± 1.5	2.6 ± 0.6	3726.7 ± 907.1	4.5 ± 1.0

Table 1 *Systemic leukocyte counts and microhemodynamic parameters*. Systemic leukocyte counts as well as microhemodynamic parameters, including inner vessel diameter, blood flow velocity, and wall shear rate, were obtained as detailed in *Materials and Methods* (mean ± SEM for *n*=4-5 per group). Taken from Sellner et al. [125].

4.1.7 CpG tube microinjection results in NF-κB pathway activation

The transcription factor NF-*κ*B is a key regulator of genes involved in inflammatory processes. Binding of TLR ligands leads to a downstream activation of NF-*κ*B and the subsequent translocation from the cytoplasm into the nucleus [132, 133], where the expression of inflammatory mediators such as TNF and IL-1 is mediated [134].

Immunostaining of phosphorylated p65, a subunit of the NF-*κ*B complex, which indicates nuclear NF-*κ*B [135], was performed with DNA nanoconstructs-microinjected cremasteric tissue to investigate the ability of CpG nanotubes to induce NF-*κ*B activation.

A clear nuclear localization of phospho-p65 could be detected in cells close to the CpG nanotube injection site 90 min upon microinjection (Fig. 15B and E), which was not present in plain tube- (Fig. 15A and D) and CpG ODN- (Fig. 15C and F) injected tissues. The majority of the phospho-p65-positive cells accumulated around the site of CpG DNA tube administration exhibited roundish nuclei, similar to multi-lobed granulocyte nuclei (Fig. 15B and E), whereas p65-positive cells with elongated nuclei are presumably tissue-resident cells, such as macrophages or mast cells.

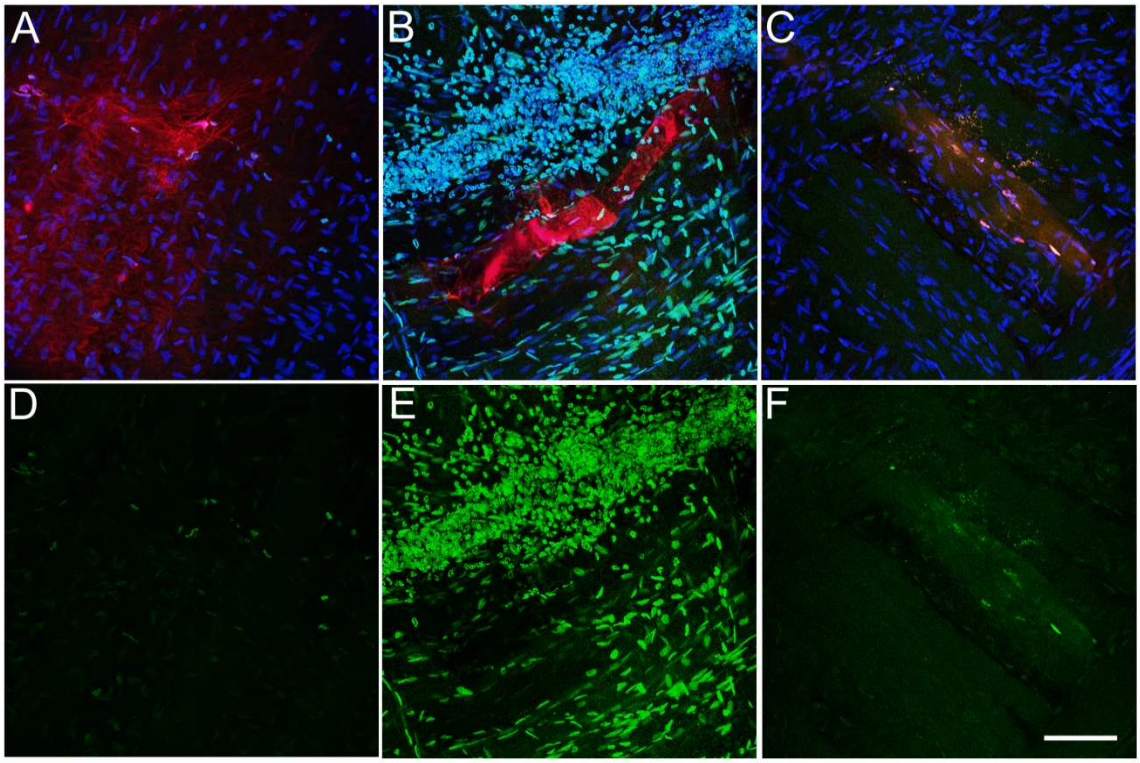

Fig. 15 *NF-κB p65 translocation occurs in the vicinity of microinjected CpG DNA nanotubes.* Confocal immunofluorescence of DNA nanotubes (red), NF-κB p65 (green), and TO-PRO (blue) counterstaining showed marked NF-κB p65 nuclear staining of cells adjacent to the injection site of CpG tubes (**B**, **E**). Injection of plain tubes (**A**, **D**) as well as of CpG ODNs into the cremasteric tissue (**C**, **F**) caused only weak nuclear p65 staining. Scale bar: 50 µm. Taken from Sellner et al. [125].

4.2 The impact of CpG nanotubes on I/R injury

4.2.1 Microdistribution of CpG DNA nanoconstructs in postischemic muscle tissue

To determine the local distribution of CpG DNA nanoconstructs within inflamed muscle tissue, real-time fluorescence intravital microscopy was used. By clamping the cremaster muscle supplying blood vessels for 30 min and subsequent release of the clamp, I/R injury and vascular inflammation were induced [136]. Since inflammation alters the tissue environment, such as the activation status of the immune system, vascular permeability [137], and the density of collagen fibers [138],

the local microdistribution of DNA nanotubes needs to be investigated to test the therapeutic potential of the constructs in the postischemic tissue.

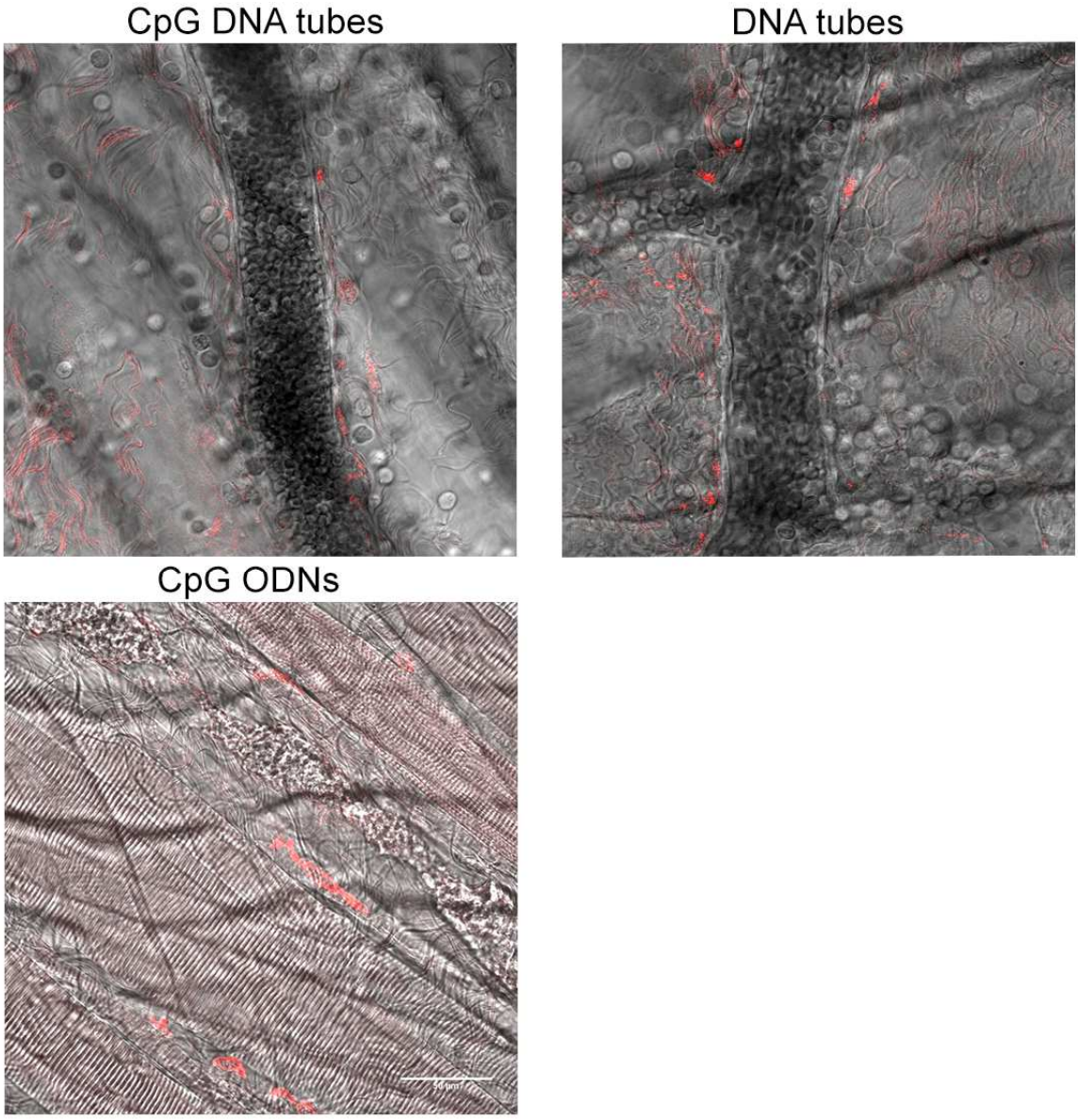

Fig. 16 *Uptake of DNA nanoconstructs by tissue macrophages in inflamed cremasteric tissue.* Confocal imaging of CpG tubes, plain tubes, and CpG ODNs microinjected in the postischemic cremaster muscle. Images show that DNA nanoconstructs (red) were internalized by tissue-resident macrophages in the inflamed cremaster tissue. The fluorescence channel images are merged with the corresponding transmitted light images depicting the muscle tissue. Scale bar: 50 µm.

By means of *in vivo* fluorescence microscopy, 30 min after microinjection of CpG DNA nanotubes (500 nM), plain nanotubes (500 nM), and CpG ODNs (12 µM), the constructs were found within cells, associated with postcapillary venules as depicted in Figure 16. The cell morphology as well as our previous experiments suggests that the DNA nanoconstructs were incorporated by tissue macrophages. Additionally, DNA tubes were prominently localized along distinct tissue structures, presumably collagen fibers (Fig. 16). However, DNA nanoconstructs could not be detected in ECs or transmigrated leukocytes. During the observation period of 90 min, the nanoconstructs remained inside macrophages and along tissue fibers (Data not shown).

4.2.2 Microinjection of CpG tubes into ischemic muscle tissue attenuates leukocyte adhesion and transmigration

Real-time fluorescence intravital microscopy was used to investigate the effects of CpG DNA nanoconstructs on leukocyte infiltration into the postischemic mouse cremaster muscle.

At baseline conditions and after release of the vascular clamp, the number of leukocytes attached to the inner vessel wall of postcapillary venules was low and did not differ among experimental groups (Data not shown). After 60 min of reperfusion, microinjection of CpG DNA nanotube or saline lead to similar numbers of firmly adherent leukocytes (Fig. 17A, CpG DNA: 3.3 +/- 0.99/10^4 µm^2; saline: 3.5 +/- 0.99/10^4 µm^2) while DNA nanotube microinjection caused highly elevated numbers of leukocytes (Fig. 17A, 10 +/- 4.59/10^4 µm^2). Within 90 min this elevated numbers after DNA nanotube administration diminished. However, the numbers of adherent

leukocytes after CpG nanotube microinjection (Fig. 17B, 1.4 +/- 0.72/10^4 μm^2) dropped under these of saline injection (Fig. 17B, 3.8 +/- 0.9/10^4 μm^2). Microinjection of CpG ODNs into the postischemic muscle tissue resulted in a similar number of adherent cells compared to microinjection of saline over the observation period of 90 min (Fig. 17B, 60 min: 2.9 +/- 0.7/10^4 μm^2; 90 min: 2.9 +/- 0.7/10^4 μm^2). Before onset of ischemia, only few transmigrated leukocytes were found within the perivenular tissue (Data not shown). Consistent with the results obtained for leukocyte firm adherence, the numbers of transmigrated leukocytes detected within the perivascular tissue were elevated after DNA nanotube application at all investigated time points (Fig. 17C, 60 min: 15 +/- 4.5/10^4 μm^2; Fig. 17D, 90 min: 22 +/- 5.8/10^4 μm^2) as compared to sham-treated mice. The numbers of transmigrated leukocytes after microinjection of CpG tubes were less than after saline at 60 min (Fig. 17C, CpG DNA nanotubes: 8.5 +/- 1.9/10^4 μm^2; saline: 12.8 +/- 2.8/10^4 μm^2) but rose after 90 min to the saline (I/R control) level (Fig. 17D, CpG DNA nanotubes: 13 +/- 2.1/10^4 μm^2; saline: 12.2 +/- 2.2/10^4 μm^2). Microinjection of CpG ODNs had an inhibitory effect on the transmigration of leukocytes at 60 min (Fig. 17C, 5 +/- 1.5/10^4 μm^2) and 90 min (Fig. 17D, 7.4 +/- 2.1/10^4 μm^2) of reperfusion.

Taken together, these data indicate that CpG ODNs attenuate the recruitment of leukocytes into ischemic tissue, whereas plain DNA tubes enhance the leukocyte response under sterile inflammatory conditions.

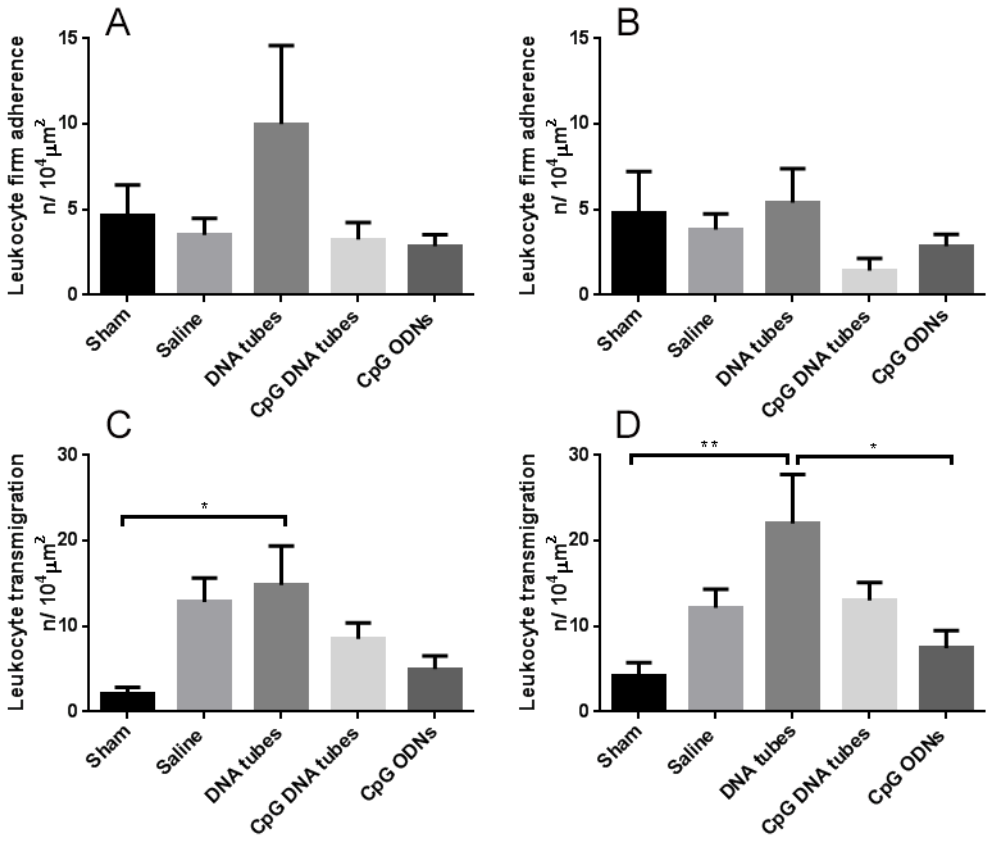

Fig. 17 *Quantitative analysis of intravascular adherence and transmigration of leukocytes after microinjection of DNA nanoconstructs into postischemic tissue at the onset of reperfusion.* Leukocyte adherence was quantified in postcapillary venules in the cremaster muscle using *in vivo* transillumination microscopy at 60 min (**A**) and 90 min (**B**) upon microinjection of CpG tubes, DNA tubes, CpG ODNs, saline, or in sham-operated animals. The numbers of adherent leukocytes were increased at 60 min and 90 min after DNA nanotube injection, whereas CpG constructs attenuated the numbers. Leukocyte transmigration was quantified at 60 min (**C**) and 90 min (**D**) after microinjection. CpG ODN injection attenuated leukocyte transmigration into the tissue, whereas DNA tube application elevated the numbers of transmigrated leukocytes (n=6, mean+/-SEM, *p<0.05, **p<0.01 vs. all groups).

4.2.3 Systemic leukocyte counts and microhemodynamic parameters

To assure intergroup comparability, systemic leukocyte counts, inner vessel diameter, blood flow, and wall shear stress were measured at the end of the experiments. No significant differences in these parameters were detected among all experimental groups (Table 2).

Experimental group	Inner vessel diameter [µm]	Blood flow velocity [mm/s]	Wall shear rate [1/s]	Systemic leukocyte counts [*10^6 /ml]
Saline	28.0 ± 0.5	2.8 ± 0.3	3978.0 ± 537.9	2.6 ± 0.3
Sham	27.8 ± 1.6	3.1 ± 0.6	4158.0 ± 825.1	3.8 ± 0.5
DNA nanotubes	27.3 ± 1.2	3.5 ± 0.2	5313.0 ± 168.1	2.1 ± 0.3
CpG nanotubes	30.1 ± 1.3	3.1 ± 0.6	3800.0 ± 587.6	3.2 ± 0.9
CpG ODNs	26.5 ± 0.7	2.6 ± 0.3	3726.0 ± 523.7	2.0 ± 0.2

Table 2 *Systemic leukocyte counts and microhemodynamic parameters*. Systemic leukocyte counts as well as microhemodynamic parameters, including inner vessel diameter, blood flow velocity, and wall shear rate, were obtained as described in *Materials and Methods* (mean ± SEM for *n*=4 per group).

4.2.4 Microinjection of CpG tubes into postischemic muscle tissue increases cellular TLR 9 expression

To determine the TLR 9 expression upon DNA nanoconstruct microinjection, confocal microscopy of TLR 9 immunostained-postischemic muscle tissue was performed.

Notably, 90 min upon microinjection of CpG DNA tubes, a multitude of cells with elongated, ramified shapes and intense TLR 9 signal were present around the injection site (Fig. 18A and E). Surprisingly, the cellular TLR 9 signal was not localized in vesicular structures but ubiquitously present over the whole cell bodies. Microinjection of CpG DNA tubes into the postischemic cremaster of a *CX_3CR1^{GFP}*

mouse revealed that these TLR 9^{high} cells are *CX$_3$CR1^{GFP}*-positive macrophages (Fig. 19A-D). I/R injury together with CpG DNA tube microinjection induced a substantial change in the morphology of these macrophages (Fig. 19B), since *CX$_3$CR1^{GFP}*-positive macrophages did not display prominent TLR 9 expression after saline injection (Fig. 19E-H). The administration of CpG ODNs in the ischemic cremaster tissue had only little impact on macrophage morphology. The cellular TLR 9 signal was markedly less pronounced and macrophages with long protrusions were not present (Fig. 18C and G). Also microinjection of plain tubes induced just weak TLR 9 expression (Fig 18B and F).

In all three groups, TLR 9 was present at blood vessel walls. Vascular TLR 9 staining was either spotted (Fig. 18B and F), or was present section-wise (Fig. 18C and G) after microinjection of plain tubes and CpG ODNs.

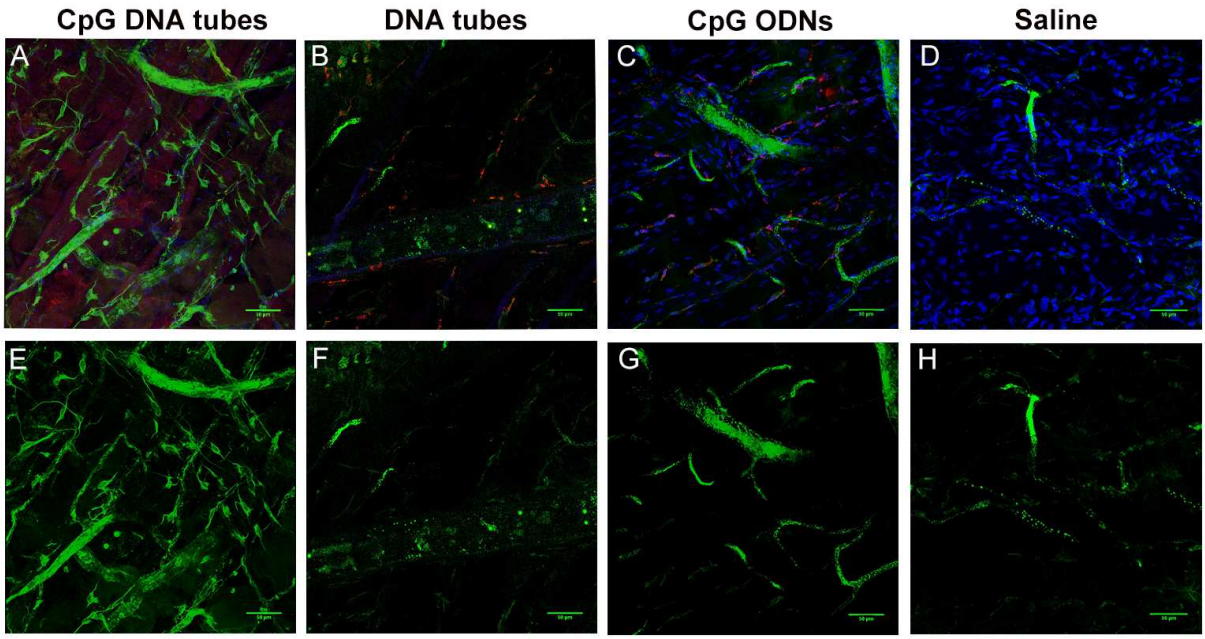

Fig. 18 *Marked TLR 9 expression in ramified macrophages upon microinjection of CpG tubes into the postischemic cremaster muscle.* Confocal immunofluorescence of CpG DNA nanoconstructs (red), TLR 9 (green), and TO-PRO (blue) counterstaining showed marked cellular TLR 9 staining after the injection of CpG tubes (**A**, **E**) into postischemic tissue. Injection of plain tubes (**B**, **F**), CpG ODNs (**C**, **G**), and saline (**D, H**) into postischemic cremasteric tissue caused only weak TLR 9 expression in interstitial cells. Scale bar: 50 µm.

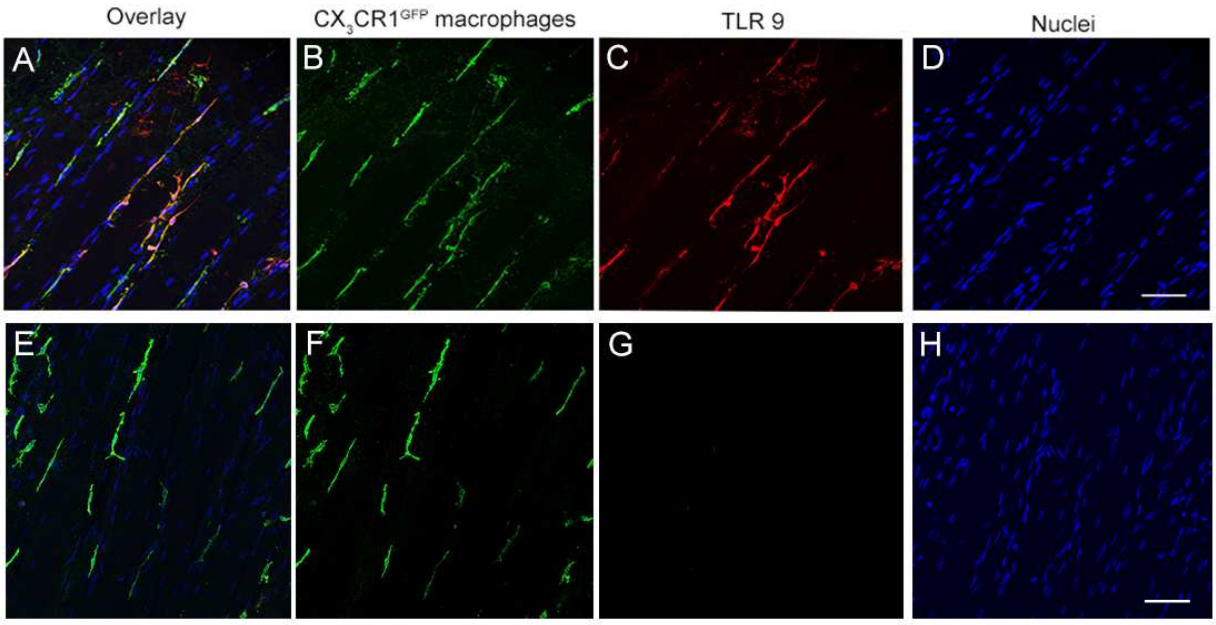

Fig. 19 *TLR 9 expression in CX_3CR1^{GFP} macrophages after injection of CpG nanoconstructs and saline into the postischemic cremaster muscle.* Confocal immunofluorescence images of CpG nanotubes (**A-D**) and saline (**E-H**) microinjected into the cremaster muscle of *CX_3CR1^{GFP}* mice, which were immunostained for TLR 9 (red) and cell nuclei (TO-PRO, blue). Injection of CpG nanotubes induced TLR 9 (red) expression (**C**) in *CX_3CR1^{GFP}*-positive macrophages (green) compared to saline (**G**). Scale bar: 50 µm.

4.3 Dexamethasone-conjugated DNA nanotubes as anti-inflammatory agents *in vivo*

4.3.1 Characterization and functionality of Dex nanotubes

Dex nanotube design, assembly, and characterization were mainly done by Samet Kocabey and Tim Liedl (Department of Physics, LMU) in close cooperation and with considerable conceptual input by the author of this thesis.

A DNA nanotube construct, consisting of 15 unique single-stranded tiles, with a ph-responsive i-motif was designed as controllable device for the intracellular release of the anti-inflammatory drug dexamethasone (Fig. 20A). In order to conjugate dexamethasone on the structure, 3 of the tiles were extended from their 3´ ends with an i-motif sequence or a random sequence, which then hybridize with Dex ODNs. The temperature-controlled assembly of the tiles into 6 parallel double helices led to

a tube structure with a designed length of ~30 nm and a diameter of ~8 nm. TEM micrographs revealed the correct assembly into nanotube structures (Fig. 20B). Plain DNA tubes, Dex nanotubes w/o i-motif, and unfolded ODNs conjugated with dexamethasone (Dex ODNs) served as control groups in all experiments. The i-motif structure is a four-stranded DNA structure that forms sequences containing stretches of cytosine residues [139-141].

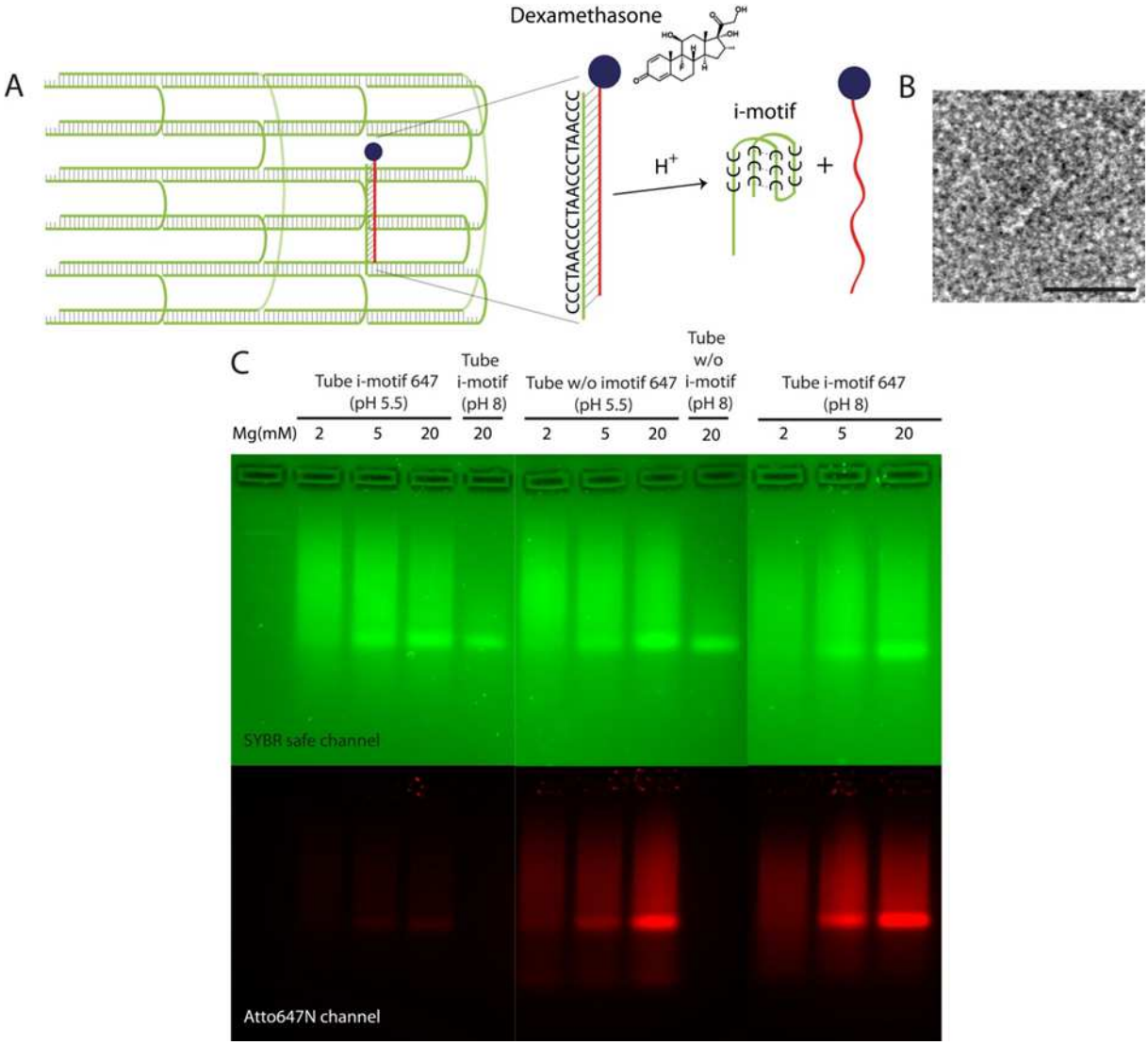

Fig. 20 *Characterization of Dex DNA nanoconstructs.* Scheme depicting the design of 6-helix nanotubes with i-motif-dependent dexamethasone release (**A**). Transmission electron micrograph of a single DNA nanotube. Scale bar 40 nm (**B**). Gel analysis of i-motif-dependent release of the hybridized ODNs labeled with Alexa 647 (red) at pH 5.5 and 37 °C from Dex nanotubes labeled with SYBR green (**C**).

Cytosines in the i-motif sequence get protonated at low pH and form a quadruple helix. This mechanism was used to release Dex ODNs upon acidic pH as illustrated in Figure 20A. To test the functionality of the i-motif-dependent release mechanism, the nanotubes were incubated in MES buffer (pH 5.5) at 37 °C and centrifuged to get rid of released single-stranded tiles. Gel analysis revealed that Alexa 647-labeled complementary tiles are still visible at structures without i-motif sequence and on structures incubated in buffer at pH 8. However, the i-motif-dependent release of hybridized ODNs at pH 5.5 could be observed since the Alexa 647 signal is very low in comparison to the control groups (Fig. 20C). The released Dex ODNs were washed out during the centrifugation process. This experiment demonstrated the i-motif-dependent release of Dex ODNs from DNA 6-helix tubes at 37 °C and under acidic pH.

4.3.2 Dexamethasone-conjugated DNA nanoconstructs do not affect macrophage viability

The synthetic glucocorticoid dexamethasone is reported to have cytotoxic effects on several cell types [142-144]. Although the dexamethasone concentrations applied *in vitro* with DEX tubes are low (40 ng/ml), the cell vitality during treatment with the different nanoconstructs were tested. For *in vitro* testing, a murine alveolar macrophage cell line (MH-S) was used in this study, since dexamethasone is a potent agent targeting the cytokine release from alveolar macrophages in asthma therapy [145, 146].

Cytotoxic effects of Dex tubes, DNA tubes, Dex ODNs, Dex tubes w/o i-motif (all at 50 nM), unconjugated dexamethasone (40 ng/ml and 1 µg/ml), and LPS (10 ng/ml)

on MH-S macrophages were examined using the WST-1 assay. Dexamethasone was used in a concentration equivalent to the concentration on Dex tubes (40 ng/ml) and in a higher dose, described to be immunosuppressive (1 µg/ml) [147]. DNA nanoconstructs, as well as free dexamethasone were not cytotoxic for MH-S cells over a time period of 12h (Fig. 21). MH-S cells were also exposed for 2 min to 70% ethanol (EtOH) and afterwards medium was added. This treatment led to cell death and served as negative control. After 6 h of incubation, the cell viability increased almost to 150% of the untreated control cells (100%), which corresponds with higher metabolic rates of NADH (mediating the complex formation of the tetrazolium salt WST-1) before macromolecular synthesis and cell division [148].

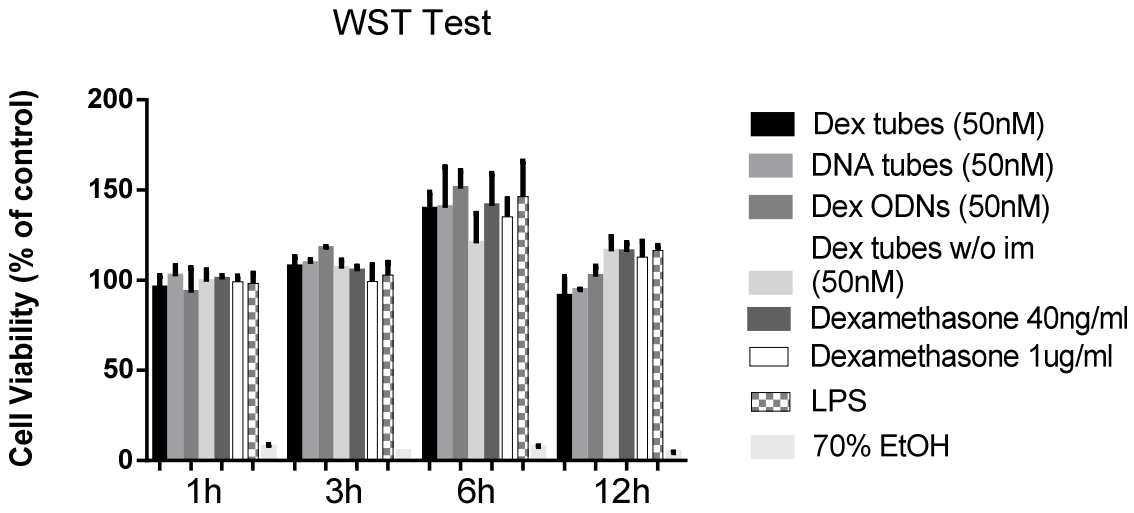

Fig. 21 *Effects of Dex nanoconstructs on MH-S macrophage cell viability.* MH-S macrophages were incubated with medium containing Dex tubes (50 nM), DNA tubes (50 nM), Dex ODNs (50 nM), Dex DNA tubes w/o i-motif (50 nM), dexamethasone (40 ng/ml and 1 µg/ml), and LPS (10 ng/ml) for 12 h. 70% ethanol was added for 2 min and served as negative control. Cell viability was evaluated using the colorimetric WST1-assay.

4.3.3 Dex tubes are effectively incorporated by macrophages

Dex tubes could be rapidly detected within MH-S macrophages. Already within 15 min of incubation with Dex nanoconstructs, Dex tubes could be detected within

intracellular vesicles (Fig. 22A), but to a lesser extent than Dex tubes w/o i-motif (Fig. 22D). Apparently, the overall uptake rate differed between the various Dex nanoconstructs, although the administered concentrations were equal. Plain DNA tubes were preferably incorporated by MH-S cells (Fig. 22B), whereas Dex ODNs could hardly be detected in phagosomal structures (Fig. 22C).

Within 6 h of incubation Dex DNA tubes and plain DNA tubes were equally present in cellular compartments of MH-S cells (Fig. 23A and B). Interestingly, at 6 h the colocalization of Alexa 546 Dex ODNs with the Alexa 488-conjugated DNA tube structure could no longer be observed, whereas Dex ODNs were still present in the endolysosomal compartments (Fig. 23C). Since the functionality of the i-motif could be shown at pH 5.5 and 37 °C (Fig. 20C), this loss of endolysosomal Alexa 546 fluorescence might indicate the escape of dexamethasone from this compartment. On the contrary, Dex tubes w/o i-motif still showed a colocalization of Alexa 546 Dex handles and the Alexa 488-linked DNA tube structure, after 6 h. Noticeable, the construct distribution changed from purely vesicular to vesicular/cytoplasmatic in the majority of MH-S cells with incorporated constructs (Fig. 23D). This phenotype was correlated with the accumulation of cells and the formation of giant cells (Data not shown), suggesting an activated status. Furthermore, within 6 h of incubation, vesicles containing Dex nanoconstructs clustered around the cellular nuclei (Fig. 23A-D). This indicates a maturation of these vesicles from early to late endosomes, which are in close proximity to the Golgi apparatus and the nucleus.

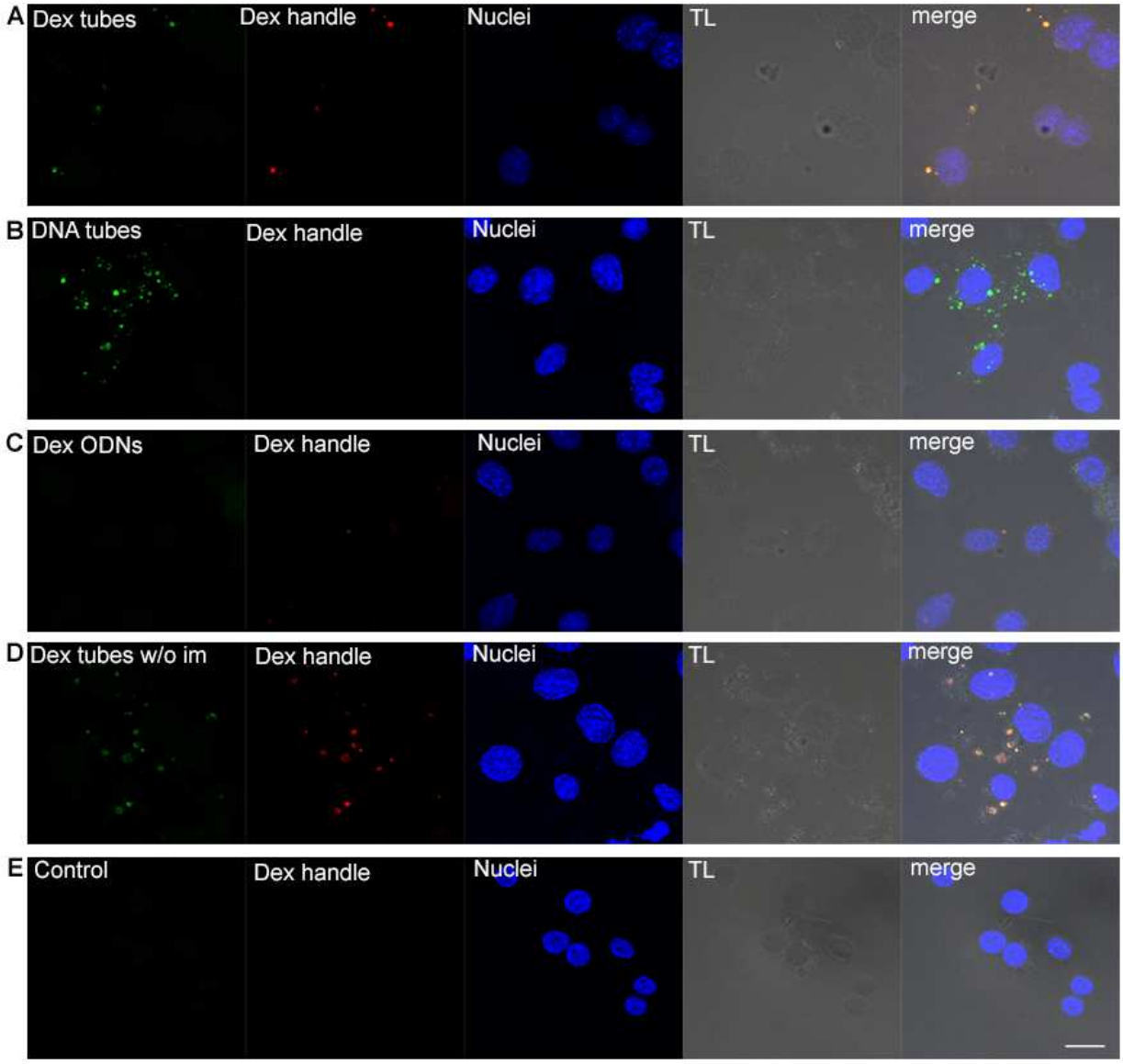

Fig. 22 *Uptake of DNA nanoconstructs by MH-S macrophages within 15 min of incubation.* MH-S cells were incubated with 50 nM Dex tubes (**A**), 50 nM plain tubes (**B**), 150 nM Dex ODNs (**C**), 50 nM Dex tubes w/o i-motif (**D**), or without additive (control) (**E**) for 15 min at 37 °C. Confocal fluorescence microscopy of Alexa 488-labeled DNA nanotubes (green), separately Alexa 546-labeled Dex handles (red) and TO-PRO (cell nuclei, blue) counterstaining showed a vesicular localization of DNA nanoconstructs within 15 min of incubation. Scale bar: 20 µm.

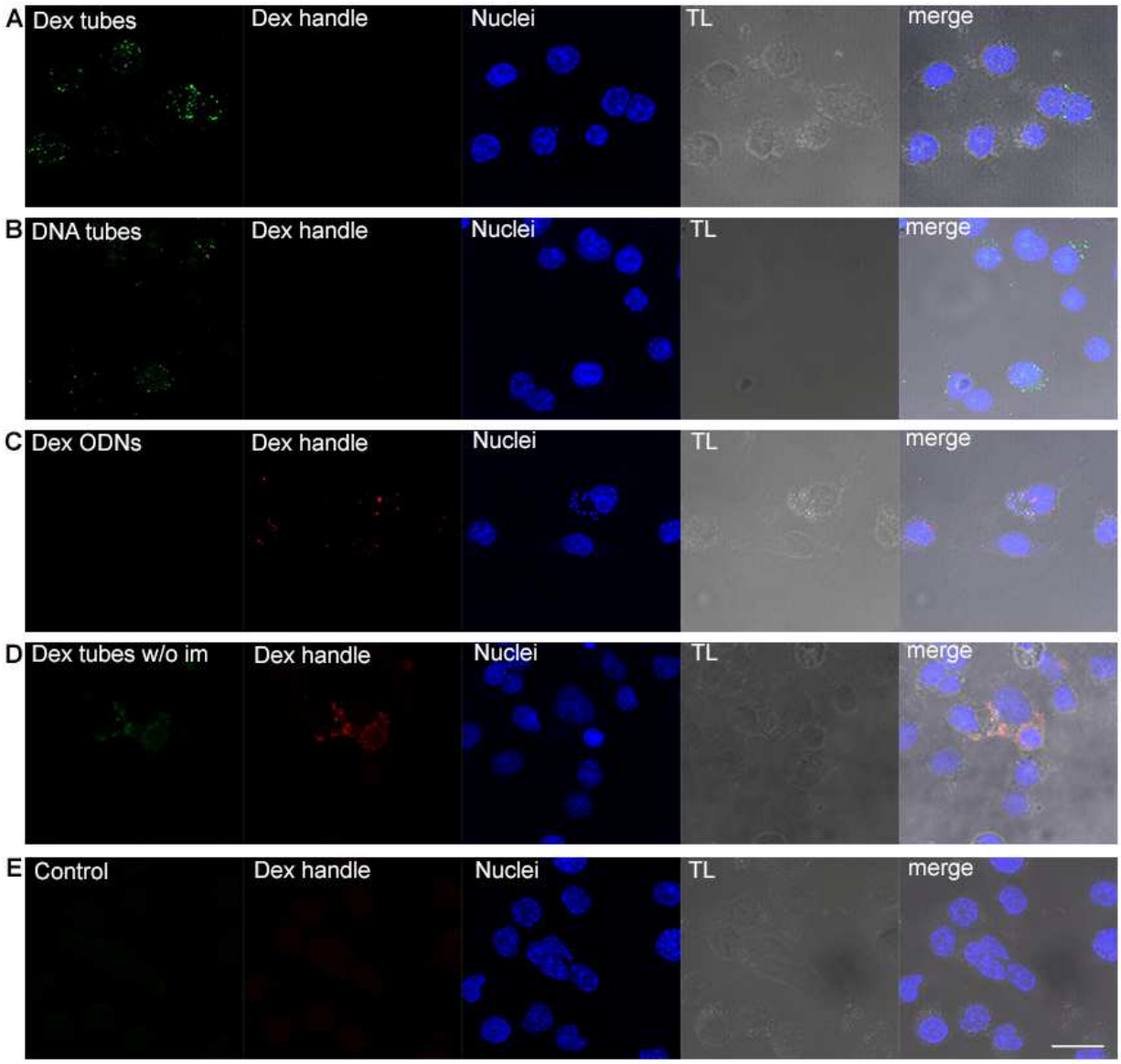

Fig. 23 *Uptake of DNA nanoconstructs by MH-S macrophages within 6 h of incubation.* MH-S cells were incubated with 50 nM Dex tubes (**A**), 50 nM plain tubes (**B**), 150 nM Dex ODNs (**C**), 50 nM Dex tubes w/o i-motif (**D**), or without additive (control) (**E**) for 6 h at 37 °C. Confocal fluorescence microscopy of Alexa 488-labeled DNA nanotubes (green), separately Alexa 546-labeled Dex handles (red) and TO-PRO (cell nuclei, blue) counterstaining revealed a vesicular localization of DNA nanoconstructs after 6 h of incubation. Scale bar: 20 µm.

Taken together, it can be concluded that the uptake of Dex nanoconstructs by MH-S cells occurs within the first minutes of incubation. DNA tubes, Dex tubes, Dex tubes w/o i-motif, and Dex ODNs are stored up to 6 h in endolysosomal compartments of MH-S macrophages, but only Dex tubes with functional i-motif lost the Dex handle signal after 6 h.

4.3.4 Dex tubes attenuate LPS-induced TNF secretion by MH-S macrophages

Next, the pH-responsive Dex nanoconstructs were tested on their ability to suppress pro-inflammatory cytokine release in response to LPS. Accordingly, MH-S alveolar macrophages were incubated for 15 min with the respective Dex nanoconstruct, which was removed prior to LPS stimulation.

Dex tubes showed a significant inhibitory effect on TNF release (12 h: 306 +/- 9.6 pg/ml) up to 12 h of LPS stimulation compared to LPS without DNA construct pretreatment (12 h: 547 +/- 35.4 pg/ml) (Fig. 24). Pretreatment with 40 ng/ml dexamethasone, a concentration equivalent to Dex tubes reduced the TNF release of MH-S cells only for 6 h (6 h: 164.1 +/- 7.3 pg/ml; 12 h: 476 +/- 13.1 pg/ml) (Fig. 24). In contrast, pretreatment with Dex tubes w/o i-motif intensified the LPS induced TNF response of MH-S cells from 6 h to 12 h of LPS stimulation (6 h: 851 +/- 40.1 pg/ml; 12 h: 1304.4 +/- 28.6 pg/ml). Plain DNA tubes did not affect the release of TNF by MH-S cells (12 h: 508.1 +/- 15.8 pg/ml) since the secreted levels were comparable to the LPS control group over 12 h. Incubation with Dex ODNs did not result in a significant inhibition of TNF release upon LPS stimulation.

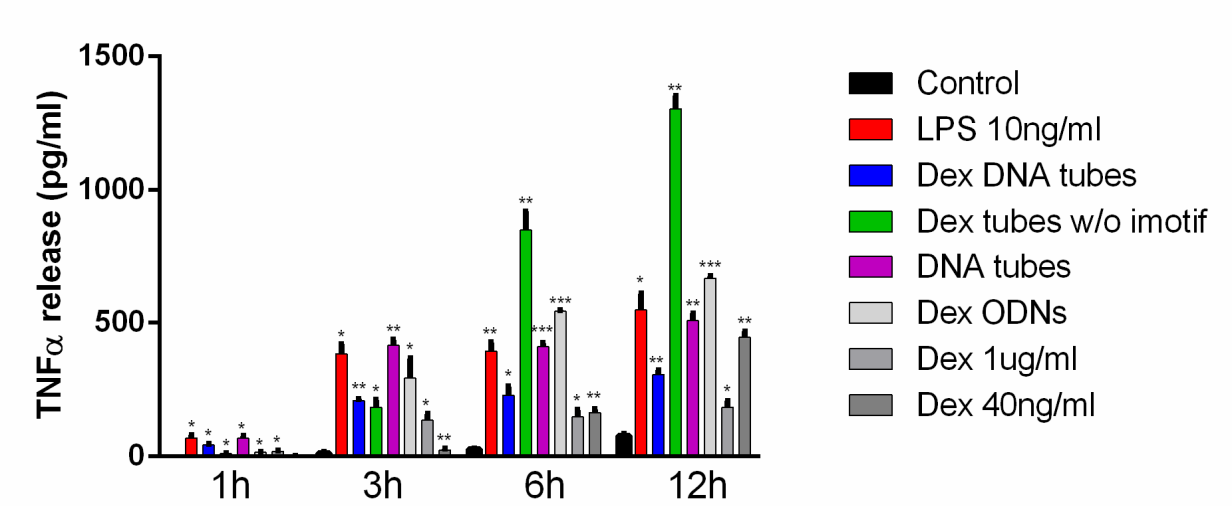

Fig. 24 *TNF release by MH-S cells induced by LPS stimulation is attenuated after pretreatment with Dex tubes.* ELISA analysis of TNF levels in supernatants of $1x10^5$ MH-S cells incubated for 1 h, 3 h, 6 h, and 12 h with LPS (10 ng/ml) and pretreated for 15 min with 50 nM Dex tubes, 50 nM Dex tubes w/o i-motif, 50 nM DNA tubes, 150 nM Dex ODNs, and dexamethasone (1 µg/ml and 40 ng/ml) or without additive (control). (n=3, mean+/-SEM; *p<0.05, **p<0.01, ***p<0.001 vs. control)

4.3.5 Microinjection of Dex tubes into postischemic muscle tissue lowers the number of adherent and transmigrated leukocytes

It has been shown that dexamethasone mediates its immunosuppressive effect by affecting the recruitment of leukocytes [149].

In vivo transillumination microscopy was performed to analyze the impact of Dex nanotubes on leukocyte infiltration. Therefore, Dex nanoconstructs as well as unconjugated dexamethasone (1 µg/ml) were microinjected into the mouse cremaster muscle at the onset of reperfusion after an ischemic period of 30 min. At baseline conditions and after release of the vascular clamp, the number of leukocytes attached to the inner vessel wall of postcapillary venules was low and did not differ among experimental groups (Data not shown). Within 60 and 90 min of reperfusion, the numbers of firmly adherent leukocytes after microinjection of Dex tubes (60 min:

4.3 +/- 1.4 /10^4 µm^2; 90 min: 2.6 +/- 1.1 /10^4 µm^2) kept at the level of saline-injected animals (60 min: 3.5 +/- 1.0 /10^4 µm^2; 90 min: 3.8 +/- 0.9 /10^4 µm^2), whereas significantly elevated numbers of adherent leukocytes could be observed after Dex ODN injection (60 min: 18.8 +/- 7.3 /10^4 µm^2; 90 min: 17.6 +/- 6.7 /10^4 µm^2) (Fig. 25A and B). Injection of unconjugated dexamethasone led to higher numbers of adherent leukocytes at both time points compared to Dex tubes (1 µg/ml; 60 min: 7.3 +/- 2.8 /10^4 µm^2; 90 min: 7.0 +/- 2.6 /10^4 µm^2). The same applies for microinjection of Dex tubes w/o i-motif (60 min: 12.6 +/- 2.6 /10^4 µm^2; 90 min: 8.8 +/- 2.4 /10^4 µm^2) and plain DNA tubes (60 min: 9.7 +/- 3.0 /10^4 µm^2; 90 min: 9.9 +/- 2.7 /10^4 µm^2) (Fig. 25A and B).

Before ischemia, only few transmigrated leukocytes were found within the perivenular tissue (Data not shown). The numbers of transmigrated leukocytes detected within the perivascular tissue after Dex DNA nanotube application (60 min: 2.8 +/- 0.9 /10^4 µm^2; 90 min: 4.2 +/- 1.6 /10^4 µm^2) were as low as in sham-operated animals (60 min: 2.2 +/- 0.7 /10^4 µm^2; 90 min: 4.2 +/- 1.6 /10^4 µm^2) at all investigated time points (Fig. 25C and D). The numbers of transmigrated leukocytes after microinjection of DNA nanotubes (60 min: 13.0 +/- 7.1 /10^4 µm^2; 90 min: 16.3 +/- 6.5 /10^4 µm^2), Dex ODNs (60 min: 10.7 +/- 2.8 /10^4 µm^2; 90 min: 16.8 +/- 3.7 /10^4 µm^2), and unconjugated dexamethasone (1 µg/ml; 60 min: 12.5 +/- 6.0 /10^4 µm^2; 90 min: 12.0 +/- 6.1 /10^4 µm^2) were comparable to the saline-injected control animals (60 min: 12.8 +/- 2.8 /10^4 µm^2; 90 min: 12.2 +/- 2.2 /10^4 µm^2). Interestingly, Dex tubes w/o i-motif had a contrary effect on leukocyte extravasation than their i-motif carrying counterparts (60 min: 21.3 +/- 4.8 /10^4 µm^2; 90 min: 24.2 +/- 5.5 /10^4 µm^2). The number of transmigrated leukocytes into the postischemic tissue was higher than in any other group (Fig. 25C and D).

Taken together, these data indicate that Dex tubes attenuate the recruitment of leukocytes into postischemic tissue, whereas Dex tubes w/o i-motif increase leukocyte recruitment under these sterile inflammatory conditions.

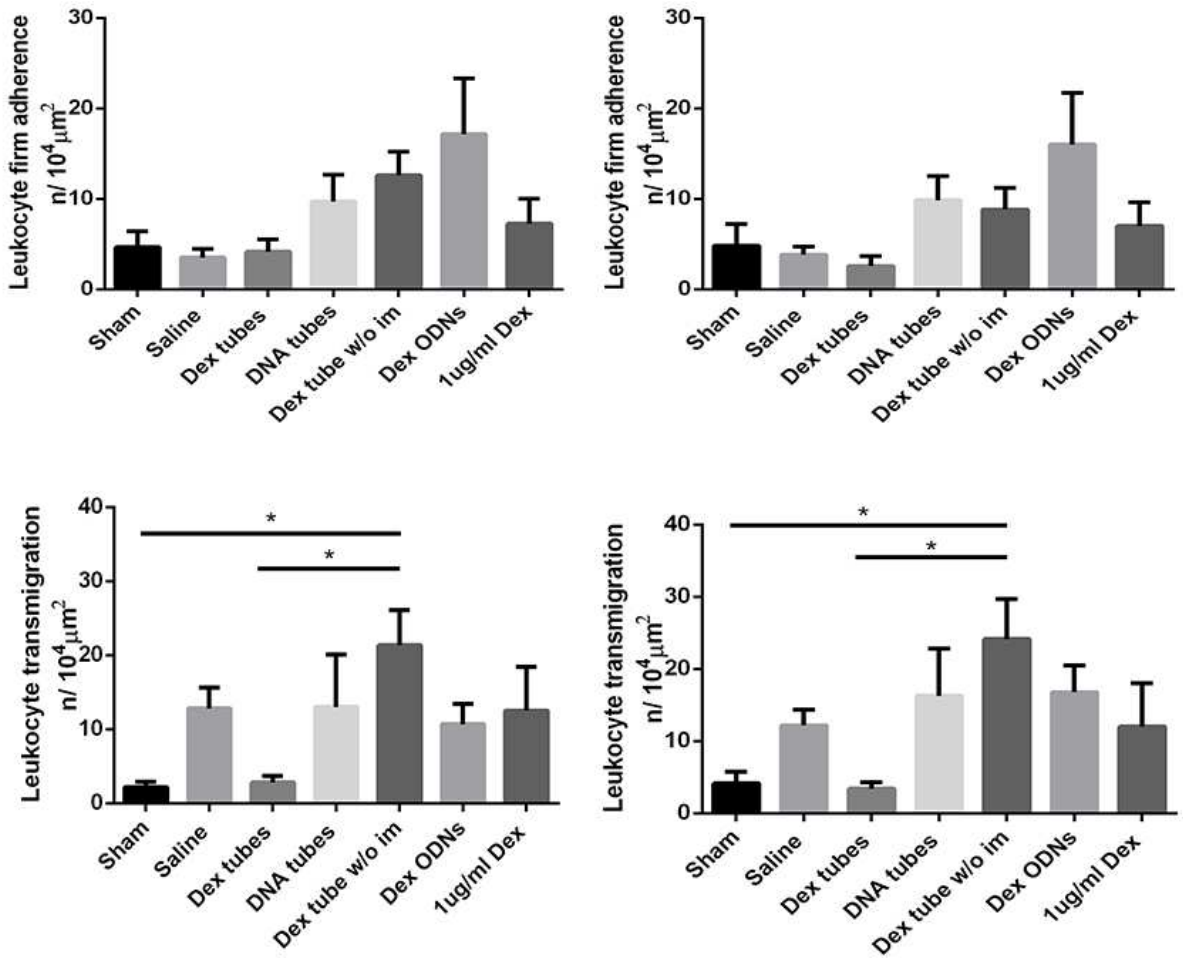

Fig. 25 *Quantitative analysis of intravascular adherence and transmigration of leukocytes after microinjection of Dex nanoconstructs.* Leukocyte adherence was quantified in postcapillary venules of the cremaster muscle using *in vivo* transillumination microscopy at 60 min (**A**) and 90 min (**B**) upon microinjection of Dex tubes, DNA tubes, Dex ODNs, Dex tubes w/o i-motif, dexamethasone, or saline into postischemic cremaster tissue at onset of reperfusion. The numbers of adherent leukocytes after injection of Dex tubes were as low as after injection of saline at 60 min and 90 min after reperfusion. Leukocyte transmigration was quantified at 60 min (**C**) and 90 min (**D**) after microinjection. Dex tube injection attenuated the transmigration of leukocytes into the tissue, whereas Dex tubes w/o i-motif induced transmigration of leukocytes into the postischemic tissue. (n=6, mean+/-SEM; *p<0.05 vs. all groups)

4.3.6 Systemic leukocyte counts and microhemodynamic parameters

Inner vessel diameter, wall shear stress, and blood flow velocities of analyzed postcapillary venules as well as leukocyte counts were determined to ensure intergroup comparability. No significant differences were present in the experimental groups (Table 3).

Experimental group	Inner vessel diameter [µm]	Blood flow velocity [mm/s]	Wall shear rate [1/s]	Systemic leukocyte counts [*10^6/ml]
Sham	27.8 ± 1.6	3.7 ± 0.3	4907 ± 446.8	3.8 ± 0.5
Saline	28.0 ± 0.5	3.1 ± 0.3	4349 ± 508.2	2.7 ± 0.3
Dex tubes	28.9 ± 2.0	3.7 ± 0.6	5294 ± 983.4	3.2 ± 0.7
Dex tubes w/o i-motif	30.5 ± 2.2	3.6 ± 0.4	4830 ± 834.6	5.2 ± 1.6
DNA tubes	27.6 ± 1.0	4.1 ± 0.4	5762 ± 728.3	4.4 ± 0.3
Dex ODNs	26.8 ± 1.8	4.0 ± 0.4	6328 ± 1177	2.4 ± 0.4
Dexamethasone 1 µg/ml	29.0 ± 2.0	3.3 ± 0.3	4372 ± 570	4.9 ± 0.9

Table 3 *Systemic leukocyte counts and microhemodynamic parameters*. Systemic leukocyte counts as well as microhemodynamic parameters, including inner vessel diameter, blood flow velocity, and wall shear rate, were obtained as detailed in *Materials and Methods* (mean ± SEM for *n*= 6 per group).

4.3.7 Dexamethasone-conjugated nanoconstructs are phagocytosed and stored in endolysosomal compartments of tissue-resident cells

Next, the cellular uptake and localization of Dex nanoconstructs in the postischemic mouse cremaster muscle was explored by means of *in vivo* fluorescence microscopy. Accordingly, fluorescently labeled Dex tubes, plain tubes, and Dex ODNs were concomitantly microinjected with LysoTracker dye in 25 µm to 50 µm distance to a postcapillary venule immediately after the release of the vascular clamp. After 60 min of reperfusion the muscle has been dissected for further analysis.

All Dex nanoconstructs were found in the endolysosomal compartment of cells present in the postischemic tissue (Fig. 26). As stated above, in the previous experiments, tissue-resident macrophages were identified as the population of phagocytes, which incorporate CpG nanoconstructs in the cremaster muscle under physiologic (Chapter 4.1) as well as under postischemic (Chapter 4.2) conditions. The morphology and the localization of cells, which incorporated Dex tubes in the postischemic cremaster, strongly suggest that these cells are tissue-resident macrophages.

However, the cellular uptake in the postischemic tissue occurs not within 5 min but within 30 min. Since the tissue is considerably damaged within 60 min of reperfusion, this might explain the delayed uptake by tissue macrophages, either by a restrained diffusion of the nanoconstructs or altered phagocytic preferences of these cells.

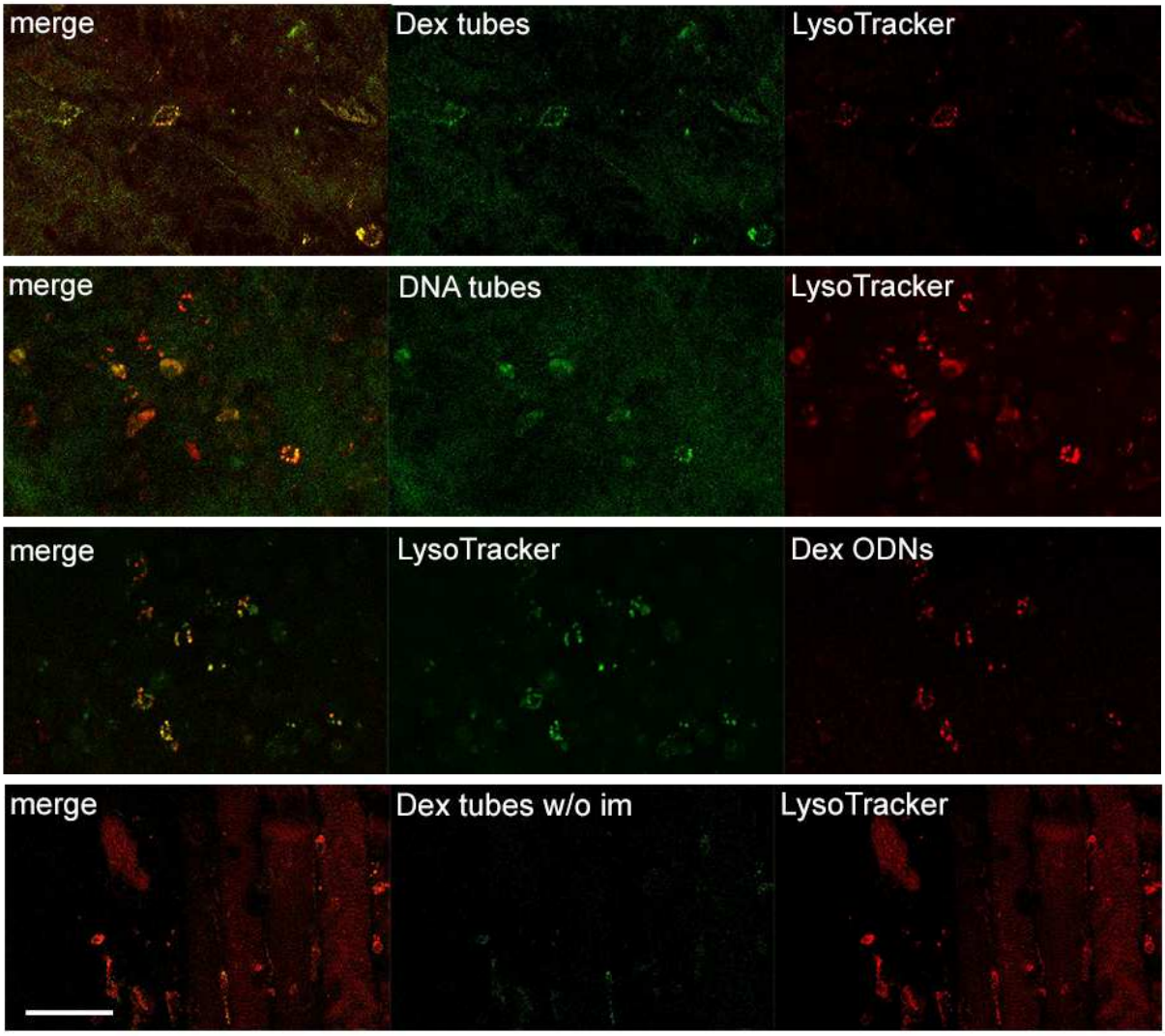

Fig. 26 *Localization of DNA nanoconstructs in the endolysosomes of tissue macrophages.* Confocal imaging of Dex tubes, DNA tubes, Dex ODNs, and Dex tubes w/o i-motif microinjected together with red or green emitting LysoTracker dye into the postischemic cremaster muscle. The fluorescence channel images were merged to determine co-localization (yellow). Images show that Dex tubes (green), DNA nanotubes (green), and Dex tubes w/o i-motif (green) were located in the cellular lysosomes (red). Dex ODNs (red) were microinjected with green LysoTracker (green) and were also detected in lysosomes. Scale bar: 50 µm.

4.3.8 Modulation of VCAM-1 and ICAM-1 expression by dexamethasone-conjugated nanoconstructs

One of the described effects of dexamethasone is the downregulation of endothelial adhesion molecules including VCAM-1 and ICAM-1 [150, 151]. To determine,

whether the downregulation of VCAM-1 and ICAM-1 contributes to the reduction of leukocyte transmigration after Dex tube application, immunostainings of postischemic cremasteric tissue for VCAM-1 and ICAM-1 and quantifications of the vascular expression using confocal microscopy were conducted.

60 min after application, VCAM-1 was continuously expressed in the microvasculature of saline-microinjected tissue, whereas Dex tube application almost completely abolished VCAM-1 fluorescence on the endothelium of vessels in close proximity to the injection site (Fig. 27A and B). PECAM-1, a marker for endothelial junctions [152], served as a vessel marker and there was no obvious effect of DNA nanoconstructs on PECAM-1 expression. Microinjection of DNA nanotubes, Dex ODNs, and Dex tubes w/o i-motif lowered the VCAM-1 expression on the endothelial surface compared to the control group, receiving saline. However, significantly more VCAM-1 was expressed on microvessels in these experimental groups than after Dex tube injection. Dex ODNs were hardly detectable after 1 h in the postischemic cremaster, probably due to degradation within the tissue (Fig. 27 and 28).

The suppressive effects of Dex tubes on ICAM-1 expression were significantly higher compared to the control group, but less pronounced than on VCAM-1 expression. Differences of microvascular ICAM-1 expression levels between saline and DNA tubes, Dex ODNs, and Dex tubes w/o i-motif-injected tissues could not be observed. The two adhesion molecules VCAM-1 and ICAM-1 are important mediators of leukocyte firm adhesion and transmigration from the blood into the tissue. The downregulation of both molecules after Dex tube injection might contribute to decreased influx of leukocytes into the tissue after I/R injury.

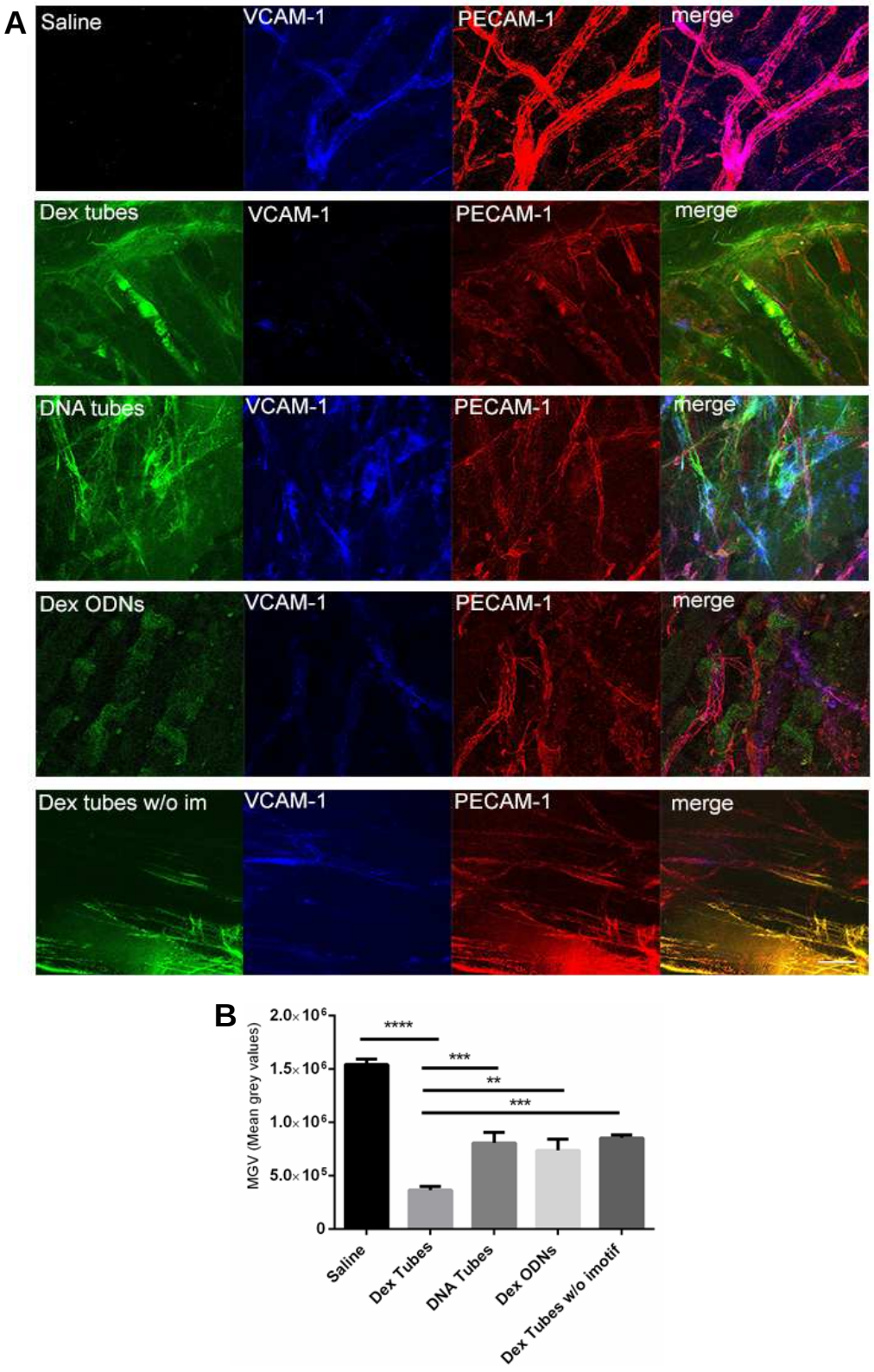

Fig. 27 *Expression patterns of VCAM-1 after application of Dex nanoconstructs into postischemic cremaster tissue.* Confocal immunofluorescence of Dex nanoconstructs (green), VCAM-1 (blue), and PECAM-1 (red) counterstaining showed significant lower VCAM-1 expression in vessels adjacent to the injection site of Dex tubes (**A, B**) compared to saline 60 min after application. Injection of DNA tubes, Dex tubes w/o i-motif as well as of Dex ODNs into the cremasteric tissue led to equivalent VCAM-1 expression levels 60 min after application (**A, B**). Scale bar: 50 µm.

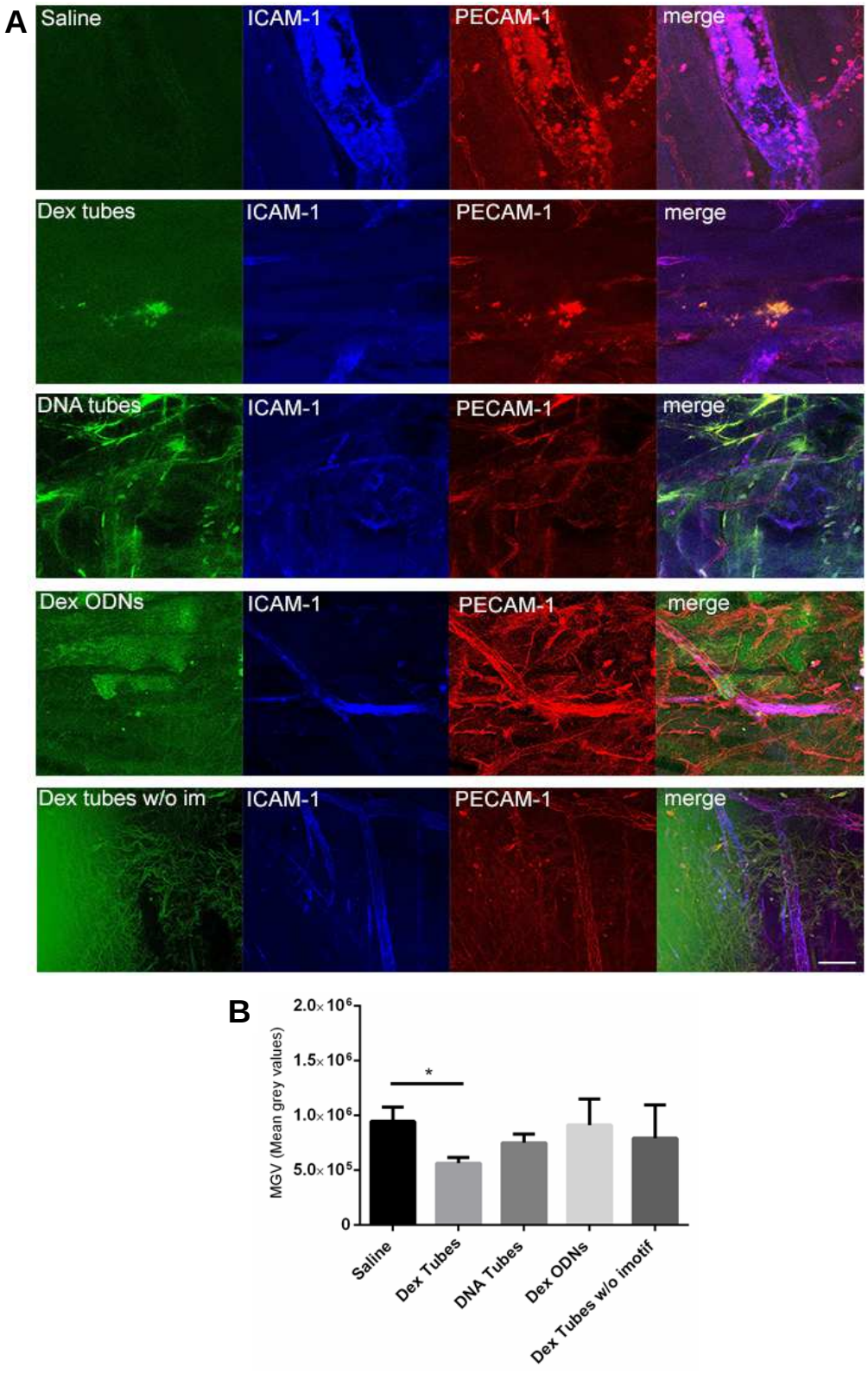

Fig. 28 *Expression patterns of ICAM-1 after application of Dex nanoconstructs into postischemic cremaster tissue.* Confocal immunofluorescence of Dex nanoconstructs (green), ICAM-1 (blue), and PECAM-1 (red) counterstaining showed significant reduction of ICAM-1 expression in vessels adjacent to the injection site of Dex tubes (**A, B**) compared to saline 60 min after application. Injection of DNA tubes, Dex tubes w/o i-motif as well as of Dex ODNs into the cremasteric tissue did not affect ICAM-1 expression 60 min after application (**A, B**). Scale bar: 50 µm.

5 Discussion

5.1 DNA nanotubes as intracellular delivery vehicles *in vivo*

Previous studies have proven that self-assembled DNA nanostructures can selectively release their payload at the target site and therefore are used as smart delivery systems in-vitro [153, 154]. Liedl and coworkers showed that CpG-conjugated DNA nanotubes, consisting of 30 helices and 62 CpG handles, led to a significantly enhanced expression of IL-6 and CD69 on isolated splenocytes compared to exposure of CpG ODNs [32]. This study was the basis for a cooperative project in the framework of the SFB1032 with the group of Tim Liedl and it was the starting point for the *in vivo* investigations of DNA nanotubes in this thesis.

In accordance with the previous work of Tim Liedl´s group, it could be demonstrated that RAW 264.7 macrophages produced considerably enhanced levels of TNF after CpG DNA nanotube exposure, whereas the cellular TNF response to CpG ODNs was low, although the applied CpG sequence “concentration” was the same. From these results and the performed stability experiments, it can be concluded that DNA nanotubes are stable over the course of application until their uptake by macrophages. This study also highlights, that complexation of CpG sequences is necessary to intensify the cellular TNF release since DNA nanotubes mixed with CpG ODNs failed to enhance this immune response.

These *in vitro* findings could be confirmed *in vivo*. Only application of CpG DNA tubes, but not the application of CpG ODNs into the murine skeletal muscle did entail immunostimulatory effects during the observation period. It has been previously described by Wu et al. that the aggregation of CpG ODNs is essential for the crosslink of TLR 9 receptors [155] and Kerkmann et al. showed that the formation of CpG ODNs to higher-ordered structures enhanced the cellular ability to produce IFN-

α [156]. Furthermore, linear CpG ODNs are quickly decomposed by exonucleases, whereas compaction and linkage to higher structures increases the resistance to DNAse substantially [153, 157]. The mechanism of action could be similar in our study. The CpG sequences are conjugated in high local densities to the tube structure, which could induce effective cross linkage of the TLR 9 receptor, causing the release of immunostimulatory mediators *in vitro* and *in vivo*.

Another requirement for the activation of TLR 9 is the cellular uptake of CpG DNA nanotubes. Phagocytosis of cellular debris and pathogens is prerequisite for the maintenance of tissue homeostasis and immune functions. Tissue-resident macrophages are professional phagocytes which fulfill these tasks [158]. It is well documented that alveolar macrophages phagocytose metal oxide NPs and as a result produce and release cytokines [159, 160]. Interestingly, surface chemistry plays a significant role in the uptake of nanomaterials and their pro-inflammatory properties. In previous works from our group, it could be demonstrated that solely negatively charged quantum dots (QDs) were taken up by perivascular macrophages from the bloodstream after intravenous administration and subsequently, leukocytes were recruited in mast cell-dependent manner [124, 136]. In a more recent study, we observed the rapid uptake of these negatively charged QDs by tissue-resident macrophages upon microinjection [161]. The uptake affinity of tissue-resident macrophages for negatively charged NPs was confirmed in the present study. Negatively charged DNA nanotubes (zeta potential; CpG tube: -13.2 +/- 0.4 mV and plain tube: -11.4 +/- 0.2 mV) could be found in the endolysosomes of tissue-resident macrophages within 5 min after microinjection.

In general, there are different routes of internalization by macrophages, such as constitutive micropinocytosis and clathrin-mediated uptake [162, 163]. A class of

receptors that mediate the endocytosis of pathogens and macromolecules in a clathrin-dependent or independent way are scavenger receptors [164, 165]. They are known for a rapid clearance of cell debris [166]. Expressed on macrophages, ECs, and smooth muscle cells, scavenger receptors recognize and bind negatively charged macromolecules, e.g., low-density lipoprotein. King et al. described that the scavenger receptor MARCO (macrophage receptor with collagenous structure) mediated the uptake of negatively charged, immune-modifying microparticles by inflammatory monocytes [167]. Minchin et al. recently showed, that the clearance of albumin-covered nanomaterials by macrophages is depending on scavenger receptor A1 (SR-A1) and MARCO [168]. The rapid internalization of DNA nanoconstructs, irrespective of the presence of a CpG motif, argues for an active uptake process, possibly receptor-mediated. The RAGE (receptor for advanced glycation end products) receptor, a pattern recognition receptor, is able to bind extracellular DNA and delivers it in the endosomal compartment to activate TLR 9 [113, 169]. This study could clearly demonstrate the rapid internalization of DNA nanotubes via the endolysosomal cellular compartment. The exact pathway of internalization and the contribution of specific scavenger or pattern recognition receptors to that process require further investigations.

Apart from macrophages, also mast cells contributed to the CpG DNA nanotube-induced immune response in the murine muscle tissue. Upon stimulation, mast cells release inflammatory mediators such as histamine, platelet-activating factor, or TNF from intracellular granula by rapid exocytosis [170, 171].

The numbers of transmigrated leukocytes upon microinjection of CpG nanotubes could be reduced to control levels in the presence of the mast cell stabilisator cromolyn [172, 173]. Mast cells, predominantly located in close vicinity to the

abluminal side of vessel walls [174], detect macrophage-derived cytokines [175, 176] via surface-localized cytokine receptors [129, 177] during the CpG nanotube-elicited inflammatory response. The uptake of DNA nanotubes by mast cells could not be detected by use of confocal microscopy, but direct mast cell activation can not be excluded. Nonetheless, the rapid increase in adherent leukocytes results from the amplification of the inflammatory signal cascade initiated by activated mast cells [178].

5.2 The impact of CpG DNA nanotubes on I/R injury

Inflammatory responses, initiated by innate immune cells, exert great influence on the extent of I/R injury [179]. The induction of this response is predominantly triggered via the activation of pattern recognition receptors, specifically TLRs, which are mainly expressed by DCs and macrophages. TLR deficiency, as well as preconditioning with their ligands has shown to be beneficial in the myocardial I/R model [180-183]. Recent studies indicate, that administration of CpG ODNs attenuates cerebral and myocardial I/R injuries [116, 184, 185]. Khandoga et al. have demonstrated the importance of TLR 2 for the transmigration of leukocytes in the I/R cremaster model [186]. Based on these results, the effects of the TLR 9 ligand CpG, conjugated to DNA nanoconstructs, on the recruitment of leukocytes in the murine cremaster I/R model were investigated.

The numbers of adherent and transmigrated leukocytes could not be significantly lowered by microinjection of CpG DNA nanotubes as compared to CpG ODNs. The conjugation of CpG to the DNA tube, which serves as delivery vehicle, could not enhance the protective effect of CpG DNA in postischemic tissue. In this context,

Zhou and colleagues could show that CpG ODNs bind to the cell surface and the immunogenic activity is enhanced at acidic extracellular pH [187] compared to neutral pH. During inflammation, the tissue pH is lowered [188, 189] and therefore association of unbound CpG ODNs compared to CpG DNA nanotubes might be preferred. This might possibly explain the greatly differing effects of CpG ODNs on leukocyte recruitment under physiological and pathological conditions. It has recently been described by Li et al., that the protective effects of CpG ODNs can be ascribed to the activation of the PI3K/AKT pathway, which promotes cell survival [116]. By strengthening the survival program of the cell prior to I/R injury, cells seem to be less susceptible to intrinsic apoptosis pathways which are triggered by DNA fragmentation, a major consequence of ischemia.

Interestingly, plain DNA tube administration implicated an enhanced transmigration of leukocytes. Although DNA has not been described yet as pro-inflammatory under ischemic conditions, it is described that the RAGE receptor, which is able to detect and bind DNA, mediates vascular injury and inflammation after global cerebral ischemia [190]. In our experiments, the externally administered DNA, in the form of DNA nanotubes, potentially induces this process. The possible mitigating effects of TLR 9 and PI3K/AKT activation due to the presence of CpG sequences in the CpG tube-treated experimental group are lacking after microinjection of DNA tubes.

A major finding was the enormous upregulation of TLR 9 expression and the morphological changes of tissue-resident macrophages after microinjection of CpG DNA constructs into the postischemic cremaster tissue. Particularly, administration of CpG DNA nanotubes resulted in a macrophage phenotype which was characterized by long protrusions and a continuous expression of TLR 9 covering the cell bodies. A connection between protrusions of different macrophages could not be detected by

means of confocal microscopy. Although TLR 9 is considered to be endosomally localized, recent publications describe a surface expression of TLR 9 on polymorphonuclear leukocytes (PMNLs) [191], splenic DCs [192], and peripheral blood mononuclear cells (PBMCs) [193], which are able to differentiate into macrophages. The dense “network” of highly ramified macrophages situated close to the scrotal cavity, might act as a barrier, similar to macrophages of many internal organs such as bladder, gut, peritoneal wall, and diaphragm, where they are positioned to build the first line of defense against invading pathogens [194].

The prevalent expression of TLR 9 in vessels, situated within the ischemic muscle tissue might exhibit another defense mechanism. The surface localization of TLR 9 allows a rapid recognition of pathogens, which is of great importance in essential organs, such as the brain. The risk of self-DNA recognition and consequently an autoimmune reaction can be minimized through a temporal upregulation or presentation of TLR 9, as Wang et al. described [195]. A general upregulation of TLR 9 in vessels could be observed in all experimental groups, but was pronounced in animals that received CpG DNA tubes and CpG ODNs, what might explain the susceptibility for the TLR 9 ligand in the I/R cremaster model.

Macrophages are probing their microenvironment and in response adapt their functional phenotype. Their ability to shift the phenotype is reversibly depending on the cytokine environment, as previously described by Suttles et al [196]. This functional plasticity of macrophages also implicates a morphological plasticity. The polarization state of macrophages is reflected by their appearance, since proinflammatory (M1) macrophages turn into flat, pancake-like cells whereas prohealing (M2) macrophages elongate their cell bodies in an *in vitro* model [197]. It is therefore not surprising, that elongated (possible M2) macrophages appear in the

postischemic cremaster tissue, where tissue is highly damaged due to inflammation and oxidative stress, triggered by reperfusion. M2 macrophages are contributing to the remodeling of the collagen network within the tissue and produce extracellular matrix components to promote wound healing processes [198]. Furthermore, the activity of M2 macrophages is strongly increased in sterile injuries [199]. Interestingly, TLR 9 agonists in combination with adenosine A_{2A} receptor ligands drive macrophages efficiently into a M2-like phenotype [200]. Adenosine, released by necrotic or apoptotic cells, is characteristic for the starting of the healing phase [201] and is recognized by the surface receptor A_{2A} on M2d macrophages [200]. A synergistic activity of adenosine and CpG ODNs may also implicate a surface localization of TLR 9. Confocal images (Fig. 19) suggest a surface localization of TLR 9 on CpG DNA nanotube-stimulated CX_3CR1-positive macrophages. But further investigations are necessary to answer the question, why CpG DNA nanotubes induce such an intensive TLR 9 expression in macrophages compared to CpG ODNs. Although CpG DNA nanotubes were not able to inhibit the infiltration of leukocytes into the ischemic muscle tissue as effective as CpG ODNs, they clearly feature an interesting tool to study macrophage morphologies under inflammatory conditions.

5.3 Dex tubes as anti-inflammatory agents *in vivo*

In this set of experiments, DNA nanotubes with amended basic structure were used. These newly generated DNA nanotubes consist of 84 nt long ODNs, forming a 6-helix structure with a length of ~30 nm and a diameter of ~6 nm. The use of 84 nt long ODNs enhanced the complementary region and compactness of the structure

itself. This implies a higher thermal stability, a higher resistance to Mg^{2+} depletion, and obstructed degradation through DNases present in the tissue [202]. DNA nanotubes could be detected up to 6 h after incubation within the cellular endolysosomes of MH-S macrophages, indicating a high “cellular” stability of the constructs, necessary for the successful intracellular delivery of the cargo. The environment in ischemic tissue *in vivo* is characterized by a low pH (pH 6.3-6.6) [203, 204], low levels of extracellular Mg^{2+} [205, 206], and elevated levels of DNase I in the serum [207, 208]. Despite this detrimental milieu, 6-helix DNA nanotubes were taken up by tissue-resident cells and were processed in their endolysosomal compartments (Fig. 26). Even though, the uptake was different from that under physiologic conditions, the rapid distribution and transport of NPs within a macrophage nanotube network, as Rehberg et al. has recently described [161], could also be observed for DNA nanotubes which have been microinjected into physiologic muscle tissue (Data not shown). This distribution of DNA nanoconstructs in a macrophage “network” was reduced in the cremasteric I/R model. Lerchenberger et al. described the remodeling and compaction of the collagen network within inflamed tissue [138], maybe causing hindered interstitial diffusion and cellular distribution of DNA nanoconstructs. Another explanation for the decelerated uptake of Dex nanoconstructs could be a reduced Fc-mediated phagocytosis and reduced TNF secretion by macrophages at acidic extracellular space [209]. Therefore, inflammatory conditions seem to have a great impact on the bioavailability of DNA nanoconstructs and the subsequent cellular reactions.

The attachment of folate receptor to the vehicle construct or the use of transfection reagent is often necessary for a successful delivery of cargo into target cells [210]. It has also been used for the selective delivery of diagnostic agents to activated

macrophages [211]. One of the biggest advantages of the DNA nanotube delivery system is that such modifications are not necessary to target tissue-resident macrophages.

Conventional therapeutic approaches operate with systemic applications of glucocorticoids, causing a bunch of side effects by affecting organs sensitive towards GCs, such as heart [212], brain [213], or bones [214]. Unwanted effects such as bone loss [215], insulin resistance [216], and sarcopenia [217] do not limit the therapeutic use of GCs in arthritis, inflammatory bowel disease, allergy, cancer, or transplant rejections. The dexamethasone concentrations used in cell culture and *in vivo* in this study were far lower than the ones therapeutically used and described as cytotoxic [142, 218]. But still, even at low concentrations, DNA nanotube-delivered dexamethasone revealed its anti-inflammatory impact without harming dexamethasone-sensitive cells such as macrophages [219]. Considering this finding in a broad context, the dosage of dexamethasone could be reduced by using DNA nanotubes as vectors without losing the pharmacological activity by selectively targeting inflammatory cells.

A key reason for the successful delivery of dexamethasone is certainly the pH-dependent conformational change of the DNA i-motif. Initially, the i-motif was discovered in human telomeric and centromeric sequences, as well as in intercalating RNA structures and proteins, interacting with cytosine repeats of DNA [220]. Nowadays, the i-motif has become an important feature in DNA nanotechnology, because it provides additional choices in design, assembly processes, and characteristics of DNA-based nanodevices. It has recently been used to fabricate nanostructures for the controlled release of small molecules [221] or the mapping of pH changes in living cells [222]. It could be demonstrated *in vitro* that the pH-

sensitive i-motif allows the controlled release of dexamethasone under acidic pH and at 37 °C (Fig. 20C). Although endosomal escape of dexamethasone *in vivo* by means of confocal microscopy could not be clearly proven, the data clearly indicate that Dex tubes enhanced the inhibition of cytokine production in response to LPS compared to a 20 times higher dose of unconjugated dexamethasone, which had no effect on leukocyte recruitment *in vivo*.

However, Dex tubes w/o i-motif enhanced the inflammatory response *in vitro* and *in vivo*. This was unexpected and could possibly be explained by the variations in the DNA sequence of the i-motif and the non-i-motif DNA tubes. The Dex tubes w/o i-motif carry a sequence solely consisting of thymine. Golenbock et al. reported that adenosine-thymine-rich DNA motifs are highly immunogenic and trigger the production of TNF and IL-6 in human and murine cells [223]. How exactly Dex tubes w/o i-motif are able to switch to this inflammatory program, needs to be further investigated.

The mechanism of action of dexamethasone is well described and starts with the binding to the cytoplasmatic glucocorticoid receptor (GR). The GR undergoes a conformational change, allowing the receptor-ligand complex to shuttle into the nucleus and actively influence gene transcription [224]. The dexamethasone/GR complex is a double-edged sword that is able to facilitate transcription, by binding to signal transducer and activator of transcription 5 (STAT5) as well as transrepression by preventing the activation of NF-*κ*B [225-227]. Since the inflammatory mediator TNF is regulated by the activation of NF-*κ*B [228] and the TNF response was substantially reduced by pretreatment with Dex tubes, the trafficking of delivered dexamethasone from the endosome into the nucleus can be assumed.

Along with the secretion of TNF, the expression of the cellular adhesion molecules VCAM-1 and ICAM-1 on the endothelium was diminished through the dexamethasone-induced repression of NF-*κ*B [229, 230]. Dex tubes could not be detected within endothelial cells by means of *in vivo* microscopy and confocal microscopy, therefore the downregulation of VCAM-1 and ICAM-1 on the endothelial surface in postischemic tissue might probably be a “secondary effect”, caused by macrophages. Shi and colleagues demonstrated that the expression of endothelial cell adhesion molecules is regulated by the inflammatory mediators TNF, IL-6, and IFN-γ, derived from macrophages, mast cells, and neutrophils [231]. In this study, TNF appeared to be the most potent of these cytokines to change expression levels of VCAM-1, ICAM-1, P-selectin, and E-selectin. These results support the view that the reduction of VCAM-1 and ICAM-1 after administration of Dex tubes is the result of a reduced TNF response. However, a direct Dex tube effect on ECs cannot be ruled out.

TNF overexpression, partly by monocytes or macrophages, is associated with a variety of diseases including HIV, cancer, rheumatoid arthritis, and Crohn´s disease [232]. TNF–directed therapies are the method of choice in the treatment of inflammatory diseases. Therefore, Dex tubes represent a promising nanomedical therapeutic alternative to the conventional anti-TNF agents, which cause a multitude of side effects due to their ubiquitous biodistribution. Considering the potential clinical use of Dex tubes, dose-response-, pharmacokinetics-, and safety-studies need to be carried out to outline therapeutic efficacy and applicability.

In summary, our findings demonstrate that DNA nanotubes allow a cell type-specific transport of dexamethasone, which lowers the effective concentration needed to gain anti-inflammatory effects.

5.4 Conclusion and future perspectives

In conclusion, this study describes a new DNA nanotube approach for the delivery of drugs or bioactive molecules into tissue-resident macrophages under physiological and pathological conditions.

Interestingly, DNA nanoconstructs were internalized by macrophages without the use of a transfection reagent or the conjugation of target-specific signals or antibodies [233]. Compared to other anionic nanomaterials, which need to be modified with receptors or signal peptides for cellular uptake [234, 235], DNA nanoconstructs can readily be designed for the molecular transportation of drugs or small molecules.

Although DNA nanoconstruct fluorescence could be detected within the cellular endolysosomes, it could not be determined whether the DNA architecture was still intact in the cells. Still, the functionality of cargo-carrying nanostructures in the mouse model was demonstrated, but for a next generation of DNA nanodevices, for example delivering RNA cargo, encoding transcription programs, construct stability, and further improvements are of great interest. But not solely stability determines the nanomedical development of DNA nanotechnology. These data convey a first impression of the distribution of DNA nanotubes and their target cells *in vivo,* but there is a general paucity of information on their long-term effects, immunogenicity and clearance. In addition to the understanding of pharmacokinetics and biodistribution, the production costs of DNA nanodevices are a major issue. Currently, large nanostructures cannot compete with polymer materials in terms of production expenses [236]. If DNA nanotechnology is able to overcome these challenges, it has the potential to serve as a programmable and multifunctional therapeutic system [237].

The results of this thesis provide new insights into the localization and the impact of DNA-based nanomaterials *in vivo* and allow for improved development of targeted therapies during inflammatory conditions.

6 References

[1] Borm PJ, Robbins D, Haubold S, Kuhlbusch T, Fissan H, Donaldson K, et al. The potential risks of nanomaterials: a review carried out for ECETOC. Part Fibre Toxicol. 2006;3:11.
[2] Khaydarov RA, Khaydarov RR, Gapurova O. Water purification from metal ions using carbon nanoparticle-conjugated polymer nanocomposites. Water Res. 2010;44:1927-33.
[3] Howes PD, Chandrawati R, Stevens MM. Bionanotechnology. Colloidal nanoparticles as advanced biological sensors. Science. 2014;346:1247390.
[4] Guo Y, Wang D, Song Q, Wu T, Zhuang X, Bao Y, et al. Erythrocyte Membrane-Enveloped Polymeric Nanoparticles as Nanovaccine for Induction of Antitumor Immunity against Melanoma. ACS Nano. 2015;9:6918-33.
[5] Singh R, Nalwa HS. Medical applications of nanoparticles in biological imaging, cell labeling, antimicrobial agents, and anticancer nanodrugs. J Biomed Nanotechnol. 2011;7:489-503.
[6] Reisch A, Klymchenko AS. Fluorescent Polymer Nanoparticles Based on Dyes: Seeking Brighter Tools for Bioimaging. Small. 2016;12:1968-92.
[7] Cai K, Wang AZ, Yin L, Cheng J. Bio-nano interface: The impact of biological environment on nanomaterials and their delivery properties. J Control Release. 2017.
[8] Monopoli MP, Aberg C, Salvati A, Dawson KA. Biomolecular coronas provide the biological identity of nanosized materials. Nature nanotechnology. 2012;7:779-86.
[9] Shang L, Nienhaus K, Nienhaus GU. Engineered nanoparticles interacting with cells: size matters. Journal of nanobiotechnology. 2014;12:5.
[10] Hirosue S, Kourtis IC, van der Vlies AJ, Hubbell JA, Swartz MA. Antigen delivery to dendritic cells by poly(propylene sulfide) nanoparticles with disulfide conjugated peptides: Cross-presentation and T cell activation. Vaccine. 2010;28:7897-906.
[11] Mahmoudi M, Saeedi-Eslami SN, Shokrgozar MA, Azadmanesh K, Hassanlou M, Kalhor HR, et al. Cell "vision": complementary factor of protein corona in nanotoxicology. Nanoscale. 2012;4:5461-8.
[12] Dobrovolskaia MA, McNeil SE. Immunological properties of engineered nanomaterials. Nature nanotechnology. 2007;2:469-78.
[13] Jones MR, Seeman NC, Mirkin CA. Nanomaterials. Programmable materials and the nature of the DNA bond. Science. 2015;347:1260901.
[14] Seeman NC. Nucleic acid junctions and lattices. Journal of theoretical biology. 1982;99:237-47.
[15] Seeman NC, Kallenbach NR. Design of immobile nucleic acid junctions. Biophysical journal. 1983;44:201-9.
[16] Benson E, Mohammed A, Gardell J, Masich S, Czeizler E, Orponen P, et al. DNA rendering of polyhedral meshes at the nanoscale. Nature. 2015;523:441-4.
[17] Han D, Pal S, Nangreave J, Deng Z, Liu Y, Yan H. DNA origami with complex curvatures in three-dimensional space. Science. 2011;332:342-6.
[18] Rothemund PW. Folding DNA to create nanoscale shapes and patterns. Nature. 2006;440:297-302.
[19] Douglas SM, Dietz H, Liedl T, Hogberg B, Graf F, Shih WM. Self-assembly of DNA into nanoscale three-dimensional shapes. Nature. 2009;459:414-8.
[20] Yan H, Park SH, Finkelstein G, Reif JH, LaBean TH. DNA-templated self-assembly of protein arrays and highly conductive nanowires. Science. 2003;301:1882-4.
[21] Park SH, Yin P, Liu Y, Reif JH, LaBean TH, Yan H. Programmable DNA self-assemblies for nanoscale organization of ligands and proteins. Nano letters. 2005;5:729-33.
[22] Sacca B, Meyer R, Erkelenz M, Kiko K, Arndt A, Schroeder H, et al. Orthogonal protein decoration of DNA origami. Angew Chem Int Ed Engl. 2010;49:9378-83.
[23] Mirkin CA, Letsinger RL, Mucic RC, Storhoff JJ. A DNA-based method for rationally assembling nanoparticles into macroscopic materials. Nature. 1996;382:607-9.
[24] Tikhomirov G, Hoogland S, Lee PE, Fischer A, Sargent EH, Kelley SO. DNA-based programming of quantum dot valency, self-assembly and luminescence. Nature nanotechnology. 2011;6:485-90.
[25] Ding B, Deng Z, Yan H, Cabrini S, Zuckermann RN, Bokor J. Gold nanoparticle self-similar chain structure organized by DNA origami. Journal of the American Chemical Society. 2010;132:3248-9.

[26] Maune HT, Han SP, Barish RD, Bockrath M, Iii WA, Rothemund PW, et al. Self-assembly of carbon nanotubes into two-dimensional geometries using DNA origami templates. Nature nanotechnology. 2010;5:61-6.
[27] Rothemund PW, Andersen ES. Nanotechnology: The importance of being modular. Nature. 2012;485:584-5.
[28] Mei Q, Wei X, Su F, Liu Y, Youngbull C, Johnson R, et al. Stability of DNA origami nanoarrays in cell lysate. Nano letters. 2011;11:1477-82.
[29] Endo M, Katsuda Y, Hidaka K, Sugiyama H. Regulation of DNA methylation using different tensions of double strands constructed in a defined DNA nanostructure. Journal of the American Chemical Society. 2010;132:1592-7.
[30] Lund K, Manzo AJ, Dabby N, Michelotti N, Johnson-Buck A, Nangreave J, et al. Molecular robots guided by prescriptive landscapes. Nature. 2010;465:206-10.
[31] Voigt NV, Torring T, Rotaru A, Jacobsen MF, Ravnsbaek JB, Subramani R, et al. Single-molecule chemical reactions on DNA origami. Nature nanotechnology. 2010;5:200-3.
[32] Schuller VJ, Heidegger S, Sandholzer N, Nickels PC, Suhartha NA, Endres S, et al. Cellular immunostimulation by CpG-sequence-coated DNA origami structures. ACS Nano. 2011;5:9696-702.
[33] Surana S, Shenoy AR, Krishnan Y. Designing DNA nanodevices for compatibility with the immune system of higher organisms. Nat Nanotechnol. 2015;10:741-7.
[34] Wei B, Dai M, Yin P. Complex shapes self-assembled from single-stranded DNA tiles. Nature. 2012;485:623-6.
[35] Douglas SM, Bachelet I, Church GM. A logic-gated nanorobot for targeted transport of molecular payloads. Science. 2012;335:831-4.
[36] Castro CE, Kilchherr F, Kim DN, Shiao EL, Wauer T, Wortmann P, et al. A primer to scaffolded DNA origami. Nature methods. 2011;8:221-9.
[37] Walsh AS, Yin H, Erben CM, Wood MJ, Turberfield AJ. DNA cage delivery to mammalian cells. ACS nano. 2011;5:5427-32.
[38] Conway JW, McLaughlin CK, Castor KJ, Sleiman H. DNA nanostructure serum stability: greater than the sum of its parts. Chem Commun (Camb). 2013;49:1172-4.
[39] You M, Peng L, Shao N, Zhang L, Qiu L, Cui C, et al. DNA "nano-claw": logic-based autonomous cancer targeting and therapy. Journal of the American Chemical Society. 2014;136:1256-9.
[40] Ko S, Liu H, Chen Y, Mao C. DNA nanotubes as combinatorial vehicles for cellular delivery. Biomacromolecules. 2008;9:3039-43.
[41] Erbacher P, Zou S, Bettinger T, Steffan AM, Remy JS. Chitosan-based vector/DNA complexes for gene delivery: biophysical characteristics and transfection ability. Pharmaceutical research. 1998;15:1332-9.
[42] Conner SD, Schmid SL. Regulated portals of entry into the cell. Nature. 2003;422:37-44.
[43] Aderem A, Underhill DM. Mechanisms of phagocytosis in macrophages. Annual review of immunology. 1999;17:593-623.
[44] May RC, Machesky LM. Phagocytosis and the actin cytoskeleton. Journal of cell science. 2001;114:1061-77.
[45] Nel AE, Madler L, Velegol D, Xia T, Hoek EM, Somasundaran P, et al. Understanding biophysicochemical interactions at the nano-bio interface. Nature materials. 2009;8:543-57.
[46] Takeshita H, Yasuda T, Nakajima T, Hosomi O, Nakashima Y, Kishi K. Mouse deoxyribonuclease I (DNase I): biochemical and immunological characterization, cDNA structure and tissue distribution. Biochemistry and molecular biology international. 1997;42:65-75.
[47] Ding XQ, Quiambao AB, Fitzgerald JB, Cooper MJ, Conley SM, Naash MI. Ocular delivery of compacted DNA-nanoparticles does not elicit toxicity in the mouse retina. PloS one. 2009;4:e7410.
[48] Yurek DM, Fletcher AM, McShane M, Kowalczyk TH, Padegimas L, Weatherspoon MR, et al. DNA nanoparticles: detection of long-term transgene activity in brain using bioluminescence imaging. Molecular imaging. 2011;10:327-39.
[49] Wynn TA, Chawla A, Pollard JW. Macrophage biology in development, homeostasis and disease. Nature. 2013;496:445-55.

[50] Cooper MD, Alder MN. The evolution of adaptive immune systems. Cell. 2006;124:815-22.
[51] Ajuebor MN, Das AM, Virag L, Flower RJ, Szabo C, Perretti M. Role of resident peritoneal macrophages and mast cells in chemokine production and neutrophil migration in acute inflammation: evidence for an inhibitory loop involving endogenous IL-10. J Immunol. 1999;162:1685-91.
[52] Farr AG, Kiely JM, Unanue ER. Macrophage-T cell interactions involving Listeria monocytogenes--role of the H-2 gene complex. J Immunol. 1979;122:2395-404.
[53] Badylak SF, Valentin JE, Ravindra AK, McCabe GP, Stewart-Akers AM. Macrophage phenotype as a determinant of biologic scaffold remodeling. Tissue engineering Part A. 2008;14:1835-42.
[54] Kohyama M, Ise W, Edelson BT, Wilker PR, Hildner K, Mejia C, et al. Role for Spi-C in the development of red pulp macrophages and splenic iron homeostasis. Nature. 2009;457:318-21.
[55] Auffray C, Sieweke MH, Geissmann F. Blood monocytes: development, heterogeneity, and relationship with dendritic cells. Annual review of immunology. 2009;27:669-92.
[56] Geissmann F, Jung S, Littman DR. Blood monocytes consist of two principal subsets with distinct migratory properties. Immunity. 2003;19:71-82.
[57] Jakubzick C, Gautier EL, Gibbings SL, Sojka DK, Schlitzer A, Johnson TE, et al. Minimal differentiation of classical monocytes as they survey steady-state tissues and transport antigen to lymph nodes. Immunity. 2013;39:599-610.
[58] Tamoutounour S, Guilliams M, Montanana Sanchis F, Liu H, Terhorst D, Malosse C, et al. Origins and functional specialization of macrophages and of conventional and monocyte-derived dendritic cells in mouse skin. Immunity. 2013;39:925-38.
[59] Swirski FK, Nahrendorf M, Etzrodt M, Wildgruber M, Cortez-Retamozo V, Panizzi P, et al. Identification of splenic reservoir monocytes and their deployment to inflammatory sites. Science. 2009;325:612-6.
[60] Shi C, Pamer EG. Monocyte recruitment during infection and inflammation. Nature reviews Immunology. 2011;11:762-74.
[61] Robbins CS, Hilgendorf I, Weber GF, Theurl I, Iwamoto Y, Figueiredo JL, et al. Local proliferation dominates lesional macrophage accumulation in atherosclerosis. Nature medicine. 2013;19:1166-72.
[62] Cheong C, Matos I, Choi JH, Dandamudi DB, Shrestha E, Longhi MP, et al. Microbial stimulation fully differentiates monocytes to DC-SIGN/CD209(+) dendritic cells for immune T cell areas. Cell. 2010;143:416-29.
[63] Arnold L, Henry A, Poron F, Baba-Amer Y, van Rooijen N, Plonquet A, et al. Inflammatory monocytes recruited after skeletal muscle injury switch into antiinflammatory macrophages to support myogenesis. The Journal of experimental medicine. 2007;204:1057-69.
[64] Hume DA, MacDonald KP. Therapeutic applications of macrophage colony-stimulating factor-1 (CSF-1) and antagonists of CSF-1 receptor (CSF-1R) signaling. Blood. 2012;119:1810-20.
[65] Masteller EL, Wong BR. Targeting IL-34 in chronic inflammation. Drug discovery today. 2014;19:1212-6.
[66] Ginhoux F, Greter M, Leboeuf M, Nandi S, See P, Gokhan S, et al. Fate mapping analysis reveals that adult microglia derive from primitive macrophages. Science. 2010;330:841-5.
[67] Yona S, Kim KW, Wolf Y, Mildner A, Varol D, Breker M, et al. Fate mapping reveals origins and dynamics of monocytes and tissue macrophages under homeostasis. Immunity. 2013;38:79-91.
[68] Hashimoto D, Chow A, Noizat C, Teo P, Beasley MB, Leboeuf M, et al. Tissue-resident macrophages self-maintain locally throughout adult life with minimal contribution from circulating monocytes. Immunity. 2013;38:792-804.
[69] Epelman S, Lavine KJ, Beaudin AE, Sojka DK, Carrero JA, Calderon B, et al. Embryonic and adult-derived resident cardiac macrophages are maintained through distinct mechanisms at steady state and during inflammation. Immunity. 2014;40:91-104.
[70] Epelman S, Lavine KJ, Randolph GJ. Origin and functions of tissue macrophages. Immunity. 2014;41:21-35.

[71] N AG, Guillen JA, Gallardo G, Diaz M, de la Rosa JV, Hernandez IH, et al. The nuclear receptor LXRalpha controls the functional specialization of splenic macrophages. Nature immunology. 2013;14:831-9.
[72] Davies LC, Rosas M, Jenkins SJ, Liao CT, Scurr MJ, Brombacher F, et al. Distinct bone marrow-derived and tissue-resident macrophage lineages proliferate at key stages during inflammation. Nature communications. 2013;4:1886.
[73] Gosselin D, Link VM, Romanoski CE, Fonseca GJ, Eichenfield DZ, Spann NJ, et al. Environment drives selection and function of enhancers controlling tissue-specific macrophage identities. Cell. 2014;159:1327-40.
[74] Gautier EL, Shay T, Miller J, Greter M, Jakubzick C, Ivanov S, et al. Gene-expression profiles and transcriptional regulatory pathways that underlie the identity and diversity of mouse tissue macrophages. Nature immunology. 2012;13:1118-28.
[75] Minkin C, Jennings JM. Carbonic anhydrase and bone remodeling: sulfonamide inhibition of bone resorption in organ culture. Science. 1972;176:1031-3.
[76] Parkhurst CN, Yang G, Ninan I, Savas JN, Yates JR, 3rd, Lafaille JJ, et al. Microglia promote learning-dependent synapse formation through brain-derived neurotrophic factor. Cell. 2013;155:1596-609.
[77] Boyle WJ, Simonet WS, Lacey DL. Osteoclast differentiation and activation. Nature. 2003;423:337-42.
[78] Lavin Y, Winter D, Blecher-Gonen R, David E, Keren-Shaul H, Merad M, et al. Tissue-resident macrophage enhancer landscapes are shaped by the local microenvironment. Cell. 2014;159:1312-26.
[79] Geissmann F, Manz MG, Jung S, Sieweke MH, Merad M, Ley K. Development of monocytes, macrophages, and dendritic cells. Science. 2010;327:656-61.
[80] Martinon F, Burns K, Tschopp J. The inflammasome: a molecular platform triggering activation of inflammatory caspases and processing of proIL-beta. Molecular cell. 2002;10:417-26.
[81] Abtin A, Jain R, Mitchell AJ, Roediger B, Brzoska AJ, Tikoo S, et al. Perivascular macrophages mediate neutrophil recruitment during bacterial skin infection. Nature immunology. 2014;15:45-53.
[82] Krausgruber T, Blazek K, Smallie T, Alzabin S, Lockstone H, Sahgal N, et al. IRF5 promotes inflammatory macrophage polarization and TH1-TH17 responses. Nature immunology. 2011;12:231-8.
[83] Davies LC, Rosas M, Smith PJ, Fraser DJ, Jones SA, Taylor PR. A quantifiable proliferative burst of tissue macrophages restores homeostatic macrophage populations after acute inflammation. European journal of immunology. 2011;41:2155-64.
[84] Jenkins SJ, Ruckerl D, Cook PC, Jones LH, Finkelman FD, van Rooijen N, et al. Local macrophage proliferation, rather than recruitment from the blood, is a signature of TH2 inflammation. Science. 2011;332:1284-8.
[85] Cailhier JF, Partolina M, Vuthoori S, Wu S, Ko K, Watson S, et al. Conditional macrophage ablation demonstrates that resident macrophages initiate acute peritoneal inflammation. J Immunol. 2005;174:2336-42.
[86] Kolaczkowska E, Goldys A, Kozakiewicz E, Lelito M, Plytycz B, van Rooijen N, et al. Resident peritoneal macrophages and mast cells are important cellular sites of COX-1 and COX-2 activity during acute peritoneal inflammation. Archivum immunologiae et therapiae experimentalis. 2009;57:459-66.
[87] Kolaczkowska E, Lelito M, Kozakiewicz E, van Rooijen N, Plytycz B, Arnold B. Resident peritoneal leukocytes are important sources of MMP-9 during zymosan peritonitis: superior contribution of macrophages over mast cells. Immunology letters. 2007;113:99-106.
[88] Biswas SK, Mantovani A. Macrophage plasticity and interaction with lymphocyte subsets: cancer as a paradigm. Nature immunology. 2010;11:889-96.
[89] Mosser DM, Edwards JP. Exploring the full spectrum of macrophage activation. Nat Rev Immunol. 2008;8:958-69.

[90] Anthony RM, Urban JF, Jr., Alem F, Hamed HA, Rozo CT, Boucher JL, et al. Memory T(H)2 cells induce alternatively activated macrophages to mediate protection against nematode parasites. Nature medicine. 2006;12:955-60.
[91] Fleming BD, Mosser DM. Regulatory macrophages: setting the threshold for therapy. Eur J Immunol. 2011;41:2498-502.
[92] Martinez FO, Sica A, Mantovani A, Locati M. Macrophage activation and polarization. Frontiers in bioscience : a journal and virtual library. 2008;13:453-61.
[93] Erwig LP, Henson PM. Immunological consequences of apoptotic cell phagocytosis. The American journal of pathology. 2007;171:2-8.
[94] Strassmann G, Patil-Koota V, Finkelman F, Fong M, Kambayashi T. Evidence for the involvement of interleukin 10 in the differential deactivation of murine peritoneal macrophages by prostaglandin E2. The Journal of experimental medicine. 1994;180:2365-70.
[95] Orkin SH, Zon LI. SnapShot: hematopoiesis. Cell. 2008;132:712.
[96] Voisin MB, Nourshargh S. Neutrophil transmigration: emergence of an adhesive cascade within venular walls. Journal of innate immunity. 2013;5:336-47.
[97] Medzhitov R. Inflammation 2010: new adventures of an old flame. Cell. 2010;140:771-6.
[98] Finegold JA, Asaria P, Francis DP. Mortality from ischaemic heart disease by country, region, and age: statistics from World Health Organisation and United Nations. International journal of cardiology. 2013;168:934-45.
[99] Yellon DM, Hausenloy DJ. Myocardial reperfusion injury. The New England journal of medicine. 2007;357:1121-35.
[100] Carden DL, Granger DN. Pathophysiology of ischaemia-reperfusion injury. J Pathol. 2000;190:255-66.
[101] Chen GY, Nunez G. Sterile inflammation: sensing and reacting to damage. Nature reviews Immunology. 2010;10:826-37.
[102] Sharma HS, Das DK. Role of cytokines in myocardial ischemia and reperfusion. Mediators of inflammation. 1997;6:175-83.
[103] Ley K. Healing without inflammation? American journal of physiology Regulatory, integrative and comparative physiology. 2003;285:R718-9.
[104] Khandoga A, Kessler JS, Meissner H, Hanschen M, Corada M, Motoike T, et al. Junctional adhesion molecule-A deficiency increases hepatic ischemia-reperfusion injury despite reduction of neutrophil transendothelial migration. Blood. 2005;106:725-33.
[105] Eltzschig HK, Collard CD. Vascular ischaemia and reperfusion injury. British medical bulletin. 2004;70:71-86.
[106] Shimamoto A, Chong AJ, Yada M, Shomura S, Takayama H, Fleisig AJ, et al. Inhibition of Toll-like receptor 4 with eritoran attenuates myocardial ischemia-reperfusion injury. Circulation. 2006;114:I270-4.
[107] Hua F, Ma J, Ha T, Kelley J, Williams DL, Kao RL, et al. Preconditioning with a TLR2 specific ligand increases resistance to cerebral ischemia/reperfusion injury. J Neuroimmunol. 2008;199:75-82.
[108] Leung PY, Stevens SL, Packard AE, Lessov NS, Yang T, Conrad VK, et al. Toll-like receptor 7 preconditioning induces robust neuroprotection against stroke by a novel type I interferon-mediated mechanism. Stroke; a journal of cerebral circulation. 2012;43:1383-9.
[109] Marsh B, Stevens SL, Packard AE, Gopalan B, Hunter B, Leung PY, et al. Systemic lipopolysaccharide protects the brain from ischemic injury by reprogramming the response of the brain to stroke: a critical role for IRF3. J Neurosci. 2009;29:9839-49.
[110] Stevens SL, Ciesielski TM, Marsh BJ, Yang T, Homen DS, Boule JL, et al. Toll-like receptor 9: a new target of ischemic preconditioning in the brain. J Cereb Blood Flow Metab. 2008;28:1040-7.
[111] Packard AE, Hedges JC, Bahjat FR, Stevens SL, Conlin MJ, Salazar AM, et al. Poly-IC preconditioning protects against cerebral and renal ischemia-reperfusion injury. Journal of cerebral blood flow and metabolism : official journal of the International Society of Cerebral Blood Flow and Metabolism. 2012;32:242-7.

[112] Kawai T, Akira S. The role of pattern-recognition receptors in innate immunity: update on Toll-like receptors. Nature immunology. 2010;11:373-84.
[113] Tian J, Avalos AM, Mao SY, Chen B, Senthil K, Wu H, et al. Toll-like receptor 9-dependent activation by DNA-containing immune complexes is mediated by HMGB1 and RAGE. Nature immunology. 2007;8:487-96.
[114] Leadbetter EA, Rifkin IR, Hohlbaum AM, Beaudette BC, Shlomchik MJ, Marshak-Rothstein A. Chromatin-IgG complexes activate B cells by dual engagement of IgM and Toll-like receptors. Nature. 2002;416:603-7.
[115] Li X, Jiang S, Tapping RI. Toll-like receptor signaling in cell proliferation and survival. Cytokine. 2010;49:1-9.
[116] Lu C, Ha T, Wang X, Liu L, Zhang X, Kimbrough EO, et al. The TLR9 ligand, CpG-ODN, induces protection against cerebral ischemia/reperfusion injury via activation of PI3K/Akt signaling. Journal of the American Heart Association. 2014;3:e000629.
[117] Yin P, Hariadi RF, Sahu S, Choi HM, Park SH, Labean TH, et al. Programming DNA tube circumferences. Science. 2008;321:824-6.
[118] Acedo M, Tarrason G, Piulats J, Mann M, Wilm M, Eritja R. Preparation of Oligonucleotide-Dexamethasone Conjugates. Bioorg Med Chem Lett. 1995;5:1577-80.
[119] Sorensen RS, Okholm AH, Schaffert D, Kodal AL, Gothelf KV, Kjems J. Enzymatic ligation of large biomolecules to DNA. ACS Nano. 2013;7:8098-104.
[120] Jung S, Aliberti J, Graemmel P, Sunshine MJ, Kreutzberg GW, Sher A, et al. Analysis of fractalkine receptor CX(3)CR1 function by targeted deletion and green fluorescent protein reporter gene insertion. Mol Cell Biol. 2000;20:4106-14.
[121] Baez S. An open cremaster muscle preparation for the study of blood vessels by in vivo microscopy. Microvascular research. 1973;5:384-94.
[122] Lipowsky HH, Zweifach BW. Application of the "two-slit" photometric technique to the measurement of microvascular volumetric flow rates. Microvascular research. 1978;15:93-101.
[123] Mempel TR, Moser C, Hutter J, Kuebler WM, Krombach F. Visualization of leukocyte transendothelial and interstitial migration using reflected light oblique transillumination in intravital video microscopy. Journal of vascular research. 2003;40:435-41.
[124] Rehberg M, Praetner M, Leite CF, Reichel CA, Bihari P, Mildner K, et al. Quantum dots modulate leukocyte adhesion and transmigration depending on their surface modification. Nano letters. 2010;10:3656-64.
[125] Sellner S, Kocabey S, Nekolla K, Krombach F, Liedl T, Rehberg M. DNA nanotubes as intracellular delivery vehicles in vivo. Biomaterials. 2015;53:453-63.
[126] Krieg AM, Yi AK, Matson S, Waldschmidt TJ, Bishop GA, Teasdale R, et al. CpG motifs in bacterial DNA trigger direct B-cell activation. Nature. 1995;374:546-9.
[127] Sasmono RT, Williams E. Generation and characterization of MacGreen mice, the Cfs1r-EGFP transgenic mice. Methods Mol Biol. 2012;844:157-76.
[128] Khandoga AG, Khandoga A, Reichel CA, Bihari P, Rehberg M, Krombach F. In vivo imaging and quantitative analysis of leukocyte directional migration and polarization in inflamed tissue. PloS one. 2009;4:e4693.
[129] Abraham SN, St John AL. Mast cell-orchestrated immunity to pathogens. Nature reviews Immunology. 2010;10:440-52.
[130] Kunder CA, St John AL, Abraham SN. Mast cell modulation of the vascular and lymphatic endothelium. Blood. 2011;118:5383-93.
[131] Guo Y, Lindbom L, Hedqvist P. Spontaneous leukocyte rolling in rat and mouse microvessels is independent of mast cell activity. Inflammation research : official journal of the European Histamine Research Society [et al]. 2000;49:325-9.
[132] Zhang G, Ghosh S. Toll-like receptor-mediated NF-kappaB activation: a phylogenetically conserved paradigm in innate immunity. The Journal of clinical investigation. 2001;107:13-9.
[133] Tak PP, Firestein GS. NF-kappaB: a key role in inflammatory diseases. The Journal of clinical investigation. 2001;107:7-11.

[134] Coussens LM, Werb Z. Inflammation and cancer. Nature. 2002;420:860-7.
[135] Maguire O, Collins C, O'Loughlin K, Miecznikowski J, Minderman H. Quantifying nuclear p65 as a parameter for NF-kappaB activation: Correlation between ImageStream cytometry, microscopy, and Western blot. Cytometry Part A : the journal of the International Society for Analytical Cytology. 2011;79:461-9.
[136] Rehberg M, Leite CF, Mildner K, Horstkotte J, Zeuschner D, Krombach F. Surface chemistry of quantum dots determines their behavior in postischemic tissue. ACS nano. 2012;6:1370-9.
[137] Juskewitch JE, Platt JL, Knudsen BE, Knutson KL, Brunn GJ, Grande JP. Disparate roles of marrow- and parenchymal cell-derived TLR4 signaling in murine LPS-induced systemic inflammation. Scientific reports. 2012;2:918.
[138] Lerchenberger M, Uhl B, Stark K, Zuchtriegel G, Eckart A, Miller M, et al. Matrix metalloproteinases modulate ameboid-like migration of neutrophils through inflamed interstitial tissue. Blood. 2013;122:770-80.
[139] Gehring K, Leroy JL, Gueron M. A tetrameric DNA structure with protonated cytosine.cytosine base pairs. Nature. 1993;363:561-5.
[140] Leroy JL, Gehring K, Kettani A, Gueron M. Acid multimers of oligodeoxycytidine strands: stoichiometry, base-pair characterization, and proton exchange properties. Biochemistry. 1993;32:6019-31.
[141] Liu D, Balasubramanian S. A proton-fuelled DNA nanomachine. Angewandte Chemie. 2003;42:5734-6.
[142] Nestler U, Winking M, Boker DK. The tissue level of dexamethasone in human brain tumors is about 1000 times lower than the cytotoxic concentration in cell culture. Neurological research. 2002;24:479-82.
[143] Migliorati G, Nicoletti I, D'Adamio F, Spreca A, Pagliacci C, Riccardi C. Dexamethasone induces apoptosis in mouse natural killer cells and cytotoxic T lymphocytes. Immunology. 1994;81:21-6.
[144] Carollo M, Parente L, D'Alessandro N. Dexamethasone-induced cytotoxic activity and drug resistance effects in androgen-independent prostate tumor PC-3 cells are mediated by lipocortin 1. Oncology research. 1998;10:245-54.
[145] Lin G, Pearson AE, Scamurra RW, Zhou Y, Baarsch MJ, Weiss DJ, et al. Regulation of interleukin-8 expression in porcine alveolar macrophages by bacterial lipopolysaccharide. The Journal of biological chemistry. 1994;269:77-85.
[146] John M, Lim S, Seybold J, Jose P, Robichaud A, O'Connor B, et al. Inhaled corticosteroids increase interleukin-10 but reduce macrophage inflammatory protein-1alpha, granulocyte-macrophage colony-stimulating factor, and interferon-gamma release from alveolar macrophages in asthma. American journal of respiratory and critical care medicine. 1998;157:256-62.
[147] Meng A, Wang B, Zhang X, Qi N, Liu D, Wu J. Additive Suppression of LPS-Induced IL-10 and TNF-alpha by Pre-treatment of Dexamethasone and SB203580 in a Murine Alveolar Macrophage Cell Line (MH-S). Inflammation. 2015;38:1260-6.
[148] Mazurek S, Michel A, Eigenbrodt E. Effect of extracellular AMP on cell proliferation and metabolism of breast cancer cell lines with high and low glycolytic rates. The Journal of biological chemistry. 1997;272:4941-52.
[149] Mancuso F, Flower RJ, Perretti M. Leukocyte transmigration, but not rolling or adhesion, is selectively inhibited by dexamethasone in the hamster post-capillary venule. Involvement of endogenous lipocortin 1. J Immunol. 1995;155:377-86.
[150] Aziz KE, Wakefield D. Modulation of endothelial cell expression of ICAM-1, E-selectin, and VCAM-1 by beta-estradiol, progesterone, and dexamethasone. Cellular immunology. 1996;167:79-85.
[151] Ito A, Miyake M, Morishita M, Ito K, Torii S, Sakamoto T. Dexamethasone reduces lung eosinophilia, and VCAM-1 and ICAM-1 expression induced by Sephadex beads in rats. European journal of pharmacology. 2003;468:59-66.
[152] Ayalon O, Sabanai H, Lampugnani MG, Dejana E, Geiger B. Spatial and temporal relationships between cadherins and PECAM-1 in cell-cell junctions of human endothelial cells. The Journal of cell biology. 1994;126:247-58.

[153] Li J, Pei H, Zhu B, Liang L, Wei M, He Y, et al. Self-assembled multivalent DNA nanostructures for noninvasive intracellular delivery of immunostimulatory CpG oligonucleotides. ACS nano. 2011;5:8783-9.
[154] Ruiz-Hernandez E, Baeza A, Vallet-Regi M. Smart drug delivery through DNA/magnetic nanoparticle gates. ACS nano. 2011;5:1259-66.
[155] Wu CC, Lee J, Raz E, Corr M, Carson DA. Necessity of oligonucleotide aggregation for toll-like receptor 9 activation. The Journal of biological chemistry. 2004;279:33071-8.
[156] Kerkmann M, Costa LT, Richter C, Rothenfusser S, Battiany J, Hornung V, et al. Spontaneous formation of nucleic acid-based nanoparticles is responsible for high interferon-alpha induction by CpG-A in plasmacytoid dendritic cells. The Journal of biological chemistry. 2005;280:8086-93.
[157] Meng W, Yamazaki T, Nishida Y, Hanagata N. Nuclease-resistant immunostimulatory phosphodiester CpG oligodeoxynucleotides as human Toll-like receptor 9 agonists. BMC biotechnology. 2011;11:88.
[158] Davies LC, Jenkins SJ, Allen JE, Taylor PR. Tissue-resident macrophages. Nature immunology. 2013;14:986-95.
[159] Haberzettl P, Duffin R, Kramer U, Hohr D, Schins RP, Borm PJ, et al. Actin plays a crucial role in the phagocytosis and biological response to respirable quartz particles in macrophages. Archives of toxicology. 2007;81:459-70.
[160] Scherbart AM, Langer J, Bushmelev A, van Berlo D, Haberzettl P, van Schooten FJ, et al. Contrasting macrophage activation by fine and ultrafine titanium dioxide particles is associated with different uptake mechanisms. Particle and fibre toxicology. 2011;8:31.
[161] Rehberg M, Nekolla K, Sellner S, Praetner M, Mildner K, Zeuschner D, et al. Intercellular Transport of Nanomaterials is Mediated by Membrane Nanotubes In Vivo. Small. 2016;12:1882-90.
[162] Weissleder R, Nahrendorf M, Pittet MJ. Imaging macrophages with nanoparticles. Nature materials. 2014;13:125-38.
[163] Kuhn DA, Vanhecke D, Michen B, Blank F, Gehr P, Petri-Fink A, et al. Different endocytotic uptake mechanisms for nanoparticles in epithelial cells and macrophages. Beilstein journal of nanotechnology. 2014;5:1625-36.
[164] Murphy JE, Vohra RS, Dunn S, Holloway ZG, Monaco AP, Homer-Vanniasinkam S, et al. Oxidised LDL internalisation by the LOX-1 scavenger receptor is dependent on a novel cytoplasmic motif and is regulated by dynamin-2. Journal of cell science. 2008;121:2136-47.
[165] Chen Y, Wang X, Ben J, Yue S, Bai H, Guan X, et al. The di-leucine motif contributes to class a scavenger receptor-mediated internalization of acetylated lipoproteins. Arteriosclerosis, thrombosis, and vascular biology. 2006;26:1317-22.
[166] Platt N, Suzuki H, Kurihara Y, Kodama T, Gordon S. Role for the class A macrophage scavenger receptor in the phagocytosis of apoptotic thymocytes in vitro. Proceedings of the National Academy of Sciences of the United States of America. 1996;93:12456-60.
[167] Getts DR, Terry RL, Getts MT, Deffrasnes C, Muller M, van Vreden C, et al. Therapeutic inflammatory monocyte modulation using immune-modifying microparticles. Sci Transl Med. 2014;6:219ra7.
[168] Mortimer GM, Butcher NJ, Musumeci AW, Deng ZJ, Martin DJ, Minchin RF. Cryptic epitopes of albumin determine mononuclear phagocyte system clearance of nanomaterials. ACS nano. 2014;8:3357-66.
[169] Sirois CM, Jin T, Miller AL, Bertheloot D, Nakamura H, Horvath GL, et al. RAGE is a nucleic acid receptor that promotes inflammatory responses to DNA. The Journal of experimental medicine. 2013;210:2447-63.
[170] Foy DS, Ley K. Intercellular adhesion molecule-1 is required for chemoattractant-induced leukocyte adhesion in resting, but not inflamed, venules in vivo. Microvascular research. 2000;60:249-60.
[171] Piliponsky AM, Chen CC, Grimbaldeston MA, Burns-Guydish SM, Hardy J, Kalesnikoff J, et al. Mast cell-derived TNF can exacerbate mortality during severe bacterial infections in C57BL/6-KitW-sh/W-sh mice. The American journal of pathology. 2010;176:926-38.

[172] Mazurek N, Berger G, Pecht I. A binding site on mast cells and basophils for the anti-allergic drug cromolyn. Nature. 1980;286:722-3.
[173] Mazurek N, Bashkin P, Petrank A, Pecht I. Basophil variants with impaired cromoglycate binding do not respond to an immunological degranulation stimulus. Nature. 1983;303:528-30.
[174] Galli SJ, Tsai M. Mast cells in allergy and infection: versatile effector and regulatory cells in innate and adaptive immunity. European journal of immunology. 2010;40:1843-51.
[175] Alam R, Forsythe PA, Stafford S, Lett-Brown MA, Grant JA. Macrophage inflammatory protein-1 alpha activates basophils and mast cells. The Journal of experimental medicine. 1992;176:781-6.
[176] Galli SJ, Tsai M. IgE and mast cells in allergic disease. Nature medicine. 2012;18:693-704.
[177] Schramm R, Thorlacius H. Neutrophil recruitment in mast cell-dependent inflammation: inhibitory mechanisms of glucocorticoids. Inflammation research : official journal of the European Histamine Research Society [et al]. 2004;53:644-52.
[178] Thorlacius H, Raud J, Rosengren-Beezley S, Forrest MJ, Hedqvist P, Lindbom L. Mast cell activation induces P-selectin-dependent leukocyte rolling and adhesion in postcapillary venules in vivo. Biochemical and biophysical research communications. 1994;203:1043-9.
[179] Eltzschig HK, Eckle T. Ischemia and reperfusion--from mechanism to translation. Nat Med. 2011;17:1391-401.
[180] Oyama J, Blais C, Jr., Liu X, Pu M, Kobzik L, Kelly RA, et al. Reduced myocardial ischemia-reperfusion injury in toll-like receptor 4-deficient mice. Circulation. 2004;109:784-9.
[181] Hua F, Ha T, Ma J, Li Y, Kelley J, Gao X, et al. Protection against myocardial ischemia/reperfusion injury in TLR4-deficient mice is mediated through a phosphoinositide 3-kinase-dependent mechanism. J Immunol. 2007;178:7317-24.
[182] Mersmann J, Berkels R, Zacharowski P, Tran N, Koch A, Iekushi K, et al. Preconditioning by toll-like receptor 2 agonist Pam3CSK4 reduces CXCL1-dependent leukocyte recruitment in murine myocardial ischemia/reperfusion injury. Critical care medicine. 2010;38:903-9.
[183] Ha T, Hu Y, Liu L, Lu C, McMullen JR, Kelley J, et al. TLR2 ligands induce cardioprotection against ischaemia/reperfusion injury through a PI3K/Akt-dependent mechanism. Cardiovascular research. 2010;87:694-703.
[184] Markowski P, Boehm O, Goelz L, Haesner AL, Ehrentraut H, Bauerfeld K, et al. Pre-conditioning with synthetic CpG-oligonucleotides attenuates myocardial ischemia/reperfusion injury via IL-10 up-regulation. Basic research in cardiology. 2013;108:376.
[185] Cao Z, Ren D, Ha T, Liu L, Wang X, Kalbfleisch J, et al. CpG-ODN, the TLR9 agonist, attenuates myocardial ischemia/reperfusion injury: involving activation of PI3K/Akt signaling. Biochim Biophys Acta. 2013;1832:96-104.
[186] Khandoga AG, Khandoga A, Anders HJ, Krombach F. Postischemic vascular permeability requires both TLR-2 and TLR-4, but only TLR-2 mediates the transendothelial migration of leukocytes. Shock. 2009;31:592-8.
[187] Hu Z, Sun S, Zhou F. The binding of CpG-oligodeoxynucleotides to cell-surface and its immunostimulatory activity are modulated by extracellular acidic pH. Vaccine. 2003;21:485-90.
[188] Menkin V. Biology of inflammation; chemical mediators and cellular injury. Science. 1956;123:527-34.
[189] Grinstein S, Swallow CJ, Rotstein OD. Regulation of cytoplasmic pH in phagocytic cell function and dysfunction. Clin Biochem. 1991;24:241-7.
[190] Kamide T, Kitao Y, Takeichi T, Okada A, Mohri H, Schmidt AM, et al. RAGE mediates vascular injury and inflammation after global cerebral ischemia. Neurochemistry international. 2012;60:220-8.
[191] Lindau D, Mussard J, Wagner BJ, Ribon M, Ronnefarth VM, Quettier M, et al. Primary blood neutrophils express a functional cell surface Toll-like receptor 9. European journal of immunology. 2013;43:2101-13.
[192] Onji M, Kanno A, Saitoh S, Fukui R, Motoi Y, Shibata T, et al. An essential role for the N-terminal fragment of Toll-like receptor 9 in DNA sensing. Nature communications. 2013;4:1949.

[193] Eaton-Bassiri A, Dillon SB, Cunningham M, Rycyzyn MA, Mills J, Sarisky RT, et al. Toll-like receptor 9 can be expressed at the cell surface of distinct populations of tonsils and human peripheral blood mononuclear cells. Infection and immunity. 2004;72:7202-11.
[194] Hume DA. Differentiation and heterogeneity in the mononuclear phagocyte system. Mucosal immunology. 2008;1:432-41.
[195] Ji Y, Zhou Y, Pan J, Li X, Wang H, Wang Y. Temporal pattern of Toll-like receptor 9 upregulation in neurons and glial cells following cerebral ischemia reperfusion in mice. The International journal of neuroscience. 2016;126:269-77.
[196] Stout RD, Jiang C, Matta B, Tietzel I, Watkins SK, Suttles J. Macrophages sequentially change their functional phenotype in response to changes in microenvironmental influences. J Immunol. 2005;175:342-9.
[197] McWhorter FY, Wang T, Nguyen P, Chung T, Liu WF. Modulation of macrophage phenotype by cell shape. Proceedings of the National Academy of Sciences of the United States of America. 2013;110:17253-8.
[198] Roszer T. Understanding the Mysterious M2 Macrophage through Activation Markers and Effector Mechanisms. Mediators of inflammation. 2015;2015:816460.
[199] Daley JM, Brancato SK, Thomay AA, Reichner JS, Albina JE. The phenotype of murine wound macrophages. Journal of leukocyte biology. 2010;87:59-67.
[200] Ferrante CJ, Pinhal-Enfield G, Elson G, Cronstein BN, Hasko G, Outram S, et al. The adenosine-dependent angiogenic switch of macrophages to an M2-like phenotype is independent of interleukin-4 receptor alpha (IL-4Ralpha) signaling. Inflammation. 2013;36:921-31.
[201] Rai NK, Tripathi K, Sharma D, Shukla VK. Apoptosis: a basic physiologic process in wound healing. The international journal of lower extremity wounds. 2005;4:138-44.
[202] Hahn J, Wickham SF, Shih WM, Perrault SD. Addressing the instability of DNA nanostructures in tissue culture. ACS Nano. 2014;8:8765-75.
[203] Hagberg H. Intracellular pH during ischemia in skeletal muscle: relationship to membrane potential, extracellular pH, tissue lactic acid and ATP. Pflugers Archiv : European journal of physiology. 1985;404:342-7.
[204] Marzouk SA, Buck RP, Dunlap LA, Johnson TA, Cascio WE. Measurement of extracellular pH, K(+), and lactate in ischemic heart. Analytical biochemistry. 2002;308:52-60.
[205] Tsukube T, McCully JD, Metz KR, Cook CU, Levitsky S. Amelioration of ischemic calcium overload correlates with high-energy phosphates in senescent myocardium. The American journal of physiology. 1997;273:H418-25.
[206] Murphy E, Steenbergen C. Ion transport and energetics during cell death and protection. Physiology (Bethesda). 2008;23:115-23.
[207] Kawai Y, Yoshida M, Arakawa K, Kumamoto T, Morikawa N, Masamura K, et al. Diagnostic use of serum deoxyribonuclease I activity as a novel early-phase marker in acute myocardial infarction. Circulation. 2004;109:2398-400.
[208] Yasuda T, Iida R, Kawai Y, Nakajima T, Kominato Y, Fujihara J, et al. Serum deoxyribonuclease I can be used as a useful marker for diagnosis of death due to ischemic heart disease. Leg Med (Tokyo). 2009;11 Suppl 1:S213-5.
[209] Bidani A, Wang CZ, Saggi SJ, Heming TA. Evidence for pH sensitivity of tumor necrosis factor-alpha release by alveolar macrophages. Lung. 1998;176:111-21.
[210] Stella B, Arpicco S, Peracchia MT, Desmaele D, Hoebeke J, Renoir M, et al. Design of folic acid-conjugated nanoparticles for drug targeting. Journal of pharmaceutical sciences. 2000;89:1452-64.
[211] Paulos CM, Turk MJ, Breur GJ, Low PS. Folate receptor-mediated targeting of therapeutic and imaging agents to activated macrophages in rheumatoid arthritis. Advanced drug delivery reviews. 2004;56:1205-17.
[212] White KP, Driscoll MS, Rothe MJ, Grant-Kels JM. Severe adverse cardiovascular effects of pulse steroid therapy: is continuous cardiac monitoring necessary? Journal of the American Academy of Dermatology. 1994;30:768-73.

[213] Sato H, Takahashi T, Sumitani K, Takatsu H, Urano S. Glucocorticoid Generates ROS to Induce Oxidative Injury in the Hippocampus, Leading to Impairment of Cognitive Function of Rats. Journal of clinical biochemistry and nutrition. 2010;47:224-32.
[214] Soybilgic A, Tesher M, Wagner-Weiner L, Onel KB. A survey of steroid-related osteoporosis diagnosis, prevention and treatment practices of pediatric rheumatologists in North America. Pediatric rheumatology online journal. 2014;12:24.
[215] Reid DM, Devogelaer JP, Saag K, Roux C, Lau CS, Reginster JY, et al. Zoledronic acid and risedronate in the prevention and treatment of glucocorticoid-induced osteoporosis (HORIZON): a multicentre, double-blind, double-dummy, randomised controlled trial. Lancet. 2009;373:1253-63.
[216] Gonzalez-Gonzalez JG, Mireles-Zavala LG, Rodriguez-Gutierrez R, Gomez-Almaguer D, Lavalle-Gonzalez FJ, Tamez-Perez HE, et al. Hyperglycemia related to high-dose glucocorticoid use in noncritically ill patients. Diabetology & metabolic syndrome. 2013;5:18.
[217] Natsui K, Tanaka K, Suda M, Yasoda A, Sakuma Y, Ozasa A, et al. High-dose glucocorticoid treatment induces rapid loss of trabecular bone mineral density and lean body mass. Osteoporosis international : a journal established as result of cooperation between the European Foundation for Osteoporosis and the National Osteoporosis Foundation of the USA. 2006;17:105-8.
[218] Stromberg T, Dimberg A, Hammarberg A, Carlson K, Osterborg A, Nilsson K, et al. Rapamycin sensitizes multiple myeloma cells to apoptosis induced by dexamethasone. Blood. 2004;103:3138-47.
[219] Ramalingam A, Hirai A, Thompson EA. Glucocorticoid inhibition of fibroblast proliferation and regulation of the cyclin kinase inhibitor p21Cip1. Mol Endocrinol. 1997;11:577-86.
[220] Gueron M, Leroy JL. The i-motif in nucleic acids. Curr Opin Struct Biol. 2000;10:326-31.
[221] Song L, Ho VH, Chen C, Yang Z, Liu D, Chen R, et al. Efficient, pH-triggered drug delivery using a pH-responsive DNA-conjugated gold nanoparticle. Adv Healthc Mater. 2013;2:275-80.
[222] Modi S, M GS, Goswami D, Gupta GD, Mayor S, Krishnan Y. A DNA nanomachine that maps spatial and temporal pH changes inside living cells. Nat Nanotechnol. 2009;4:325-30.
[223] Sharma S, DeOliveira RB, Kalantari P, Parroche P, Goutagny N, Jiang Z, et al. Innate immune recognition of an AT-rich stem-loop DNA motif in the Plasmodium falciparum genome. Immunity. 2011;35:194-207.
[224] Henneicke H, Gasparini SJ, Brennan-Speranza TC, Zhou H, Seibel MJ. Glucocorticoids and bone: local effects and systemic implications. Trends in endocrinology and metabolism: TEM. 2014;25:197-211.
[225] Ogawa S, Lozach J, Benner C, Pascual G, Tangirala RK, Westin S, et al. Molecular determinants of crosstalk between nuclear receptors and toll-like receptors. Cell. 2005;122:707-21.
[226] Scheinman RI, Gualberto A, Jewell CM, Cidlowski JA, Baldwin AS, Jr. Characterization of mechanisms involved in transrepression of NF-kappa B by activated glucocorticoid receptors. Molecular and cellular biology. 1995;15:943-53.
[227] Caldenhoven E, Liden J, Wissink S, Van de Stolpe A, Raaijmakers J, Koenderman L, et al. Negative cross-talk between RelA and the glucocorticoid receptor: a possible mechanism for the antiinflammatory action of glucocorticoids. Mol Endocrinol. 1995;9:401-12.
[228] Rahman MM, McFadden G. Modulation of NF-kappaB signalling by microbial pathogens. Nature reviews Microbiology. 2011;9:291-306.
[229] Xia YF, Liu LP, Zhong CP, Geng JG. NF-kappaB activation for constitutive expression of VCAM-1 and ICAM-1 on B lymphocytes and plasma cells. Biochemical and biophysical research communications. 2001;289:851-6.
[230] Lee CW, Lin WN, Lin CC, Luo SF, Wang JS, Pouyssegur J, et al. Transcriptional regulation of VCAM-1 expression by tumor necrosis factor-alpha in human tracheal smooth muscle cells: involvement of MAPKs, NF-kappaB, p300, and histone acetylation. Journal of cellular physiology. 2006;207:174-86.
[231] Zhang J, Alcaide P, Liu L, Sun J, He A, Luscinskas FW, et al. Regulation of endothelial cell adhesion molecule expression by mast cells, macrophages, and neutrophils. PloS one. 2011;6:e14525.

[232] Davis JM, Colangelo J. Small-molecule inhibitors of the interaction between TNF and TNFR. Future medicinal chemistry. 2013;5:69-79.
[233] Petros RA, DeSimone JM. Strategies in the design of nanoparticles for therapeutic applications. Nature reviews Drug discovery. 2010;9:615-27.
[234] Sudimack J, Lee RJ. Targeted drug delivery via the folate receptor. Advanced drug delivery reviews. 2000;41:147-62.
[235] Kelly C, Jefferies C, Cryan SA. Targeted liposomal drug delivery to monocytes and macrophages. Journal of drug delivery. 2011;2011:727241.
[236] Keefe AD, Pai S, Ellington A. Aptamers as therapeutics. Nature reviews Drug discovery. 2010;9:537-50.
[237] Chen YJ, Groves B, Muscat RA, Seelig G. DNA nanotechnology from the test tube to the cell. Nature nanotechnology. 2015;10:748-60.

7 Appendix

7.1 Lab equipment and consumables

Table 4 Lab consumables

Consumables	Manufacturer
1.5 ml and 2 ml tubes	Eppendorf, Hamburg, Germany
15 ml and 50 ml tubes	BD Falcon, Heidelberg, Germany
Aqua ad injectabilia	Braun, Melsungen, Germany
Baysilone-Paste, hochviskos	Bayer, Leverkusen, Germany
BD Discardit II	BD, Heidelberg, Germany
BD Microlance 3	BD, Heidelberg, Germany
BD Plastipak	BD, Heidelberg, Germany
Borosilicate micropipettes GB150-TF-8P	Science Product, Hofheim, Germany
Natriumchlorid 0,9 % Lsg.	Braun, Melsungen, Germany
Sterican 100, 0,30 x 12 mm, 30G	Braun, Melsungen, Germany
BD Falcon round bottom tubes	BD, Heidelberg, Germany

Table 5 Lab equipment

Equipment	Manufacturer
Elektrotom 500-BF	KLSMartin, Tuttlingen, Germany
Eppendorf Research Plus 10, 100, 1000 µl	Eppendorf, Hamburg, Germany
Femtojet microinjector	Eppendorf, Hamburg, Germany
Incubator BD 115	Binder, Tuttlingen, Germany
Infinite F200 Multiplate reader	Tecan, Männedorf, Switzerland
Gallios flow cytometer	Beckman Coulter, Krefeld, Germany
Leitz Labovert	Leica, Wetzlar, Germany
Patchstar Micromanipulator	Scientifica, Uckfield, UK
PC-10 Puller	Narishige, London, UK

Pipetboy comfort	Integra Biosciences, Ziezers, Switzerland
Universal 30RF	Hettich, Tuttlingen, Germany
Vortex Genie 2	Bender&Hobein, Zurich, Switzerland
Coulter ACT Counter	Beckman Coulter, Krefeld, Germany

Table 6 Chemicals

Chemicals	**Manufacturer**
Cromolyn sodium salt	SigmaAldrich, Taufkirchen, Germany
Dexamethasone	SigmaAldrich, Taufkirchen, Germany
Ketamin	Zoetis, Berlin, Germany
Pentobarbital	Merial, Hallbergmoos, Germany
Xylazin	Bayer, Leverkusen, Germany

7.2 Cell culture consumables

Table 7 Cell culture consumables

Consumable	**Manufacturer**
Dulbecco´s modified eagle medium	Thermo Scientific, Bonn, Germany
RPMI-1640 medium	Merck Millipore, Berlin, Germany
Phosphate-buffered saline	Braun, Melsungen, Germany
Trypsin-EDTA (0.5 %)	Thermo Scientific, Bonn, Germany
2-Mercaptoethanol (50 mM)	Thermo Scientific, Bonn, Germany
Fetal calf serum	Merck Millipore, Berlin, Germany
Lipopolysaccharides from *E. coli*	SigmaAldrich, Taufkirchen, Germany
WST-1 Reagent	SigmaAldrich, Taufkirchen, Germany
Mouse TNF-alpha DuoSet ELISA	R&D Systems, Wiesbaden, Germany

7.3 Immunohistochemistry consumables

Table 8 Primary and secondary antibodies

Primary or secondary antibody	Manufacturer
Alexa Fluor 488, goat anti rat, IgG (H+L)	Life Technologies, Carlsbad, USA
Alexa Fluor 546, donkey anti goat, IgG (H+L)	Life Technologies, Carlsbad, USA
Alexa Fluor 546, goat anti rabbit, IgG (H+L)	Life Technologies, Carlsbad, USA
Alexa Fluor 633, goat anti rabbit, IgG (H+L)	Life Technologies, Carlsbad, USA
Alexa Fluor 633, goat anti rat, IgG (H+L)	Life Technologies, Carlsbad, USA
CD31, rat, mAb	BD, Heidelberg, Germany
CD45, rat, mAb	BioLegend, Fell, Germany
CD106, rat, mAb	BioLegend, Fell, Germany
F4/80, rat, mAb	Abcam, Cambridge, UK
Glucocorticoid receptor, rabbit, mAb	Santa Cruz, Heidelberg, Germany
Histone H3 (citrulline R2+R8+R17), rabbit, pAb	Abcam, Cambridge, UK
CD45, rat, mAb	BioLegend, Fell, Germany
NF-κB p65 (acetyl K310), rabbit, pAb	Abcam, Cambridge, UK
PECAM-1(M20), goat, mAb	Santa Cruz, Heidelberg, Germany
TLR 9, mouse, mAb	Abcam, Cambridge, UK
TLR 9, rabbit, mAb	Abcam, Cambridge, UK

Table 9 Fluorescent dyes

Fluorescent dye	Manufacturer
FluoSpheres, 2 µm	Life Technologies, Carlsbad, USA
LysoTracker Red DND-99	Life Technologies, Carlsbad, USA
LysoTracker Green DND-26	Life Technologies, Carlsbad, USA
TO-PRO-3 Iodid	Thermo Scientific, Bonn, Germany

Table 10 Microscope equipment and consumables

Equipment and consumables	Manufacturer
LMPlanFI 20x/0.4 NA	Olympus, Münster, Germany
Plan Apochromat 40x/1.4 NA oil	Leica, Wetzlar, Germany
Plan Apochromat 63x/1.4 NA oil	Leica, Wetzlar, Germany
Plan Apochromat 63x/1.0 NA water	Leica, Wetzlar, Germany
TCS SP5 SMD	Leica, Wetzlar, Germany
Glass coverslips 25 x 25 mm	VWR, Radnor, USA
Rolera EM-C^2 cameras	Qimaging, Surrey, Canada
VisiScope A1 imaging system	Visitron Systems, Puchheim, Germany
VWR Superfrost Micro Slide	VWR, Radnor, USA

Table 11 Consumables

Consumables	Manufacturer
Paraformaldehyde	SigmaAldrich, Taufkirchen, Germany
PermaFlour^{TM} Aqueous Mounting Medium	Beckman Coulter, Krefeld, Germany
Triton X-100	SigmaAldrich, Taufkirchen, Germany
Bovine Serum Albumin	SigmaAldrich, Taufkirchen, Germany

7.4 Abbreviations

3D	Three-dimensional
BSA	Bovine serum albumin
CD	Cluster of differentiation
Csfr1	Colony stimulating factor 1 receptor
CO_2	Carbondioxide
$CoCl_2$	Cobalt(II)chloride
CpG	-C-phosphate-G-
cQD	carboxyl Quantum Dot
CX_3CR1	CX3 chemokine receptor 1
Cy3	Cyanine-3
DAMP	Damage associated pattern
DC	Dendritic cell
DCC	Dicyclohexylcarbodiimid
DCM	Dichloromethane
Dex	Dexamethasone
DLS	Dynamic light scattering
DMAP	*N,N*-Dimethylaminopyridine
DMEM	Dulbecco´s modified eagle medium
DMF	Dimethylformamide
DNA	Deoxyribonucleic acid
dUTP	Deoxyuridine-triphosphatase
ECs	Endothelial cells
EDTA	Ethylenediaminetetraacetic acid
EGFP	Enhanced green fluorescent protein
Fc	Fragment crystallizable region
FCS	Fetal calf serum
GaAsP	Gallium arsenide phosphide
GC	Glucocorticoids
GR	Glucocorticoid receptor
HPLC	High performance liquid chromatography

HPSF	High purity salt free
ICAM-1	Intercellular adhesion molecule 1
IgG	Immunoglobulin G
IL	Interleukin
IFN-α	Interferon alpha
IFN-γ	Interferon gamma
IκB	Inhibitor of kappa B
IKK	IκB Kinase
IR	Ischemia/reperfusion
IRAK	Interleukin-1 receptor associated kinase
kb	Kilo-base
kDa	Kilo Dalton
LPS	Lipopolysaccharide
mAb	Monoclonal antibody
M-CSF	Macrophage colony-stimulating factor
MeOH	Methanol
MES	2-(*N*-morpholino)ethanesulfonic acid
MgCl2	Magnesium chloride
MIP	Macrophage inflammatory protein
MMP	Matrixmetalloproteinase
MWCO	Molecular weight cut-off
MYD88	Myeloid differentiation primary response gene 88
NaOAc	Sodium acetate
NF-κB	Nuclear factor 'kappa-light-chain-enhancer' of activated B- cells
NOD	Nucleotide-binding oligomerization domain receptor
NP	Nanoparticle
nt	Nucleotides
ODN	Oligodeoxynucleotide
PAA	Polyacrylamid
pAb	Polyclonal antibody
PAMP	Pathogen associated pattern
PBMC	Peripheral blood mononuclear cell
PBS	Phosphate buffered saline

PECAM-1	Platelet endothelial cell adhesion molecule 1
PFA	Para-formaldhehyde
PMNL	Polymorphonuclear leukocyte
Poly-A	Polyadenylation
STAT5	Signal transducer and activator of transcription 5
TBE	Tris/Borate/EDTA
TdT	Terminal deoxynucleotidyl transferase
TEM	Transmission electron microscopy
THF	Tetrahydrofurane
TLR	Toll-like receptor
TNF	Tumor necrosis factor
Tris-HCl	Tris hydrochloride
VCAM-1	Vascular cell adhesion molecule 1
WST-1	Water soluble tetrazolium salt 1

7.5 Publications and presentations

7.5.1 Publications

Dexamethasone-conjugated DNA nanotubes as anti-inflammatory agents *in vivo*

Sabine Sellner*, Samet Kocabey*, Tao Zhang, Fritz Krombach, Tim Liedl, Markus Rehberg

Submitted at Biomaterials

Microglial CX3CR1 promotes adult neurogenesis by inhibiting Sirt 1/p65 signaling independent of CX3CL1

Sabine Sellner, Paricio-Montesinos Ricardo, Spieß Alena, Masuch Anette, Erny Daniel, Harsan Laura A., von Elverfeldt Dominik, Schwabenland Marius, Biber Knut, Staszewski Ori, Lira Sergio, Jung Steffen, Prinz Marco, Blank Thomas

Acta Neuropathologica Communications, 2016 Sep17;4(1):102

Influence of surface modifications on the spatio-temporal microdistribution of quantum dots *in vivo*

Katharina Nekolla, Kerstin Kick, Sabine Sellner, Karina Mildner, Stefan Zahler, Dagmar Zeuschner, Fritz Krombach, Markus Rehberg

Small, 2016 May;12(19):261-51

Intercellular transport of nanomaterials is mediated by membrane nanotubes *in vivo*

Markus Rehberg, Anna K. Nekolla, Sabine Sellner, Karina Mildner, Dagmar Zeuschner, Fritz Krombach

Small, 2016 Apr;12(14):1882-90

Multi-photon microscopy of non-fluorescent nanoparticles *in vitro* and *in vivo*

Steffen Dietzel, Stefanie Hermann, Yan Kugel, Sabine Sellner, Bernd Uhl, Stephanie Hirn, Fritz Krombach, Markus Rehberg

Small, 2016 Apr;12(14):3245-57

A microfluidics approach to study the accumulation of molecules at basal lamina interfaces

Fabienna Arends, Sabine Sellner, Philipp Seifert, Ulrich Gerland, Markus Rehberg, Oliver Lieleg

Lab on a chip, 2015 Aug 21, 15(16)

DNA nanoconstructs as intracellular delivery vehicles *in vivo*

Sabine Sellner*, Samet Kocabey*, Anna K. Nekolla, Fritz Krombach, Tim Liedl, Markus Rehberg

Biomaterials. 2015, 53:453-63

*These authors contribute equally.

7.5.2 Oral presentations

DNA Nanotubes - Intracellular Delivery Vehicles *in vivo*

Sabine Sellner, Samet Kocabey, Fritz Krombach, Tim Liedl, Markus Rehberg

Emerging Methods and Technologies for Medical Research Conference,

September 1-2 2015, Stockholm, Sweden

DNA Nanotubes - Intracellular Delivery Vehicles *in vivo*

Sabine Sellner, Samet Kocabey, Fritz Krombach, Tim Liedl, Markus Rehberg

Kolloquium über experimentelle Pathophysiologie

June 30 2014, Munich, Germany

DNA Nanotubes - Intracellular Delivery Vehicles *in vivo*

Sabine Sellner, Samet Kocabey, Fritz Krombach, Tim Liedl, Markus Rehberg

SFB 1032 Retreat 2014, February 24-25, Frauenchiemsee, Germany

7.5.3 Poster presentations

The impact of DNA nanotubes in physiologic and inflamed tissue

Sabine Sellner, Samet Kocabey, Fritz Krombach, Tim Liedl, Markus Rehberg

SFB 1032 evaluation 2016, January 28-29, Munich, Germany

Localization and immunogenic properties of DNA nanotubes under physiological and pathophysiological conditions

Sabine Sellner, Samet Kocabey, Fritz Krombach, Tim Liedl, Markus Rehberg

SFB 1032 Retreat 2015, February 3-5, Altötting, Germany

Localization and immunogenic properties of DNA nanotubes *in vivo*

Sabine Sellner, Samet Kocabey, Fritz Krombach, Tim Liedl, Markus Rehberg

2nd IBN International Symposium Nanomedicine and Nanoassay 2014, December 8-9, Singapur

Localization and immunogenic properties of DNA nanotubes *in vivo*

Sabine Sellner, Samet Kocabey, Fritz Krombach, Tim Liedl, Markus Rehberg

CeNS Venice Workshop 2014, September 22-26, Venice, Italy

DNA nanotubes as intracellular delivery vehicles *in vivo*

Sabine Sellner, Samet Kocabey, Fritz Krombach, Tim Liedl, Markus Rehberg

International Physics of Living Systems Network Conference 2014, July 21-24, Munich, Germany

DNA nanotubes as intracellular delivery vehicles *in vivo*

Sabine Sellner, Samet Kocabey, Fritz Krombach, Tim Liedl, Markus Rehberg

7. International Nanotoxicology Congress 2014, April 23-26, Antalya, Turkey